INVESTIGATION OF ATMOSPHERIC OZONE IMPACTS OF 3-METHOXY-3-METHYL-1-BUTANOL

Final Report to the

Kuraray Co. Ltd
Contract UCR- 09070726

By

William P. L. Carter[1], Wendy S. Goliff[1],
Roger Atkinson,[2] Janet Arey[2] and Sara M. Aschmann[2]

July 8, 2010

[1]Center for Environmental Research and Technology
College of Engineering
University of California
Riverside, California 92521

[2]Air Pollution Research Center
University of California
Riverside, California 92521

ABSTRACT

An experimental and modeling study was carried out to assess the impacts of 3-Methoxy-3-methyl-1-butanol (MMB) on ground-level ozone formation. The rate constant for the reaction of MMB with OH radicals was measured to be $(1.64 \pm 0.06) \times 10^{-11}$ cm^3 $molecule^{-1}$ s^{-1} at 296 ± 2 K, which is over a factor of 2 higher than previously estimated. Acetone, methyl acetate, and 3 methoxy-3-methylbutanal were identified as products of this reaction, with yields of 3 ± 1%, 34 ± 8, and approximately 33-47%, respectively. Glycolaldehyde was also observed but was not quantified. These data were used to derive a mechanism for the atmospheric reactions of MMB, for use in calculating its atmospheric ozone impacts using the SAPRC-07 mechanism. To evaluate the predictive capability of this mechanism, incremental reactivity environmental chamber experiments were carried out to determine the effects of adding MMB to irradiations of reactive organic gas (ROG) surrogate - NO_x mixtures representing ambient conditions. The results were reasonably consistent with the new MMB mechanism derived in this work. This mechanism was then used to calculate the atmospheric ozone impact of MMB in the MIR and other SAPRC-07 ozone reactivity scales. The MIR calculated for MMB was 2.78 grams O_3 per gram VOC, which is higher than calculated for it previously using an estimated mechanism, but slightly lower than the MIR for the mixture used to represent anthropogenic VOCs from all sources in the reactivity calculations. The environmental chamber experiments also indicated that MMB does not form measurable secondary organic aerosol under the conditions of our experiments.

ACKNOWLEDGEMENTS AND DISCLAIMERS

This work was funded by Kuraray Co. Ltd. through contract UCR- 09070726. The environmental chamber experiments for this project were carried out at the College of Engineering Center for Environmental Research and Technology (CE-CERT) at the University of California at Riverside (UCR) under the supervision of William Carter and Wendy Goliff. The experiments at CE-CERT were carried out primarily by Qi Li and Kurt Bumiller. Mr. Dennis Fitz also provided assistance in administering this project at CE-CERT, and Ms. Kathy Cocker provided assistance in conducting the experiments and processing the data. The kinetic and mechanistic experiments were carried out by Roger Atkinson, Janet Arey and Sara Aschmann at the Air Pollution Research Center (APRC) at UCR. We also wish to thank Mr. Wally Albers of CBC America Corporation for supporting this project and for helpful discussions.

Although Kuraray Co. Ltd. funded this work, the contents of this report reflect only the opinions and conclusions of the primary author. Mention of trade names and commercial products does not constitute endorsement or recommendation for use.

TABLE OF CONTENTS

INTRODUCTION 1

EXPERIMENTAL METHODS 3
- Kinetic and Mechanistic Studies 3
  - Kinetic Experiments 3
  - Product Determination Experiments 3
  - Materials 4
- Environmental Chamber Experiments 4
  - Chamber Description 4
  - Analytical Instrumentation 6
  - Sampling methods 9
  - Characterization Methods 9
  - Experimental Procedures 10
  - Materials 11

KINETIC AND MECHANISTIC RESULTS 12
- Kinetics of OH + 3-Methoxy-3-methyl-1-butanol 12
- Products of OH + 3-Methoxy-3-methyl-1-butanol 12

MECHANISM AND MODELING METHODS 17
- Base Mechanism 17
- Mechanism for 3-Methoxy-3-Methyl-1-Butanol 18
- Representation of Chamber Conditions 26
- Atmospheric Reactivity Simulations 26

RESULTS AND DISCUSSION 27
- Characterization Results 27
- Incremental Reactivity and Mechanism Evaluation Results 30
- Atmospheric Reactivity Calculation 33
- Effects of MMB on Secondary Aerosol Formation 37

CONCLUSIONS 39

REFERENCES 40

APPENDIX A. BASE MECHANISM LISTING 44

LIST OF TABLES

Table 1. List of analytical and characterization instrumentation for the UCR EPA chamber. 7

Table 2. Estimated rate constants for OH radical abstractions from various positions in the 3-methoxy-3-methyl-1-butanol molecule. 18

Table 3. Mechanism used for the atmospheric reactions of 3-methoxy-3-methyl-1-butanol. 19

Table 4. Products predicted to be formed in the atmospheric reactions of 3-methoxy-3-methyl-1-butanol and the model species used to represent their subsequent reactions. 22

Table 5. Mechanism used for the atmospheric reactions of the MMB oxidation product 3-methoxy-3-methyl butyraldehyde. 24

Table 6. Products predicted to be formed in the atmospheric reactions of $CH_3OC(CH_3)(CH_3)CH_2CHO$ and the model species used to represent their subsequent reactions. 25

Table 7. Summary of experiments carried out for this project. 28

Table 8. Summary of initial concentrations and selected gas-phase results of the incremental reactivity experiments. 30

Table 9. Summary of conditions of scenarios used for reactivity assessment 34

Table 10. Calculated atmospheric incremental reactivities for 3-methoxy-3-methyl-1-butanol and the base ROG mixture 36

Table A-1. List of model species used in the base SAPRC-07 mechanism, including the VOC species used in the chamber and atmospheric reactivity simulations. 44

Table A-2. Reactions and rate constants in the base SAPRC-07 mechanism used in this work. See Carter (2009a) for documentation. 48

Table A-3. Summary of photolysis rates used in chamber and ambient simulations. 65

LIST OF FIGURES

Figure 1. Schematic of the UCR EPA environmental chamber reactors and enclosure. 5

Figure 2. Spectrum of the light sources used in the UCR EPA chamber, with intensities normalized to give the same NO_2 photolysis rates. A representative solar spectrum is also shown. 5

Figure 3. Plot of Equation (I) for the gas-phase reaction of OH radicals with 3-methoxy-3-methyl-1-butanol at 296 ± 2 K, with di-*n*-butyl ether as the reference compound. 13

Figure 4. Plots of the amounts of product observed against the amounts of 3-methoxy-3-methyl-1-butanol reacted with OH radicals.. 13

Figure 5. Total ion chromatogram of a GC-MS analysis (DB-5 column) of a coated-SPME fiber exposed to the chamber contents after reaction. 14

Figure 6. Mass spectra of peaks #1a, 2a, 3a, and 3 in Figure 5. (Peaks 1b and 2b had an essentially identical mass spectra as peaks 1a and 2a, respectively)..... 15

Figure 7. Plots of best fit HONO offgasing parameters against UCR EPA run number. 29

Figure 8. Experimental and calculated results of the incremental reactivity experiments with added MMB. 32

Figure 9. Comparisons of ozone reactivity of MMB in the MIR scale with those for isomeric compounds and other representative VOCs. 37

Figure 10. Plots of average PM reactivities in incremental reactivity experiments for all VOCs for which PM data are available in UCR EPA chamber reactivity experiments..... 38

INTRODUCTION

Ozone in photochemical smog is formed from the gas-phase reactions of volatile organic compounds (VOCs) and oxides of nitrogen (NO_x) in sunlight, and control of both VOCs and NO_x is required to attain air quality standards for ozone. Many different types of VOCs are emitted into the atmosphere, each reacting at different rates and having different mechanisms for their reactions. Because of this, they can differ significantly in their effects on ozone formation, or their "reactivity". In recognition of this, the U.S. EPA has exempted volatile organic certain compounds with ozone impacts expected to be less than ethane from regulations as VOC ozone precursors (Dimitriades, 1999; RRWG, 1999, EPA, 2005), and the California Air Resources Board (CARB) has adopted regulations with reactivity-based adjustments for several types of VOC sources (CARB 1993, 2000) and is investigating their use for other sources (CARB, 2008).

The compound 3-methoxy-3-methyl-1-butanol (MMB) (CAS number 56539-66-3) is an essential ingredient of certain odorant products, whose normal use would result in it being emitted into the atmosphere. Because of this, it may be subject to regulation as a VOC ozone precursor, unless its ozone impact can be shown to be sufficiently low that it can be exempted as an ozone precursor. Although until this study there has been no known experimental data concerning the atmospheric reactions or ozone impact of this compound, ozone impacts of MMB have been calculated in the MIR and other reactivity scales, based on an estimated mechanism derived using various structural-reactivity methods (Carter, 2009a). The most recently derived MIR value for MMB is 1.47 grams O_3 per gram VOC. This makes MMB less reactive than the base reactive organic gas (ROG) mixture used to represent total anthropogenic VOCs (whose MIR is 3.52 grams O_3 per gram VOC), but more reactive than ethane (whose MIR is 0.27 grams O_3 per gram VOC), the compound the U.S. EPA uses as the borderline for determining if a compound can be exempted as having negligible ozone impact (Dimitriades, 1999, EPA, 2005). If this reactivity estimate is correct, MMB should be regulated less strictly than other VOCs in any reactivity-based regulatory scheme, but it would be still too reactive to be exempt from regulation in a mass-based regulatory scheme as having an negligible ozone impact.

These conclusions about MMB's ozone impact depend on the reliability of the mechanism used for this compound in the reactivity calculations, which is based entirely on estimates. We are aware of no previously available environmental chamber data to test the ability of our current mechanism for this compound to calculate its ozone impact, nor are we aware of any experimental data concerning its major expected atmospheric reaction, which is reaction with OH radicals. Therefore, the rate at which it reacts in the atmosphere and the mechanisms of the subsequent reactions all had to be estimated, using various structure-reactivity methods. Although these estimates are not considered to be overly uncertain for this type of compound, and such estimated mechanisms have performed well in simulating chamber data for many (though not all) glycol ethers, the estimated rate constant or branching ratio estimates are at best only good to within ±30% under the best of circumstances, and can be further off in some cases. Without experimental verification the possibility of unexpected reactions or rate constants cannot be totally ruled out.

To address the uncertainty in current ozone impact estimates for MMB, we carried out kinetic and mechanistic studies to measure the rate constant for the reaction of MMB with OH radicals and determine its major oxidation products, environmental chamber studies to test the ability of current the mechanism to predict its ozone impacts, and a modeling study to update the atmospheric reaction mechanism of MMB based on the results of the laboratory and chamber experiments and to estimate its atmospheric

ozone impacts. The kinetic and mechanistic studies were carried out at the Air Pollution Research Center (APRC) at the University of California at Riverside (UCR) by Roger Atkinson, Janet Arey and Sara M. Aschmann, and the environmental chamber and modeling studies were carried out at the College of Engineering Center for Environmental Research and Technology (CE-CERT) at UCR under the direction of William P. L. Carter. The methods, results, and conclusions of these studies are discussed in this report.

EXPERIMENTAL METHODS

Kinetic and Mechanistic Studies

Experiments were carried out in a ~7000 L all-Teflon chamber at APRC, equipped with two parallel banks of blacklamps for irradiation and a Teflon-coated fan to ensure rapid mixing of reactants, in the presence of ~735 Torr total pressure of purified dry air at 296 ± 2 K. OH radicals were generated from the photolysis of CH_3ONO in air at wavelengths >300 nm, and NO was also added to the reactant mixtures to suppress the formation of O_3 and hence of NO_3 radicals. Additional information concerning the chamber and experimental methods used is available in numerous publications describing similar studies carried out by Atkinson and co-workers (see, for example, Tuazon et al., 2005 and Aschmann and Atkinson, 2008).

Kinetic Experiments

The rate constant for the reaction of OH radicals with 3-methoxy-3-methyl-1-butanol was measured using a relative rate technique in which the disappearance rate of 3-methoxy-3-methyl-1-butanol was determined relative to that of a reference compound, whose rate constant is reliably known. Di-*n*-butyl ether was used as the reference compound in this study. The data analysis method employed is discussed in the Results of the Kinetic and Mechanistic Studies section, below.

The procedures used for the kinetic experiments were as follows. The initial reactant concentrations (molecule cm^{-3}) were: CH_3ONO, ~2.4×10^{14}; NO, ~2.4×10^{14}; and 3-methoxy-3-methyl-1-butanol and di-*n*-butyl ether, ~2.4×10^{13} each. Irradiations were carried out at 20% of the maximum light intensity for up to 15 min, resulting in consumption of up to 38% and 56% of 3-methoxy-3-methyl-1-butanol and di-*n*-butyl ether, respectively. The concentrations of 3-methoxy-3-methyl-1-butanol and di-*n*-butyl ether and selected products (see below) were measured during the experiments by gas chromatography with flame ionization detection (GC-FID). Gas samples of 100 cm^3 volume were collected from the chamber onto Tenax-TA solid adsorbent with subsequent thermal desorption at ~205 ^oC onto a 30 m DB-1701 megabore column, initially held at -40 °C and then temperature programmed to 250 °C at 8 °C min^{-1}. Replicate analyses of the 3-methoxy-3-methyl-1-butanol and di-*n*-butyl ether within the chamber prior to reaction agreed to within typically ≤3%.

Product Determination Experiments

Products were analyzed by GC-FID as described above. GC-FID response factor calibrations were carried out by introducing measured amounts of the chemicals (3-methoxy-3-methyl-1-butanol, acetone and methyl acetate) into the chamber and conducting several replicate GC-FID analyses as described above. In addition, carbonyl products were identified by collection onto a 65 μm polydimethylsiloxane/divinylbenzene Solid Phase MicroExtraction (SPME) fiber pre-coated with *O*-(2,3,4,5,6-pentafluorobenzyl)hydroxyl amine (PFBHA) for on-fiber derivatization of carbonyl compounds, with subsequent thermal desorption and analysis by positive chemical ionization GC-MS (PCI GC-MS) using methane as the CI gas in an Agilent 5975 Inert XL Mass Selective Detector with a 60 m DB-5 capillary column (250 μm i.d., 0.25 μm phase) operated in the scanning mode. Each carbonyl group derivatized to an oxime added 195 mass units to the compound's molecular weight. Methane-CI gives protonated molecules $[M+H]^+$ and smaller adduct ions at $[M+29]^+$ and $[M+41]^+$, and also a $[M+H-198]^+$ fragment, where M is the molecular weight of the oxime. In addition, hydroxycarbonyls have

characteristic $[M+H-H_2O]^+$ fragment ions. Analogous GC-MS analyses were also conducted of samples collected onto Tenax-TA solid adsorbent, with concurrent GC-FID analyses on BD-5 and DB-1701 columns, in order to determine the identity of the peak(s) observed.in the GC-FID analyses.

Materials

The MMB sample used for the kinetic and mechanistic studies were obtained from Aldrich Chemical, with a stated purity of 98+%. The methyl nitrite was synthesized as described previously (see, for example, Tuazon et al., 2005 and Aschmann and Atkinson, 2008).

Environmental Chamber Experiments

Chamber Description

All of the environmental chamber experiments for this project were carried out using the UCR EPA environmental chamber at CE-CERT. This chamber was constructed under EPA funding to address the needs for an improved environmental chamber database for mechanism evaluation (Carter, 2002). The objectives, design, construction, and results of the initial evaluation of this chamber facility are described in more detail elsewhere (Carter, 2002; Carter, 2004, Carter et al., 2005a). A brief description of the chamber is also given below.

The UCR EPA chamber consists of two ~85,000-liter Teflon® reactors located inside a 16,000 cubic ft temperature-controlled "clean room" that is continuously flushed with purified air. The clean room design is employed in order to minimize background contaminants into the reactor due to permeation or leaks. Two alternative light sources can be used. The first consists of a 200 KW argon arc lamp with specially designed UV filters that give a UV and visible spectrum similar to sunlight. Banks of blacklights are also present to serve as an alternative lower cost light source when blacklight irradiation is sufficient. Blacklights have a good representation of sunlight in the UV portion of the spectrum that affects most photolysis reactions of interest, and their use is sufficient for test compounds whose mechanisms involve photoreactive compounds whose action spectra can be estimated (Carter et al., 1995a). Since this is believed to be the case for MMB, they were used for all experiments for this project. The interior of the enclosure is covered with reflective aluminum panels in order to maximize the available light intensity and to attain sufficient light uniformity, which is estimated to be ±10% or better in the portion of the enclosure where the reactors are located (Carter, 2002). A diagram of the enclosure and reactors is shown in Figure 1, and spectra of the light sources are shown in Figure 2.

The dual reactors are constructed of flexible 2 mil Teflon® film, which is the same material used in the other UCR Teflon chambers used for mechanism evaluation (e.g., Carter et al., 1995b; Carter, 2000a, and references therein). A semi-flexible framework design was developed to minimize leakage and simplify the management of large volume reactors. The Teflon film is heat-sealed into separate sheets for the top, bottom, and sides (the latter sealed into a cylindrical shape) that are held together and in place using bottom frames attached to the floor and moveable top frames. The moveable top frame is held to the ceiling by cables that are controlled by motors that raise the top to allow the reactors to expand when filled or lower the top to allow the volume to contract when the reactors are being emptied or flushed. These motors in turn are controlled by pressure sensors that raise or lower the reactors as needed to maintain slight positive pressure. During experiments the top frames are slowly lowered to maintain continuous positive pressure as the reactor volumes decrease due to sampling or leaks. The experiment is terminated once the volume of one of the reactor reaches about 1/3 the maximum value, where the time this took varied depending on the amount of leaks in the reactor, but was greater than the duration of most

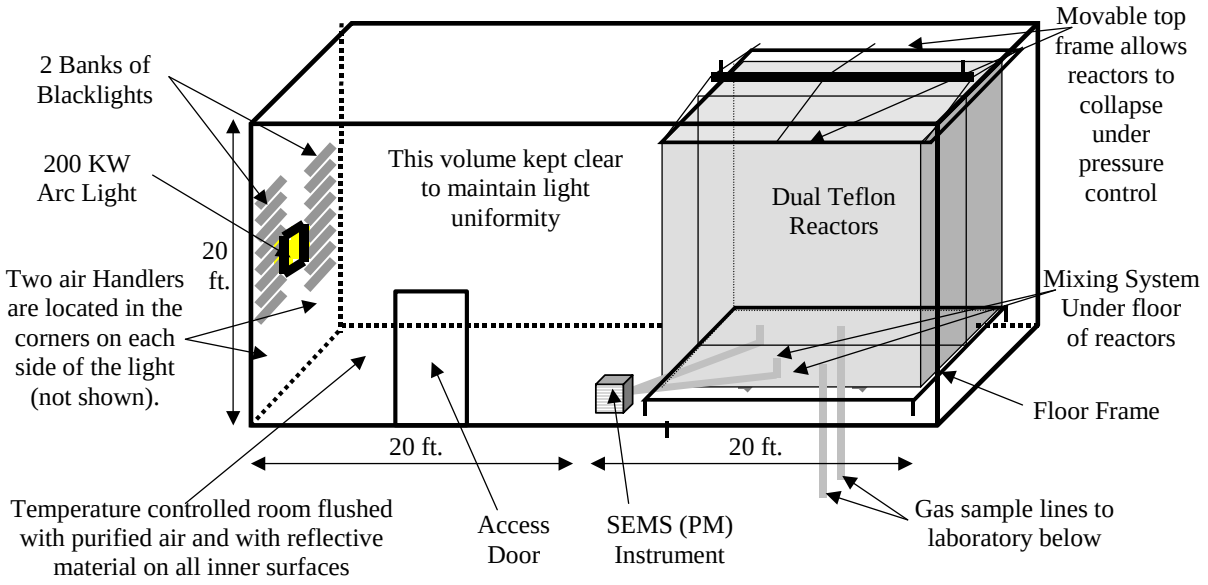

Figure 1. Schematic of the UCR EPA environmental chamber reactors and enclosure.

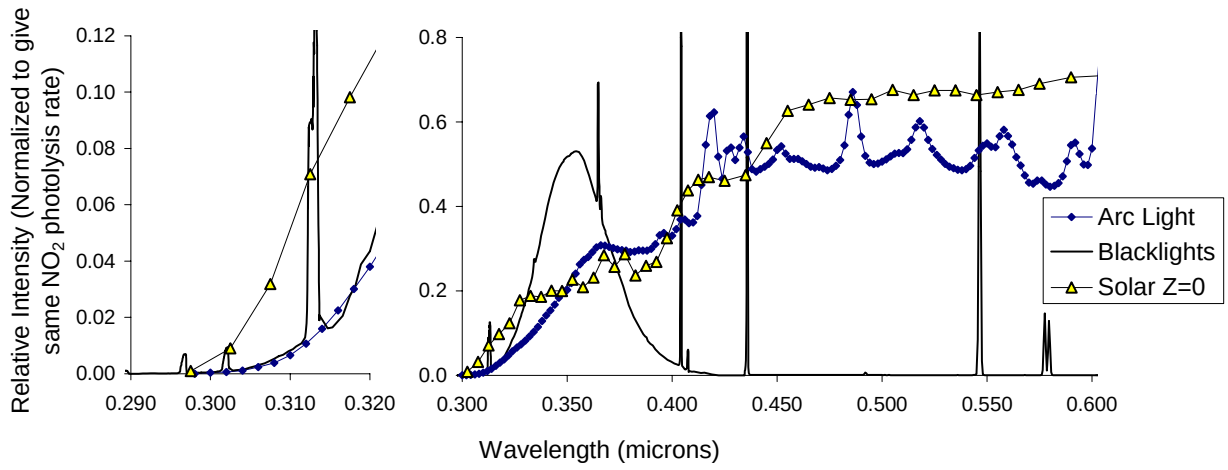

Figure 2. Spectrum of the light sources used in the UCR EPA chamber, with intensities normalized to give the same NO_2 photolysis rates. A representative solar spectrum is also shown.

of the experiments discussed in this report. Since at least some leaks are unavoidable in large Teflon film reactors, the constant positive pressure is important to minimize the introduction of enclosure air into the reactor that may otherwise result.

As indicated in Figure 1, the floor of the reactors has openings for a high volume mixing system for mixing reactants within a reactor and also for exchanging reactants between the reactors to achieve equal concentrations in each. This utilizes four 10" Teflon pipes with Teflon-coated blowers and flanges to either blow air from one side of a reactor to the other, or to move air between each of the two reactors. Teflon-coated air-driven metal valves are used to close off the openings to the mixing system when not in use, and during the irradiation experiments.

An AADCO air purification system that provides dry purified air at flow rates up to 1500 liters min^{-1} is used to supply the air to flush the enclosure and to flush and fill the reactors between experiments. The air is further purified by passing it through cartridges filled with Purafil® and heated Carulite 300® which is a Hopcalite® type catalyst and also through a filter to remove particulate matter. The measured NO_x, CO, and non-methane organic concentrations in the purified air were found to be less than the detection limits of the instrumentation employed (see Analytical Equipment, below).

The chamber enclosure is located on the second floor of a two-floor laboratory building that was designed and constructed specifically to house this facility (Carter et al., 2002). Most of the analytical instrumentation is located on the ground floor beneath the chamber, with sampling lines leading down as indicated in Figure 1.

Analytical Instrumentation

Table 1 gives a listing of the analytical and characterization instrumentation whose data were utilized for this project. Other instrumentation was available and used for some of these experiments, as discussed by Carter 2002a and Carter et al., 2005a, but the data obtained were not characterized for modeling and thus not used in the mechanism evaluations for this project. The table includes a brief description of the equipment, species monitored, and their approximate sensitivities, where applicable. These are discussed further in the following sections.

Ozone, CO, NO, and NO_y were monitored using commercially available instruments as indicated in Table 1. The instruments were spanned for NO, NO_2, and CO and zeroed prior to all experiments using the gas calibration system indicated in Table 1, and a prepared calibration gas cylinder with known amounts of NO and CO. O_3 and NO_2 spans were conducted by gas phase titration using the calibrator during this period. Span and zero corrections were made to the NO, NO_2, and CO data as appropriate based on the results of these span measurements, and the O_3 spans indicated that the UV absorption instrument was performing within its specifications.

Organic reactants were measured by gas chromatography with FID detection as described elsewhere (Carter et al., 1995b); see also Table 1. The surrogate gaseous compounds ethylene, propylene, n-butane and trans-2-butene were monitored by using 30 m megabore GS-Alumina column and the loop sampling system. The second signal of the same GC outfitted with FID, loop sampling system and 30 m megabore DB-5 column was used to analyze surrogate liquid components toluene, n-octane and m-xylene. The sampling methods employed for injecting the sample with the test compounds on the GC column depended on the volatility or "stickiness" of the compounds. For analyses of more volatile species such as MMB the same loop method was suitable.

Table 1. List of analytical and characterization instrumentation for the UCR EPA chamber.

Type	Model or Description	Species	Sensitivity	Comments
Ozone Analyzer	Dasibi Model 1003-AH. UV absorption analysis.	O_3	2 ppb	Standard monitoring instrument.
NO - NO_y Analyzer	Teco Model 42 C with external converter. Chemiluminescent analysis for NO, NOy by catalytic conversion.	NO NO_y	1 ppb 1 ppb	Useful for NO and initial NO_2 monitoring. Converter close-coupled to the reactors so the "NO_y" channel should include HNO_3 as well as NO_2, PANs, organic nitrates, and other species converted to NO by the catalyst.
CO Analyzer	Thermo Environmental Instruments Inc. Model 48 C	CO	50 ppb	Standard monitoring instrument
GC-FID Instruments	Dual Agilent 6890 Series II GC with dual columns, loop injectors and FID detectors. Controlled by computer interfaced to network.	VOCs	~10 ppbC	30 m x 0.53 mm GS-Alumina column used for the analysis of light hydrocarbons such as ethylene, propylene, n-butane and trans-2-butene and 30 m x 0.53 mm DB-5 column used for the analysis of C_{5+} alkanes and aromatics, such as toluene and m-xylene. Loop injection is suitable for low to medium volatility VOCs that are not too "sticky" to pass through valves. Two 30 m x 0.32 mm DB-5 column measure C_{5+} alkanes and aromatics, such as toluene and m-xylene. This was also used for the analysis of MMB.
LC-DAD-TOF analysis of carbonyls	Agilent 1200 series Liquid Chromatography - Diode Array Detector – Agilent 6210 Time-of-Flight Mass Spectrometer. Used for analysis of carbonyls derivatized with 2,4-dinitro-phehylhydrazine (DNPH)	carbonyl products	~3ppb	5 µm Deltabond AK Resolution (Thermo Scientific, 200mm x 4.6 mm ID) column was used. Diode array detector wavelength 360nm. Agilent 6210 Mass spectrometer operated in negative Atmospheric Pressure Chemical Ionization (-APCI) mode.
Gas Calibrator	Model 146C Thermo Environmental Dynamic Gas Calibrator	N/A	N/A	Used for calibration of NO_x and other analyzers. Instrument acquired early in project and under continuous use.
Data Acquisition Sytem	Windows PC with custom LabView software, 16 analog input, 40 I/O, 16 thermo-couple, and 8 RS-232 channels.	N/A	N/A	Used to collect data from most monitoring instruments and control sampling solenoids. In-house LabView software was developed using software developed by Sonoma Technology for ARB for the Central California Air Quality Study as the starting point.
Temperature sensors	Various thermocouples, radiation shielded thermocouple housing	Tempera-ture	~0.1 ^oC	Primary measurement is thermocouples inside reactor. However, comparison with temperature measurements in the sample line suggest that irradiative heating may bias these data high by ~2.5^oC (Carter, 2004).

Table 1 (continued)

Type	Model or Description	Species	Sensitivity	Comments
Humidity Monitor	General Eastern HYGRO-M1 Dew Point Monitor	Humid-ity	Dew point range: -40 - 50°C	Instrument performs as expected, but dew point below the performance range for most of the experiments discussed in this report, except for those with added humidity.
Spectro-radiometer	LiCor LI-1800 Spectroradiometer	300-850 nm Light Spect-rum	Adequate	Resolution relatively low but adequate for this project. Used to obtain relative spectrum. Also gives an absolute intensity measurement on surface useful for assessing relative trends.
QSL Spherical Irradiance Sensor	Biospherical QSL-2100 PAR Irradiance Sensor. Responds to 400-700 nm light.	Spherical Broad-band Light Intensity	Adequate	Provides a measure of absolute intensity and light uniformity that is more directly related to photolysis rates than light intensity on surface. Gives more precise measurement of light intensity trends than NO_2 actinometry, but is relatively sensitive to small changes in position.
Scanning Mobility Particle Sizer (SMPS)	TSI 3080L column, TSI 3077 ^{85}Kr neutralizer, and TSI 3771 CPC. Instrument design, control, and operation Similar to that described in Cocker et al. (2001)	Aerosol number and size distribut-ions	Adequate	Provides information on size distribution of aerosols in the 28-735 nm size range, which accounts for most of the aerosol mass formed in our experiments. Data can be used to assess effects of VOCs on secondary PM formation.

Both the GC instruments were controlled and their data were analyzed using Agilent ChemStation software installed on a dedicated PC. The GC's were spanned using the prepared calibration cylinder with known amounts of ethylene, propane, propylene, n-butane, n-hexane, toluene, n-octane and m-xylene in ultrapure nitrogen. Analyses of the span mixture were conducted approximately every day an experiment was run, and the results were tracked for consistency.

The surrogate components analyzed by the above system were calibrated by repeated analysis of a standard mixture containing these compounds, and verified by injecting and sampling known amounts of the compound in calibration chamber of known volume. The amounts of gaseous compounds injected were determined by vacuum methods, using an MKS Baratron precision pressure gauge, and bulbs of known volume, determined by weighing when filled with water. The amounts of liquid compounds injected were determined by measuring amounts injected using microliter syringes. The volumes of the calibration chambers were determined by injecting and analyzing compounds whose analyses have been calibrated previously.

The GC analysis of MMB was calibrated by injecting a quantitative amount of the compound in the chamber reactors. The chamber reactors have a known volume and therefore contain a known concentration of the injected compound. The calibration factor was then determined as a result of the GC analyses conducted prior to the start of the irradiations.

As indicated in Table 1, aerosol number and size distributions were also measured in conjunction with our experiments. The instrumentation employed is similar to that described by Cocker et al. (2001),

and is the same as employed in our previous studies of coatings VOCs (Carter and Malkina, 2005). Particle size distributions are obtained using a scanning mobility particle sizer (SMPS) equipped with a 3077 ^{85}Kr charger, a 3081L cylindrical long column, and a 3771 condensation particle counter (CPC). Flow rates of 2.5 LPM and 0.25 LPM for sheath and aerosol flow, respectively, are maintained using Labview 6.0-assisted PID control of MKS proportional solenoid control valves. Both the sheath and aerosol flow are obtained from the reactor enclosure. The data inversion algorithm described by Collins et al. (2002) converts CPC counts versus time to particle size distribution.

Most of the instruments other than the GCs and aerosol instrument were interfaced to a PC-based computer data acquisition system under the control of a LabView program written for this purpose. These data, and the GC data from the Agilent ChemStation computer, were collected over the CE-CERT computer network and merged into Excel files that are used for applying span, zero, and other corrections, and preparation of the data for modeling.

Data on gas-phase carbonyl compounds was also obtained using an Agilent 1200 Liquid Chromatography – Diode Array Detector – Time-of-Flight (LC-DAD-TOF) Mass Spectrometer as described in Table 1. Acetonitrile and water were used as eluents. The total flow rate of eluents was kept at 1ml/min and acetonitrile concentration was programmed to be 40-70% (0-35 min) and 70% (35-40 min). UV absorption (wavelength: 360 nm) was monitored by Agilent 1200 series Diode Array Detector, followed by accurate mass measurement by Agilent 6210 Time-of-Flight. Ionization was done by atmospheric pressure chemical ionization (APCI) method in negative ion mode. Mass accuracy was routinely calibrated with tuning mix (Agilent Technology, G1969-85020) to be within 5 ppm error. This mass measurement enables determination of the molecular weights of unknown carbonyl products.

Sampling methods

Samples for analysis by the continuous monitoring instruments were withdrawn alternately from the two reactors and zero air, under the control of solenoid valves that were in turn controlled by the data acquisition system discussed above. For most experiments the sampling cycle was 5 minutes for each reactor, the zero air, or (for control purposes) the chamber enclosure. The program controlling the sampling sent data to the data acquisition program to indicate which state was being sampled, so the data could be appropriately apportioned when being processed. Data taken less than 3-4 minutes after the sample switched were not used for subsequent data processing. The sampling system employed is described in more detail by Carter (2002).

Samples for GC analysis of surrogate compounds were taken at approximately every 20-minute directly from each of the reactors through the separate sample lines attached to the bottom of the reactors. The GC sample loops were flushed for a desired time with the air from the reactor being sampled.

The sample air containing carbonyls was passed through cartridges coated with 2,4-dinitrophenylhydrazine (DNPH) (Sep-Pak® DNPH-Silica Cartridge, Waters, Part No. WAT037500) at flow rates ~1L/min and carbonyls are derivatized to be hydrazones in situ. The cartridges were eluted with 5 mL HPLC-grade acetronitrile and 10 µL of each extract was injected to LC-DAD-TOF.

Characterization Methods

Use of chamber data for mechanism evaluation requires that the conditions of the experiments be adequately characterized. This includes measurements of temperature, humidity, light and wall effects characterization. Wall effects characterization is discussed in detail by Carter (2004) and updated by Carter and Malkina (2005) and Carter (2007) and most of that discussion is applicable to the experiments

for this project. The instrumentation used for the other characterization measurements is summarized in Table 1, above, and these measurements are discussed further below.

Temperature was monitored during chamber experiments using calibrated thermocouples attached to thermocouple boards on our computer data acquisition system. The temperature in each of the reactors was continuously measured using relatively fine gauge thermocouples that were located ~1 foot above the floor of the reactors. These thermocouples were not shielded from the light, though it was hoped that irradiative heating would be minimized because of their small size. Experiments where the thermocouple for one of the reactors was relocated to inside the sample line indicated that radiative heating is probably non-negligible, and that a correction needs to be made for this by subtracting ~2.5^{o}C from the readings of the thermocouples in the reactors. This is discussed by Carter (2004).

Light Spectrum and Intensity. The spectrum of the light source in the 300-850 nm region was previously measured using a LiCor LI-1800 spectroradiometer, which is periodically calibrated at the factory. Spectroradiometer readings were taken periodically, though the relative spectra were found to have very little variation during the course of these experiments. The absolute light intensity is measured by carrying out NO_2 actinometry experiments periodically using the quartz tube method of Zafonte et al. (1977) modified as discussed by Carter et al. (1995b). In most cases the quartz tube was located in front of the reactors. Since this location is closer to the light than the centers of the reactors, the measurement at this location is expected to be biased high, so the primary utility of these data are to assess potential variation of intensity over time. However, several special actinometry experiments were conducted prior to the experiments carried out for this project where the quartz tube was located inside the reactors, to provide a direct measurement of the NO_2 photolysis rates inside the reactors. The photolysis rates used when modeling these experiments were the same as used by Carter (2009b,c) when modeling the recently completed experiments for several halopropenes.

Experimental Procedures

The reaction bags were collapsed to the minimum volume by lowering the top frames, then cleaned by emptying and refilling them at least six times after each experiment, and then filled with dry purified air on the nights before experiments. Span measurements were generally made on the continuous instruments prior to injecting the reactants for the experiments. The reactants were then injected through Teflon injection lines (that are separate from the sampling lines) leading from the laboratory below to the reactors. The common reactants were injected in both reactors simultaneously, and were mixed by using the reactor-to-reactor exchange blowers and pipes for 10 minutes. The valves to the exchange system were then closed and the other reactants were injected to their respective sides and mixed using the in-reactor mixing blowers and pipes for 1 minute. The contents of the chamber were then monitored for at least 30 minutes prior to irradiation, and samples were taken from each reactor for GC analysis.

Once the initial reactants are injected, stabilized, and sampled, the light or lights employed (blacklights in the case of this project) are turned on to begin the irradiation. During the irradiation the contents of the reactors are kept at a constant positive pressure by lowering the top frames as needed, under positive pressure control. The reactor volumes therefore decrease during the course of the experiments, in part due to sample withdrawal and in part due to small leaks in the reactor. A typical irradiation experiment ended after about 6 hours, by which time the reactors are typically down to about half their fully filled volume. Larger leaks are manifested by more rapid decline of reactor volumes, and the run is aborted early if the volume declines to about 1/3 the maximum. This was the case for a few of the experiments discussed in this report. After the irradiation the reactors were emptied and filled six times as indicated above.

The procedures for injecting the various types of reactants were as follows. The NO, and NO_2 were prepared for injection using a vacuum rack. Known pressures of NO, measured with MKS Baratron capacitance manometers, were expanded into Pyrex bulbs with known volumes, which were then filled with nitrogen (for NO) or purified air (for NO_2). In order to maintain constant NO/NO_2 ratios the same two bulbs of specified volume were utilized in most of experiments. The contents of the bulbs were then flushed into the reactor(s) with nitrogen. For experiments with added CO, the CO was purified by passing it through an in-line activated charcoal trap and flushing it into the reactor at a known rate for the amount of time required to obtain the desired concentration. Measured volumes of volatile liquid reactants were injected, using a micro syringe, into a 2 ft long Pyrex injection tube surrounded with heat tape and equipped with one port for the injection of the liquid and other ports to attach bulbs with gas reactants. For injections into both reactors (e.g, the NO_x and base ROG surrogate components in incremental reactivity experiments), one end of the injection tube was attached to the "Y"-shape glass tube (equipped with stopcocks) that was connected to reactors and the other end of injection tube was connected to a nitrogen source. The injections into a single reactor (e.g., for MMB in the reactivity experiments) was similar except the "Y" tube was not used.

The procedures for injection of the hydrocarbon surrogate components were as follows. A cylinder containing n-butane, trans-2-butene, propylene and ethylene in nitrogen, was used for injecting the gaseous components of the surrogate. The cylinder was attached to the injection system and a gas stream was introduced into reactors at controlled flow for certain time to obtain desired concentrations. A prepared liquid mixture with the appropriate ratios of toluene, n-octane and m-xylene was utilized for injection of these surrogate components, using the procedures as discussed above for pure liquid reactants. All the gas and liquid reactants intended to be the same in both reactors were injected at the same time. The injection consisted of opening the stopcocks and flushing the contents of the bulbs and the liquid reactants with nitrogen, with the liquid reactants being heated slightly using heat that surrounded the injection tube. The flushing continued for approximately 10 minutes.

MMB was introduced to the chamber prior to an experiment using the following procedure: A specific volume of MMB was injected into a three neck, distillation round bottom flask. The flask was located in an oven set to 70C. The flask was continuously purged with clean air into the injection lines to the chamber. The flask was continuously purged at a flow rate of 900cc/min over a duration of approximately 90min until all the visible liquid was evaporated away and the concentration was reproducible as detected by the GC-FID.

Materials

The sources of the NO, CO and the various base case surrogate compounds came from various commercial vendors as employed in previous projects at our laboratory. The sample of MMB used for the chamber experiments was provided by Kuraray. No significant impurities were detected in any of the GC analyses of these samples.

KINETIC AND MECHANISTIC RESULTS

Kinetics of OH + 3-Methoxy-3-methyl-1-butanol

The rate constant for the reactions of 3-methoxy-3-methyl-1-butanol was determined using a relative rate method as discussed above in the Experimental Methods section, using di-n-butyl ether as the reference compound. It is expected that both MMB and di-*n*-butyl ether are consumed primarily by reactions with OH radicals under atmospheric conditions and also under the conditions of the kinetic experiments, i.e.,

$$\text{OH + 3-methoxy-3-methyl-1-butanol} \rightarrow \text{products} \quad (1)$$

$$\text{OH + di } n\text{-butyl ether} \rightarrow \text{products} \quad (2)$$

If these are the only significant reactions and there is no dilution or other loss processes, then,

$$\ln\left(\frac{[\text{MMB}]_{t0}}{[\text{MMB}]_t}\right) = \frac{k_1}{k_2} \ln\left(\frac{[\text{Ether}]_{t0}}{[\text{Ether}]_t}\right) \quad (\text{I})$$

where [MMB]to and [Ether]to are the concentrations of 3-methoxy-3-methyl-1-butanol and the di-*n*-butyl ether, respectively, at time t0, [MMB]t and [Ether]t are the corresponding concentrations at time t, and k_1 and k_2 are the rate constants for reactions (1) and (2), respectively. A plot of ln([MMB]to/[MMB]t) against ln([Ether]to/[Ether]t) should then be a straight line of slope k_1/k_2 and zero intercept.

The experimental data are plotted in accordance with Equation (I) in Figure 3, and a least-squares analysis leads to the rate constant ratio $k_1/k_2 = 0.582 \pm 0.020$, where the indicated error is the two least-squares standard deviation. This rate constant ratio k_1/k_2 can be placed on an absolute basis using a rate constant for the reaction of OH radicals with di-*n*-butyl ether of $k_2 = 2.81 \times 10^{-11}$ cm^3 molecule^{-1} s^{-1} at 296 K (Mellouki et al., 1995), resulting in

$$k_1 = (1.64 \pm 0.06) \times 10^{-11} \text{ cm}^3 \text{ molecule}^{-1} \text{ s}^{-1} \text{ at } 296 \pm 2 \text{ K},$$

where the indicated error is two least-squares standard deviations and does not include the uncertainty in the rate constant k_2.

Products of OH + 3-Methoxy-3-methyl-1-butanol

Acetone and methyl acetate were identified as products of the OH + 3-methyloxy-3-methyl-1-butanol by matching of retention times of authentic standards introduced into the chamber with GC peaks in irradiated CH_3ONO - NO - 3-methoxy-3-methyl-1-butanol - air mixtures. While acetone and methyl acetate react with OH radicals, their rate constants for these reactions are lower than that for OH + 3-methoxy-3-methyl-1-butanol by a factor of ~50-100, and hence corrections for secondary reactions of acetone and methyl acetate were negligible (<1%). Plots of the amounts of acetone and methyl acetate formed against the amounts of 3-methoxy-3-methyl-1-butanol are shown in Figure 4, and least-squares analyses lead to acetone and methyl acetate formation yields of 3 ± 1% and 34 ± 8%, respectively, where the indicated errors are the two least-squares standard deviations combined with estimated uncertainties in the GC-FID response factors of ±5% each for 3-methoxy-3-methyl-1-butanol, acetone and methyl acetate.

GC-MS analyses of the coated SPME fibers exposed to the chamber contents after reaction showed (Figure 3) the presence of three products, each with two mono-oximes (*syn* and *anti*). In addition, the di-oximes of glyoxal, $(CHO)_2$, were present, eluting at longer retention times than shown in Figure 3. One of these product mono-carbonyls (carbonyl #1) had a molecular weight of 60, as evident from the

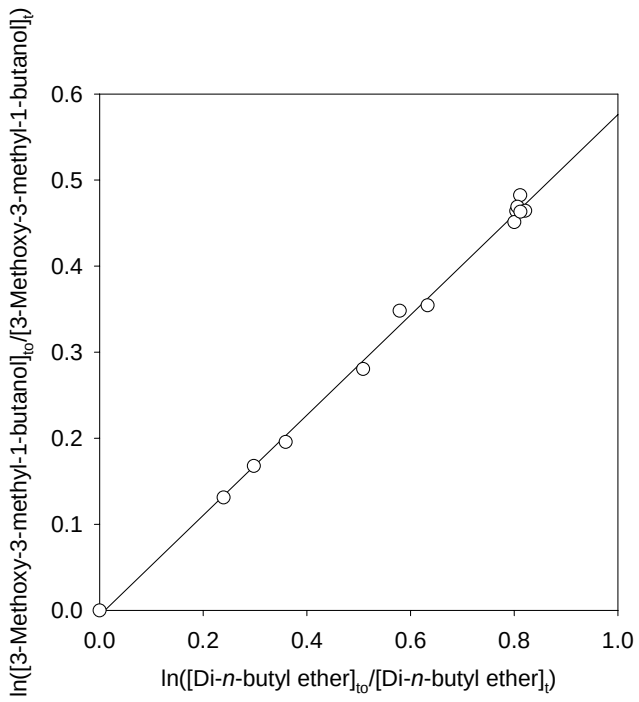

Figure 3. Plot of Equation (I) for the gas-phase reaction of OH radicals with 3-methoxy-3-methyl-1-butanol at 296 ± 2 K, with di-*n*-butyl ether as the reference compound. Data are from three experiments.

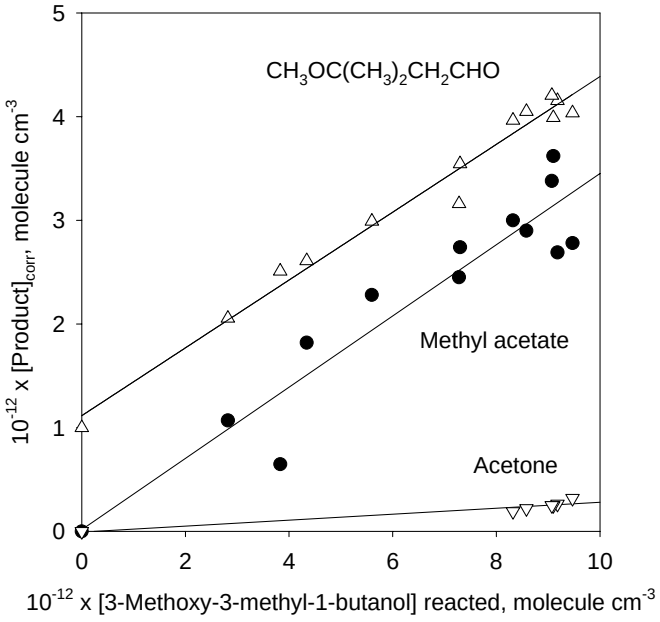

Figure 4. Plots of the amounts of product observed against the amounts of 3-methoxy-3-methyl-1-butanol reacted with OH radicals. The data for $CH_3OC(CH_3)_2CH_2CHO$ have been corrected for secondary reaction with OH radicals (see text) and have been displaced vertically by 1.0 x 10^{12} molecule cm^{-3} for clarity.

presence of two oxime peaks (1a and 1b in Figure 3) with identical mass spectra with ion peaks at 256 u $[M+H]^+$ and 296 u $[M+41]^+$, and with a strong fragment ion at 238 u $[M+H-H_2O]^+$ (Figure 4) This carbonyl product is attributed to glycolaldehyde, $HOCH_2CHO$. The second mono-carbonyl (carbonyl #2) had two oxime peaks (2a and 2b in Figure 5) with identical mass spectra with ion peaks at 298 u $[M+H]^+$ and 338 u $[M+41]^+$, and with an intense fragment ion at 280 u $[M+H-H_2O]^+$ and much less intense fragment ions at 320 u $[M+41-H_2O]^+$ and 100 u $[M+H-198]^+$ (Figure 5). These peaks are either (a) oximes of a molecular weight 102 hydroxycarbonyl or (b) oximes of two co-eluting carbonyl-containing products of molecular weight 84 (perhaps $C_4H_4O_2$) and 102. The third mono-carbonyl (carbonyl #3) had two oxime peaks (3a and 3b in Figure 5) with similar mass spectra, with an intense ion peak at 280 u and a much less intense fragment ion at 114 u $[M+H-198]^+$ (Figure 6c and Figure 6d). These are probably from the oximes of a carbonyl-containing product of molecular weigh 116 that also contains a methoxy group (since the dominant ion would then be a loss of 32 = CH_3OH as we observed in separate analyses of 4,4-dimethoxy-2-butanone). This would be consistent with formation of $CH_3OC(CH_3)_2CH_2CHO$.

In order to obtain more information concerning the carbonyl products indicated by the GC-MS analyses of the coated SPME fibers, we also conducted GC-MS analyses of samples collected onto Tenax cartridges from an OH + 3-methoxy-3-methyl-1-butanol reaction. These were analyzed by GC-FID on a DB-1701 column (as used previously) and on a DB-5 column, and by GC-MS on a DB-5 column. The peaks on the GC-MS total ion chromatogram can be readily correlated with those from the GC-FID analysis on the DB-5 column. GC-MS analysis showed the presence of an early-eluting molecular weight 74 compound that we attribute to methyl acetate. The major GC-FID product peak is consistent with a molecular weight 116 compound, and this is the GC-FID peak we can quantify by estimating its GC-FID response and OH reaction rate constant as discussed below. This peak is attributed to $CH_3OC(CH_3)_2CH_2$ CHO.

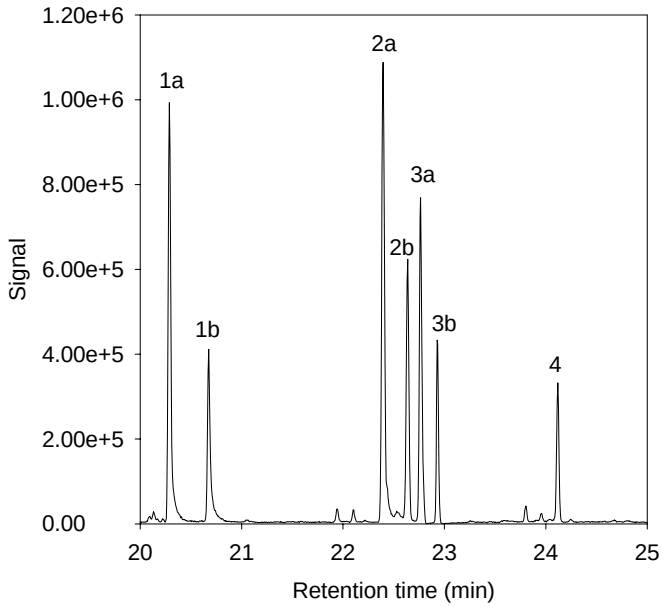

Figure 5. Total ion chromatogram of a GC-MS analysis (DB-5 column) of a coated-SPME fiber exposed to the chamber contents after reaction. The portion of the chromatogram containing mon-oximes is shown. Peak #4 is from the derivatizing agent. See Figure 6 for mass spectra of selected peaks.

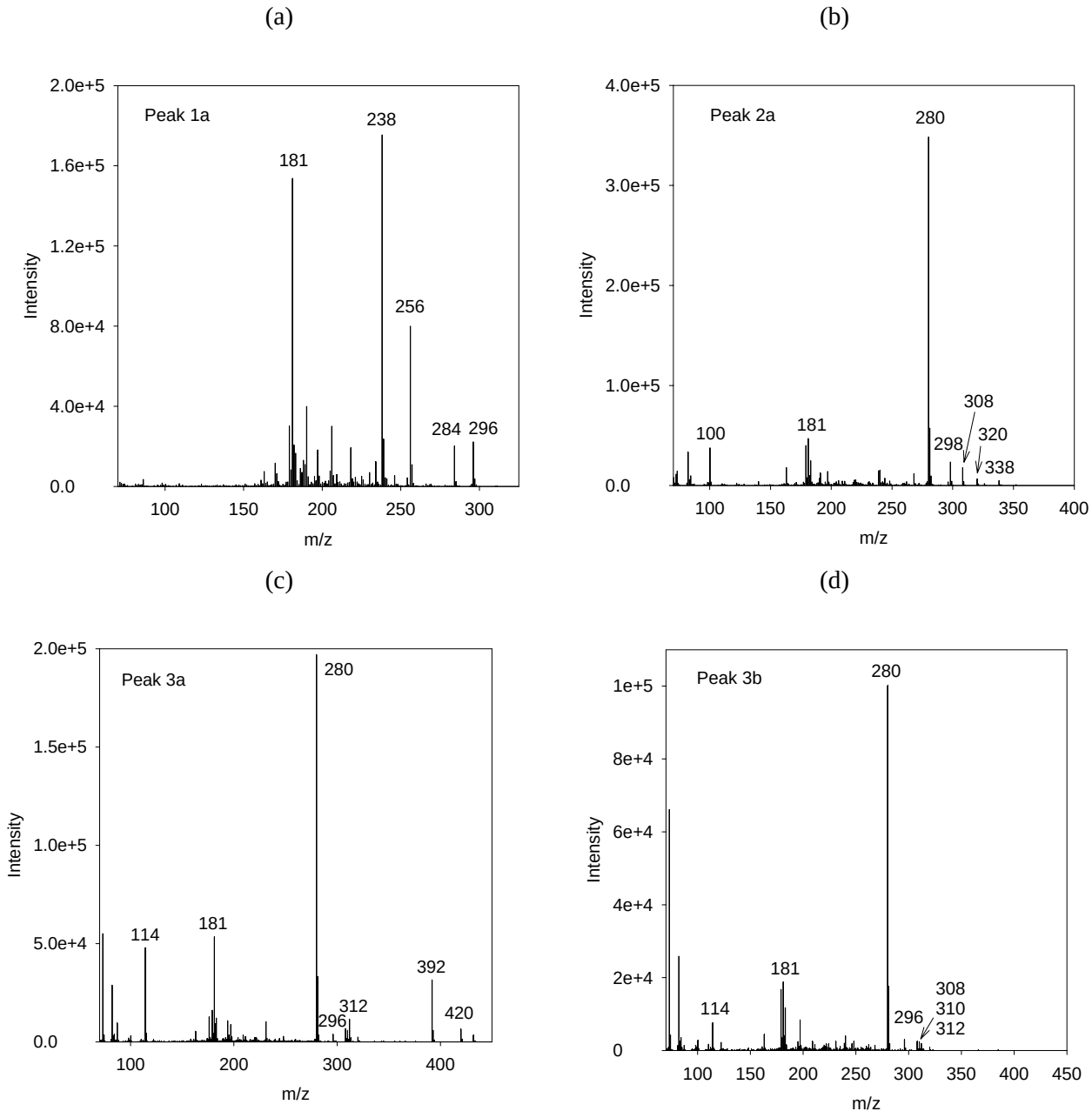

Figure 6. Mass spectra of peaks #1a, 2a, 3a, and 3 in Figure 5. (Peaks 1b and 2b had an essentially identical mass spectra as peaks 1a and 2a, respectively). M/z = 181 is a fragment associated with the derivatizing agent portion of the oxime. For interpretation see text.

Data taken during the LC-DAD-TOF analyses of the DNPH sampling for carbonyls carried out in conjunction with the environmental chamber experiments with added MMB also indicated that the major carbonyl product of this reaction had a molecular weight of 116. This is also consistent with this product being $CH_3OC(CH_3)_2CH_2CHO$.

Using the Effective Carbon Number concept (Scanlon and Willis, 1985), the FID response factor of $CH_3OC(CH_3)_2CH_2CHO$ is estimated to be 4.0/4.5 = 0.89 of that for 3-methoxy-3-methyl-1-butanol. This carbonyl can be assumed to have a rate constant for reaction with OH radicals of $\sim 2.4 \times 10^{-11}$ cm^3 $molecule^{-1}$ s^{-1} at room temperature. The GC-FID analysis of the reacted OH + 3-methoxy-3-methyl-1-butanol mixtures showed the presence of one significant GC product peak eluting ~1.5 min earlier than 3-methoxy-3-methyl-1-butanol. If this GC peak is $CH_3OC(CH_3)_2CH_2CHO$, then after correction for reaction with OH radicals (Figure 2) the data result in a formation yield of ~33%.

MECHANISM AND MODELING METHODS

Base Mechanism

The starting point for the chemical mechanism evaluated in this work is the SAPRC-07 mechanism as documented by Carter (2009a). This is a complete update of the SAPRC-99 mechanism of Carter (2000a), but it is very similar to it in its major features. The reactions and rate constants in this mechanism are given in tables in Appendix A to this report, and complete documentation of this mechanism is given by Carter (2009a). Files and software implementing this chemical mechanism are available at the SAPRC mechanism web site[1], with the chemical mechanism simulation computer programs available there being essentially the same as those employed in this work.

As discussed previously (Carter, 2000a,b, 2009a), the current SAPRC mechanisms consists of a "base mechanism" that represents the reactions of the inorganic species and common organic products and lumped organic radical model species and "operators", and separate mechanisms for the initial reactions of the many types other organic compounds that are not in the base mechanism. The compounds, or groups of compounds, that are not included in the base mechanism but for which mechanism assignments have been made, are referred to as detailed model species. The latter include all the base ROG surrogate constituents and compounds whose reactivities are being assessed (3-methoxy-3-methyl-1-butanol, or MMB, in this case). These compounds can either be represented explicitly, with separate model species with individual reactions or sets of reactions for each, or using lumped model species similar to those employed in the "fixed parameter" version of SAPRC (Carter, 2000b, 2009a). The latter approach is used when modeling complex mixtures in ambient simulations or simulations of experiments with complex mixtures, but the other approach, representing each compound explicitly, is more appropriate when evaluating mechanisms for individual compounds or simple mixtures. This is because the purpose of mechanism evaluations against chamber data is to assess the performance of the mechanism itself, not to assess the performance lumping approaches. The latter is most appropriately assessed by comparing simulations of explicit and condensed versions of the same mechanism in ambient simulations.

In this work, all of the organic constituents in the environmental chamber experiments were represented explicitly using separate model species for each compound, while complex mixture of emitted species in the atmospheric reactivity simulations were represented using the appropriate lumped model species for the fixed parameter mechanism, as indicted in Table A-1 in Appendix A. The reactions and rate constants in the base mechanism are given in Table A-2, and the photolysis rates used are given in Table A-3. These photolysis rates were calculated from applicable actinic flux or light source characterization data and absorption cross-sections and quantum yields given by Carter (2009a).

The version of the SAPRC-07 mechanism used in this work is the same as that employed in our recent studies of other VOCs (e.g., Carter, 2009b,c), but incorporated several corrections relative to the version used previously These corrections are discussed in Appendix E of Carter (2009a), and primarily concern hydroperoxide and peroxy + peroxy reactions that are not important in affecting ozone formation and have no significant effect on calculations of ozone impacts of VOCs.

[1] Reports and files concerning the latest version of the SAPRC chemical mechanisms and their associated reactivity scales are available at http://www.cert.ucr.edu/ ~carter/SAPRC.

Mechanism for 3-Methoxy-3-Methyl-1-Butanol

Like other glycols and ethers, 3-methoxy-3-methyl-1-butanol is expected to be consumed in the atmosphere primarily by reaction with OH radicals. The initial reaction is expected to be abstraction of one of the 5 types of hydrogen atoms forming H_2O and the corresponding alkyl radical. Based on structure-reactivity estimates primarily developed by Kwok and Atkinson (1995) for abstractions from these 5 positions in the molecule, the SAPRC-07 mechanism estimation system derives rate constants for reaction at each of these 5 positions in the molecule, as shown on Table 2. Based on these estimated partial rate constants, a total rate constant for this OH + MMB reaction of 7.1 x 10^{-12} cm^3 $molec^{-1}$ s^{-1} is derived, and this was used in the existing mechanism for this compound used by Carter (2009a) to estimate its atmospheric ozone impact.

However, as discussed above the OH + MMB rate constant measured in this work was 1.64 x 10^{-11} cm^3 $molec^{-1}$ s^{-1} which is more than a factor of 2 higher than the estimated value used previously. The reason for this discrepancy is unknown. Generally the estimation methods for such OH abstraction reactions from alcohols and ethers perform better than this (Kwok and Atkinson, 1995; Carter, 2000a), so a discrepancy of this magnitude is unexpected. In order for the estimated mechanism to predict the observed methyl acetate yield of 34%, it is necessary to assume that Reaction (3), forming the $CH_3OC(CH_3)(CH_3)CH(\cdot)CH_2OH$ radical that is predicted to be the precursor to methyl acetate (see Table 3, discussed below), occurs approximately 46% of the time. This gives a partial rate constant for reaction (3) that is approximately a factor of 5 higher than the value estimated using the method of Kwok and Atkinson (1995). This is still not sufficient to account for the discrepancy in the total rate constant, and in order to account for this we assume that Reaction (2) occurs almost a factor of 2 higher than estimated. Reactions at the methyl group (Reactions 1, 4 or 5) are expected to be relatively less important and it is unlikely that discrepancies in estimation of their partial rate constants would be enough to account for the discrepancy for the total rate constant.

The subsequent reactions for the estimated for the radicals formed in the presence of O_3 in air, and estimated fractions for reactions at various alternative competing pathways, are summarized in Table 3. If the alkyl radical has an OH substituent next to it then it will react with O_2 to form HO_2 and a

Table 2. Estimated rate constants for OH radical abstractions from various positions in the 3-methoxy-3-methyl-1-butanol molecule.

Rxn. No.	Hydrogen Abstracted	Rate constant (x 10^{-12} cm^3 $molec^{-1}$ s^{-1})		
		Est'd [a]	Used [b]	Ratio [c]
1	$CH_3OC(CH_3)(CH_3)CH_2CH_2O–H$	0.18	0.18	1
2	$CH_3OC(CH_3)(CH_3)CH_2CH(–H)OH$	4.01	7.62	1.9
3	$CH_3OC(CH_3)(CH_3)CH(–H)CH_2OH$	1.42	7.12	5.0
4	$CH_3OC(CH_3)(CH_2–H)CH_2CH_2OH$	0.34	0.34	1
5	$H–CH_2OC(CH_3)(CH_3)CH_2CH_2OH$	1.15	1.15	1
	Total k(OH + MMB)	7.10	16.40	2.3

[a] Estimated using the structure-reactivity methods of Kwok and Atkinson (1995) as used in the SAPRC-99/07 mechanism generation system.

[b] As used in this work. See text and footnotes 1-3 on Table 3.

[c] Ratio of rate constant used for this pathway relative to the estimated value.

Table 3. Mechanism used for the atmospheric reactions of 3-methoxy-3-methyl-1-butanol.

Reaction	Fract. Reacting Rxn.	Total	Notes
$CH_3OC(CH_3)(CH_3)CH_2CH_2OH$ + OH (Total k = 1.64 x 10^{-11} cm^3 $molec^{-1}$ s^{-1})	*Est'd	Used	
$\rightarrow H_2O + CH_3OC(CH_3)(CH_3)CH_2CH_2O\cdot$	2.5%*	1.1%	1
$\rightarrow H_2O + CH_3OC(CH_3)(CH_3)CH_2CH(\cdot)OH$	56.5%*	46.4%	2
$\rightarrow H_2O + CH_3OC(CH_3)(CH_3)CH(\cdot)CH_2OH$	20.0%*	43.4%	3
$\rightarrow H_2O + CH_3OC(CH_3)(CH_2\cdot)CH_2CH_2OH$	4.8%*	2.1%	1
$\rightarrow H_2O + CH_3C(CH_3)(CH_2CH_2OH)OCH_2\cdot$	16.2%*	7.0%	1
$CH_3OC(CH_3)(CH_3)CH_2CH_2O\cdot$			
$+ O_2 \rightarrow CH_3OC(CH_3)(CH_3)CH_2CHO + HO_2\cdot$	10.0%	0.1%	4
$\rightarrow CH_3OC(CH_3)(CH_2\cdot)CH_2CH_2OH$	90.0%	1.0%	
$CH_3OC(CH_3)(CH_2\cdot)CH_2CH_2OH + O_2 \rightarrow CH_3OC(CH_3)(CH_2OO\cdot)CH_2CH_2OH$		1.0%	5
$CH_3OC(CH_3)(CH_2OO\cdot)CH_2CH_2OH$			6,7
$+ NO \rightarrow CH_3OC(CH_3)(CH_2ONO_2)CH_2CH_2OH$	9.8%	0.1%	
$+ NO \rightarrow NO_2 + CH_3OC(CH_3)(CH_2O\cdot)CH_2CH_2OH$	90.2%	0.9%	
$CH_3OC(CH_3)(CH_2O\cdot)CH_2CH_2OH$			4
$\rightarrow HCHO + CH_3OC(\cdot)(CH_3)CH_2CH_2OH$	50.2%	0.4%	
$\rightarrow CH_3OC(CH_3)(CH_2OH)CH_2CH(\cdot)OH$	49.8%	0.4%	
$CH_3OC(\cdot)(CH_3)CH_2CH_2OH + O_2 \rightarrow CH_3OC(OO\cdot)(CH_3)CH_2CH_2OH$		0.4%	5
$CH_3OC(OO\cdot)(CH_3)CH_2CH_2OH$			6
$+ NO \rightarrow CH_3OC(CH_3)(ONO_2)CH_2CH_2OH$	6.5%	0.0%	
$+ NO \rightarrow NO_2 + CH_3OC(O\cdot)(CH_3)CH_2CH_2OH$	93.5%	0.4%	
$CH_3OC(O\cdot)(CH_3)CH_2CH_2OH \rightarrow CH_3C(O)OCH_3 + .CH_2CH_2OH$		0.4%	4,5
$.CH_2CH_2OH + O_2 \rightarrow .OOCH_2CH_2OH$		0.4%	5
$.OOCH_2CH_2OH + NO \rightarrow NO_2 + .OCH_2CH_2OH$		0.4%	
$.OCH_2CH_2OH$			8
$+ O_2 \rightarrow HCOCH_2OH + HO_2\cdot$	19.5%	0.1%	
$\rightarrow HCHO + .CH_2OH$	80.5%	0.3%	
$.CH_2OH + O_2 \rightarrow HCHO + HO_2\cdot$		0.3%	5
$CH_3OC(CH_3)(CH_2OH)CH_2CH(\cdot)OH + O_2 \rightarrow CH_3OC(CH_3)(CH_2CHO)CH_2OH + HO_2\cdot$		0.4%	5
$CH_3OC(CH_3)(CH_3)CH_2CH(\cdot)OH + O_2 \rightarrow CH_3OC(CH_3)(CH_3)CH_2CHO + HO_2\cdot$		46.4%	5
$CH_3OC(CH_3)(CH_3)CH(\cdot)CH_2OH + O_2 \rightarrow CH_3OC(CH_3)(CH_3)CH(OO\cdot)CH_2OH$		43.4%	5
$CH_3OC(CH_3)(CH_3)CH(OO\cdot)CH_2OH$			6,7
$+ NO \rightarrow CH_3OC(CH_3)(CH_3)CH(ONO_2)CH_2OH$	9.8%	4.3%	
$+ NO \rightarrow NO_2 + CH_3OC(CH_3)(CH_3)CH(O\cdot)CH_2OH$	90.2%	39.1%	
$CH_3OC(CH_3)(CH_3)CH(O\cdot)CH_2OH$			4
$\rightarrow HCOCH_2OH + CH_3OC(\cdot)(CH_3)CH_3$	99.5%	39.1%	5
$\rightarrow CH_3OC(CH_3)(CH_3)CHO + .CH_2OH$	0.5%	~0%	9
$CH_3OC(\cdot)(CH_3)CH_3 + O_2 \rightarrow CH_3OC(OO\cdot)(CH_3)CH_3$		39.1%	5
$CH_3OC(OO\cdot)(CH_3)CH_3$			6
$+ NO \rightarrow CH_3OC(CH_3)(CH_3)ONO_2$	3.9%	1.5%	
$+ NO \rightarrow NO_2 + CH_3OC(O\cdot)(CH_3)CH_3$	96.1%	37.6%	

Table 3 (continued)

Reaction	Fract. Reacting Rxn.	Total	Notes
$CH_3OC(O\cdot)(CH_3)CH_3$			10
$\rightarrow CH_3C(O)CH_3 + CH_3O\cdot$	13.0%	4.9%	
$\rightarrow CH_3C(O)OCH_3 + CH_3\cdot$	87.0%	32.7%	
$CH_3O\cdot + O_2 \rightarrow HCHO + HO_2\cdot$		4.9%	5
$CH_3\cdot + O_2 \rightarrow CH_3OO\cdot$		32.7%	5
$CH_3OC(CH_3)(CH_2\cdot)CH_2CH_2OH + O_2 \rightarrow CH_3OC(CH_3)(CH_2OO\cdot)CH_2CH_2OH$		2.1%	5
$CH_3OC(CH_3)(CH_2OO\cdot)CH_2CH_2OH$			6,7
$+ NO \rightarrow CH_3OC(CH_3)(CH_2ONO_2)CH_2CH_2OH$	9.8%	0.2%	
$+ NO \rightarrow NO_2 + CH_3OC(CH_3)(CH_2O\cdot)CH_2CH_2OH$	90.2%	1.9%	
$CH_3OC(CH_3)(CH_2O\cdot)CH_2CH_2OH$			4
$\rightarrow HCHO + CH_3OC(\cdot)(CH_3)CH_2CH_2OH$	50.2%	0.9%	
$\rightarrow CH_3OC(CH_3)(CH_2OH)CH_2CH(\cdot)OH$	49.8%	0.9%	
$CH_3OC(\cdot)(CH_3)CH_2CH_2OH + O_2 \rightarrow CH_3OC(OO\cdot)(CH_3)CH_2CH_2OH$		0.9%	5
$CH_3OC(OO\cdot)(CH_3)CH_2CH_2OH$			6
$+ NO \rightarrow CH_3OC(CH_3)(ONO_2)CH_2CH_2OH$	6.5%	0.1%	
$+ NO \rightarrow NO_2 + CH_3OC(O\cdot)(CH_3)CH_2CH_2OH$	93.5%	0.9%	
$CH_3OC(O\cdot)(CH_3)CH_2CH_2OH \rightarrow CH_3C(O)OCH_3 + .CH_2CH_2OH$		0.9%	4,5
$.CH_2CH_2OH + O_2 \rightarrow .OOCH_2CH_2OH$		0.9%	5
$.OOCH_2CH_2OH + NO \rightarrow NO_2 + .OCH_2CH_2OH$		0.9%	5,6
$.OCH_2CH_2OH + O_2$			8
$+ O_2 \rightarrow HCOCH_2OH + HO_2\cdot$	19.5%	0.2%	
$\rightarrow HCHO + .CH_2OH$	80.5%	0.7%	
$.CH_2OH + O_2 \rightarrow HCHO + HO_2\cdot$		0.7%	5
$CH_3OC(CH_3)(CH_2OH)CH_2CH(\cdot)OH + O_2 \rightarrow CH_3OC(CH_3)(CH_2CHO)CH_2OH + HO_2\cdot$		0.9%	5
$CH_3C(CH_3)(CH_2CH_2OH)OCH_2\cdot + O_2 \rightarrow CH_3C(CH_3)(CH_2CH_2OH)OCH_2OO\cdot$		7.0%	5
$CH_3C(CH_3)(CH_2CH_2OH)OCH_2OO\cdot$			6,7
$+ NO \rightarrow CH_3C(CH_3)(CH_2CH_2OH)OCH_2ONO_2$	9.8%	0.7%	
$+ NO \rightarrow NO_2 + CH_3C(CH_3)(CH_2CH_2OH)OCH_2O\cdot$	90.2%	6.3%	
$CH_3C(CH_3)(CH_2CH_2OH)OCH_2O\cdot$			4
$+ O_2 \rightarrow CH_3C(CH_3)(CH_2CH_2OH)OCHO + HO_2\cdot$	87.0%	5.5%	
$\rightarrow HCHO + CH_3C(O\cdot)(CH_3)CH_2CH_2OH$	2.1%	0.1%	
$\rightarrow CH_3C(CH_3)(CH(\cdot)CH_2OH)OCH_2OH$	11.0%	0.7%	
$CH_3C(O\cdot)(CH_3)CH_2CH_2OH \rightarrow CH_3C(O)CH_3 + .CH_2CH_2OH$		0.1%	4,5
$.CH_2CH_2OH + O_2 \rightarrow .OOCH_2CH_2OH$		0.1%	5
$.OOCH_2CH_2OH + NO \rightarrow NO_2 + .OCH_2CH_2OH$		0.1%	5,6
$.OCH_2CH_2OH$			8
$+ O_2 \rightarrow HCOCH_2OH + HO_2\cdot$	19.5%	0.0%	
$\rightarrow HCHO + .CH_2OH$	80.5%	0.1%	
$.CH_2OH + O_2 \rightarrow HCHO + HO_2\cdot$		0.1%	5
$CH_3C(CH_3)(CH(\cdot)CH_2OH)OCH_2OH + O_2 \rightarrow CH_3C(CH_3)(CH(OO\cdot)CH_2OH)OCH_2OH$		0.7%	5
$CH_3C(CH_3)(CH(OO\cdot)CH_2OH)OCH_2OH$			6,7
$+ NO \rightarrow CH_3C(CH_3)(OCH_2OH)CH(ONO_2)CH_2OH$	9.8%	0.1%	
$+ NO \rightarrow NO_2 + CH_3C(CH_3)(CH(O\cdot)CH_2OH)OCH_2OH$	90.2%	0.6%	
$CH_3C(CH_3)(CH(O\cdot)CH_2OH)OCH_2OH \rightarrow HCOCH_2OH + CH_3C(\cdot)(CH_3)OCH_2OH$		0.6%	4,5
$CH_3C(\cdot)(CH_3)OCH_2OH + O_2 \rightarrow CH_3C(OO\cdot)(CH_3)OCH_2OH$		0.6%	5

Table 3 (continued)

Reaction	Fract. Reacting Rxn.	Fract. Reacting Total	Notes
$CH_3C(OO\cdot)(CH_3)OCH_2OH$			6
$+ NO \rightarrow CH_3C(CH_3)(ONO_2)OCH_2OH$	3.9%	0.0%	
$+ NO \rightarrow NO_2 + CH_3C(O\cdot)(CH_3)OCH_2OH$	96.1%	0.6%	
$CH_3C(O\cdot)(CH_3)OCH_2OH$			4
$\rightarrow CH_3C(O)OCH_2OH + CH_3\cdot$	95.0%	0.6%	
$\rightarrow CH_3C(O)CH_3 + .OCH_2OH$	5.0%	0.0%	
$CH_3\cdot + O_2 \rightarrow CH_3OO\cdot$		0.6%	5
$.OCH_2OH + O_2 \rightarrow HCOOH + HO_2\cdot$		0.0%	5

Notes:

1 Fraction for reaction at this position derived from the ratio of the rate constant for reaction at this position estimated using the assignments in the SAPRC07 mechanism estimation system (Carter, 2009a), relative to the total OH + MMB rate constant measured in this work.

2 Fraction reacted at this position derived from the fractions reacted at the other positions in the molecule, to yield 100% reaction at all positions.

3 Fraction reacted at this position adjusted to obtain the 34% methyl acetate yield measured in this work.

4 Rate constants for competing reactions of this alkoxy radical estimated using the procedures in the SAPRC-99 and SAPRC-07 mechanism estimation system. See Carter (2000a, 2009a).

5 Estimated or assumed to be the major atmospheric reaction of this radical

6 Nitrate yield estimated using the procedures in the SAPRC-99 and SAPRC-07 mechanism estimation system as discussed by Carter (2000a, 2009a).

7 Although this parameter could reasonably be adjusted to some extent to improve fits to chamber data, adjustment does not significantly improve fits to the data. See text.

8 Branching ratios of this radical are the same as used in the OH + ethene mechansim, which also forms this radical.

9 This minor route is neglected when generating the full mechanism, so subsequent reactions of the species formed are ignored.

10 Branching ratios for this radical derived based on ratios of methyl acetate to acetone yields from methyl t-butyl ether (Tuazon et al., 1991; Smith et al., 1991). This gives a methyl acetate / acetone yield ratio that is reasonably consistent with that observed in this work for MMB.

carbonyl product, e.g.,

$$CH_3OC(CH_3)(CH_3)CH_2CH(\cdot)OH + O_2 \rightarrow CH_3OC(CH_3)(CH_3)CH_2CHO + HO_2$$

Otherwise, the alkyl radical alkyl radical then adds O_2 forming the corresponding peroxy radical, which in the presence of NO_x reacts primarily with NO to form the corresponding organic nitrate or NO_2 and the corresponding alkoxy radical, e.g.

$$CH_3OC(CH_3)(CH_3)CH(\cdot)CH_2OH + O_2 \rightarrow CH_3OC(CH_3)(CH_3)CH(OO\cdot)CH_2OH$$
$$CH_3OC(CH_3)(CH_3)CH(OO\cdot)CH_2OH + NO \rightarrow CH_3OC(CH_3)(CH_3)CH(ONO_2)CH_2OH$$
$$CH_3OC(CH_3)(CH_3)CH(OO\cdot)CH_2OH + NO \rightarrow NO_2 + CH_3OC(CH_3)(CH_3)CH(O\cdot)CH_2OH$$

In the absence of NO_x the peroxy radicals will either react with HO_2 to form the corresponding hydroperoxide, or (to a lesser extent) react with other peroxy radicals forming either alkoxy radicals or disproportionation products, e.g.

$$CH_3OC(CH_3)(CH_3)CH(OO\cdot)CH_2OH + HO_2 \rightarrow CH_3OC(CH_3)(CH_3)CH(OOH)CH_2OH$$
$$CH_3OC(CH_3)(CH_3)CH(OO\cdot)CH_2OH + RO_2 \rightarrow RO\cdot + O_2 + CH_3OC(CH_3)(CH_3)CH(O\cdot)CH_2OH$$
$$CH_3OC(CH_3)(CH_3)CH(OO\cdot)CH_2OH + RO_2 \rightarrow ROH + O_2 + CH_3OC(CH_3)(CH_3)C(O)CH_2OH$$
$$CH_3OC(CH_3)(CH_3)CH(OO\cdot)CH_2OH + RO_2 \rightarrow R'CHO + O_2 + CH_3OC(CH_3)(CH_3)CH(OH)CH_2OH$$

The latter processes are not shown on Table 3 because they are not important under conditions where O_3 formation occurs, where the peroxy radicals react primarily with NO. The alkoxy radicals formed from the reactions of peroxy radicals with NO or with other peroxy radicals can react in various ways depending on the structure of the radical. These are shown on Table 3.

Except for the initial OH + MMB reaction, discussed above, the branching ratios shown on Table 3 were derived using the various estimation associated with the SAPRC-07 mechanism generation system (Carter, 2000a, 2009a). The products predicted to be formed by the mechanism listed in Table 3 are listed in Table 4, along with an indication of their representation in the model, which is discussed further below. The major predicted products are 3-methyl-3-methoxy butyraldehyde, formaldehyde, glycolaldehyde, and methyl acetate. As discussed above, the branching ratio for the OH + MMB reaction forming the precursor to methyl acetate (Reaction 3 on Table 2) was adjusted to predict the 34% yield of methyl acetate observed in the product studies discussed above, but no other adjustments to the mechanism were made based on the product yield data.

The prediction of the C_6 aldehyde 3-methyl-3-methoxy butyraldehyde, or $CH_3OC(CH_3)(CH_3)$-CH_2CHO, as the major product is reasonably consistent with the results of the product studies discussed

Table 4. Products predicted to be formed in the atmospheric reactions of 3-methoxy-3-methyl-1-butanol and the model species used to represent their subsequent reactions.

Product	Yield	Model Species
$CH_3OC(CH_3)(CH_3)CH_2CHO$	47%	MMBprod [a]
HCHO [b]	42%	HCHO
$HCOCH_2OH$	40%	CCHO
$CH_3C(O)OCH_3$	34%	Neglected [c]
$CH_3C(CH_3)(CH_2CH_2OH)OCHO$	6%	PROD2
$CH_3C(O)CH_3$	5%	ACET
$CH_3OC(CH_3)(CH_3)CH(ONO_2)CH_2OH$	4%	RNO3
$CH_3OC(CH_3)(CH_3)ONO_2$	2%	RNO3
$CH_3OC(CH_3)(CH_2CHO)CH_2OH$	1%	RCHO
$CH_3C(CH_3)(CH_2CH_2OH)OCH_2ONO_2$	1%	RNO3
$CH_3C(O)OCH_2OH$	1%	PROD2
$CH_3OC(CH_3)(CH_3)CHO$	~0%	RCHO

[a] Model species added to the mechanism to explicitly represent this major product species is represented for more accurate reactivity calculation. The mechanism and the product representation used for this compound are given in Table 5 and Table 6, respectively.

[b] Includes formaldehyde formed in reactions of $CH_3OO\cdot$, which are part of the base mechanism and therefore not shown on Table 3.

[c] Reactions of methyl acetate is assumed to make a negligible contribution to MMB's reactivity because of its low reactivity.

above, where the data indicate that this compound is formed with an estimated yield of ~33%. Although the ~47% yield derived from our estimated mechanism is somewhat higher than the ~33% yield derived from estimated GC response factors, they are probably consistent to within the uncertainties of the estimates.

The predicted formation of glycolaldehyde is consistent with the results of the product study discussed above, except that the yield of glycolaldehyde could not be quantified. The product study could obtain no information on formaldehyde yields since formaldehyde is also formed in the reactions of the methyl nitrite that was used as the OH radical source. The formation of formaldehyde and glycolaldehyde as the other major products could not be confirmed our chamber data because they were not be quantified from the analytical methods employed, and also they are known or predicted to be formed to some extent from the reactions of components of the base ROG surrogate used in the chamber experiments. However, the prediction of acetone as a minor product is consistent with the product study, which indicates a 3±1% yield for this compound. The other minor products could not be monitored using our available instrumentation.

Because the oxidation product 3-methoxy-3-methyl butyraldehyde is predicted to be formed in relatively high yields and is also expected to be quite reactive, it is appropriate that its subsequent reactions be represented explicitly when calculating MMB's ozone impacts. There are no known data for its atmospheric reaction rates or reaction mechanisms, but they can be estimated using the procedures incorporated in the SAPRC-07 mechanism generation system (Carter, 2000a, 2009a). The major atmospheric reactions of such aldehydes are expected to be reaction with OH and NO_3 radicals and photolysis. The rate constants for the reactions with OH and NO_3 radicals can be estimated based on those measured for other aldehydes, and the photolysis rates are assumed to be the same as those used in the mechanism for propionaldehyde and the lumped higher aldehyde species RCHO. The reactions of the radicals subsequently formed are estimated using the same procedures as used for those formed in the initial OH + MMB reaction, given in Table 3. The estimated mechanism derived in this way is given on Table 5, and the products predicted to be formed are given in Table 6.

In terms of model species used in the base SAPRC-07 mechanism, the mechanism used in this work for the initial atmospheric reactions of MMB and its product 3-methoxy-3-methyl butyraldehyde are as follows.

MMB + OH → 0.465 HO2 + 0.899 RO2C + 0.07 RO2XC + 0.07 zRNO3 + 0.133 xHO2 + 0.333 xMEO2 + 0.088 xHCHO + 0.401 xCCHO + 0.014 xRCHO + 0.051 xACET + 0.465 MMBprod + 0.061 xPROD2 + 0.535 yROOH

$CH_3OC(CH_3)(CH_3)CH_2CHO$ + OH → 0.891 RCO3 + 0.157 RO2C + 0.013 RO2XC + 0.013 zRNO3 + 0.069 xHO2 + 0.026 xMEO2 + 0.001 xRCO3 + 0.021 xCO + 0.031 xHCHO + 0.052 xRCHO + 0.005 xACET + 0.002 xPROD2 + 0.032 xGLY + 0.036 NROG + 0.109 yROOH

$CH_3OC(CH_3)(CH_3)CH_2CHO$ + NO3 → RCO3 + HNO3

$CH_3OC(CH_3)(CH_3)CH_2CHO$ + HV → HO2 + 1.823 RO2C + 0.107 RO2XC + 0.107 zRNO3 + CO + 0.117 xHO2 + 0.776 xMEO2 + 01.047 xHCHO + 0.117 xACET + 0.776 NROG + yROOH

The rate constants used are given in Table 3 and Table 5, above. The reactions of the model species used in the base mechanism are given in Appendix A to this report. This mechanism was used in all model simulations for MMB in this report unless indicated otherwise.

Table 5. Mechanism used for the atmospheric reactions of the MMB oxidation product 3-methoxy-3-methyl butyraldehyde.

Reaction	Fraction Reacting	
	Rxn.	Total
Reaction with OH		
$CH_3OC(CH_3)(CH_3)CH_2CHO$ ($kOH=2.16 \times 10^{-11}$ cm^3 $molec^{-1}$ s^{-1})		
$+ OH \rightarrow H_2O + CH_3C(CH_3)(CH_2CHO)OCH_2\cdot$	5%	5.3%
$+ OH \rightarrow H_2O + CH_3OC(CH_3)(CH_2\cdot)CH_2CHO$	2%	1.6%
$+ OH \rightarrow H_2O + CH_3OC(CH_3)(CH_3)CH(\cdot)CHO$	4%	4.0%
$+ OH \rightarrow H_2O + CH_3OC(CH_3)(CH_3)CH_2C(O)\cdot$	89%	89.1%
$CH_3C(CH_3)(CH_2CHO)OCH_2\cdot + O_2 \rightarrow CH_3C(CH_3)(CH_2CHO)OCH_2OO\cdot$		5.3%
$CH_3C(CH_3)(CH_2CHO)OCH_2OO\cdot + NO \rightarrow NO_2 + CH_3C(CH_3)(CH_2CHO)OCH_2O\cdot$		4.8%
$CH_3C(CH_3)(CH_2CHO)OCH_2O\cdot + O_2 \rightarrow CH_3C(CH_3)(CH_2CHO)OCHO + HO_2\cdot$		4.4%
$CH_3OC(CH_3)(CH_2\cdot)CH_2CHO + O_2 \rightarrow CH_3OC(CH_3)(CH_2OO\cdot)CH_2CHO$		1.6%
$CH_3OC(CH_3)(CH_2OO\cdot)CH_2CHO + NO \rightarrow NO_2 + CH_3OC(CH_3)(CH_2O\cdot)CH_2CHO$		1.4%
$CH_3OC(CH_3)(CH_2O\cdot)CH_2CHO \rightarrow HCHO + CH_3OC(\cdot)(CH_3)CH_2CHO$		1.4%
$CH_3OC(\cdot)(CH_3)CH_2CHO + O_2 \rightarrow CH_3OC(OO\cdot)(CH_3)CH_2CHO$		1.4%
$CH_3OC(OO\cdot)(CH_3)CH_2CHO + NO \rightarrow NO_2 + CH_3OC(O\cdot)(CH_3)CH_2CHO$		1.3%
$CH_3OC(O\cdot)(CH_3)CH_2CHO \rightarrow CH_3C(O)OCH_3 + HCOCH_2\cdot$		1.3%
$HCOCH_2\cdot + O_2 \rightarrow HCOCH_2OO\cdot$		1.3%
$HCOCH_2OO\cdot + NO \rightarrow NO_2 + HCOCH_2O\cdot$		1.3%
$HCOCH_2O\cdot \rightarrow HCHO + HCO\cdot$		1.2%
$HCO\cdot + O_2 \rightarrow CO + HO_2\cdot$		2.0%
$CH_3OC(CH_3)(CH_3)CH(\cdot)CHO + O_2 \rightarrow CH_3OC(CH_3)(CH_3)CH(OO\cdot)CHO$		4.0%
$CH_3OC(CH_3)(CH_3)CH(OO\cdot)CHO + NO \rightarrow NO_2 + CH_3OC(CH_3)(CH_3)CH(O\cdot)CHO$		3.6%
$CH_3OC(CH_3)(CH_3)CH(O\cdot)CHO \rightarrow HCOCHO + CH_3OC(\cdot)(CH_3)CH_3$		2.9%
$CH_3OC(\cdot)(CH_3)CH_3 + O_2 \rightarrow CH_3OC(OO\cdot)(CH_3)CH_3$		2.9%
$CH_3OC(OO\cdot)(CH_3)CH_3 + NO \rightarrow NO_2 + CH_3OC(O\cdot)(CH_3)CH_3$		2.8%
$CH_3OC(O\cdot)(CH_3)CH_3 \rightarrow CH_3C(O)OCH_3 + CH_3\cdot$		2.4%
$CH_3\cdot + O_2 \rightarrow CH_3OO\cdot$		2.4%
$CH_3OC(CH_3)(CH_3)CH_2C(O)\cdot + O_2 \rightarrow CH_3OC(CH_3)(CH_3)CH_2C(O)OO\cdot$		89.1%
38 reactions with yields less than 1.0% were ignored.		
Reaction with NO_3		
$CH_3OC(CH_3)(CH_3)CH_2CHO$ ($kNO_3 = 3.81 \times 10^{-15}$ cm^3 $molec^{-1}$ s^{-1})		
$+ NO_3 \rightarrow HNO_3 + CH_3OC(CH_3)(CH_3)CH_2C(O)\cdot$		100%
$CH_3OC(CH_3)(CH_3)CH_2C(O)\cdot + O_2 \rightarrow CH_3OC(CH_3)(CH_3)CH_2C(O)OO\cdot$		100%
38 reactions with yields less than 1.0% were ignored.		
Photolysis Reaction		
$CH_3OC(CH_3)(CH_3)CH_2CHO$ (PHOT=C2CHO, same rate constant as RCHO)		
$+ h\nu \rightarrow CH_3OC(CH_3)(CH_3)CH_2\cdot + HCO\cdot$	100%	100%
$CH_3OC(CH_3)(CH_3)CH_2\cdot + O_2 \rightarrow CH_3OC(CH_3)(CH_3)CH_2OO\cdot$		100%
$CH_3OC(CH_3)(CH_3)CH_2OO\cdot$		
$+ NO \rightarrow CH_3OC(CH_3)(CH_3)CH_2ONO_2$	7%	7.0%
$+ NO \rightarrow NO_2 + CH_3OC(CH_3)(CH_3)CH_2O\cdot$	93%	93.0%
$CH_3OC(CH_3)(CH_3)CH_2O\cdot \rightarrow HCHO + CH_3OC(\cdot)(CH_3)CH_3$		93.0%

Table 5 (continued)

Reaction	Fraction Reacting	
	Rxn.	Total
$CH_3OC(\cdot)(CH_3)CH_3 + O_2 \rightarrow CH_3OC(OO\cdot)(CH_3)CH_3$		93.0%
$CH_3OC(OO\cdot)(CH_3)CH_3$		
$+ NO \rightarrow CH_3OC(CH_3)(CH_3)ONO_2$	4%	3.7%
$+ NO \rightarrow NO_2 + CH_3OC(O\cdot)(CH_3)CH_3$	96%	89.3%
$CH_3OC(O\cdot)(CH_3)CH_3$		
$\rightarrow CH_3C(O)CH_3 + CH_3O\cdot$	13%	11.7%
$\rightarrow CH_3C(O)OCH_3 + CH_3\cdot$	87%	77.6%
$CH_3O\cdot + O_2 \rightarrow HCHO + HO_2\cdot$		11.7%
$CH_3\cdot + O_2 \rightarrow CH_3OO\cdot$		77.6%
$HCO\cdot + O_2 \rightarrow CO + HO_2\cdot$		100.0%
38 reactions with yields less than 1.0% were ignored.		

Table 6. Products predicted to be formed in the atmospheric reactions of $CH_3OC(CH_3)(CH_3)CH_2CHO$ and the model species used to represent their subsequent reactions.

Product	Yield	Model Species
<u>OH Reaction Products</u>		
$CH_3OC(CH_3)(CH_3)CH_2C(O)OO\cdot$	89%	RCO3
HCHO [a]	6%	HCHO
$CH_3C(CH_3)(CH_2CHO)OCHO$	4%	RCHO
$CH_3C(O)OCH_3$	4%	NROG
HCOCHO	3%	GLY
CO	2%	CO
$CH_3OC(CH_3)(CH_3)CHO$	1%	RCHO
$CH_3C(CH_3)(CH_2CHO)OCH_2ONO_2$	1%	RNO3
$CH_3C(O)CH_3$	1%	ACET
<u>NO_3 Reaction Products</u>		
$CH_3OC(CH_3)(CH_3)CH_2C(O)OO\cdot$	100%	RCO3
<u>Photolysis products</u>		
HCHO [a]	183%	HCHO
CO	100%	CO
$CH_3C(O)OCH_3$	78%	Neglected [b]
$CH_3C(O)CH_3$	12%	ACET
$CH_3OC(CH_3)(CH_3)CH_2ONO_2$	7%	RNO3
$CH_3OC(CH_3)(CH_3)ONO_2$	4%	RNO3

[a] Includes formaldehyde formed from $CH_3OO\cdot$.

[b] Reactions of methyl acetate are assumed to make a negligible contribution to MMB's reactivity because of its low reactivity.

Representation of Chamber Conditions

The procedures used in the model simulations of the environmental chamber experiments for this project are the same as those used for the experiments with various tetrafluoropropenes (Carter, 2009b,c), and are based on those discussed in detail by Carter (2004) and employed in the studies of Carter and Malkina (2005) and Carter et al. (2005b), updated for SAPRC-07 as discussed by Carter (2009a). Carter (2004) should be consulted for details of the characterization model and chamber effects parameters employed. The temperatures used when modeling were the averages of the temperatures measured in the reactors, corrected as discussed by Carter (2004).

The light intensity for the blacklight experiments declines slowly with time when the lights are new, though the rate of decline decreases as the lights age (Carter et al., 1995b; Carter, 2004, 2007). The characterization of the light intensity for the previous set of reported experiments is discussed by Carter (2007), and based on extrapolating the light intensity assignments for the experiments carried out then to the current experiments we assign a light intensity corresponding to an NO_2 photolysis rate of 0.115 min^{-1} for the experiments modeled in this report. Model simulations of the control experiments for this and the tetrafluoropropene (Carter, 2009b,c) projects indicate that this is an appropriate assignment. The blacklight spectral distribution given by Carter et al. (1995b) was found to be appropriate for the blacklights in this chamber and is used when modeling the runs in this chamber using the blacklight light source.

The chamber effects parameters used when modeling the experiments in this chamber were the same as those given by Carter (2004) except for the HONO offgasing parameters, which were derived based on results of characterization runs carried out in conjunction with these experiments as discussed below. As discussed by Carter (2004), the chamber effects model currently used for this chamber represents both the chamber radical source and background NO_x offgasing by HONO offgasing, whose magnitude is determined by the chamber effects parameter RN-I, which is the ratio of the HONO offgasing rate to the NO_2 photolysis rate. The RN-I parameter that best fits the characterization data tends to vary over time depending on the conditions of the chamber, and the results of the characterization experiments applicable to modeling the experiments discussed in this report, and the assignment of the RN-I values used, are given in the Characterization Results section, below.

The initial reactant concentrations used in the model simulations were based on the experimentally measured values. However, the calibration of the MMB measurements were based on calculated amounts of compound injected and the volume of the reactors, which were measured by injecting known quantities of CO or NO_x, and measuring the CO or NO_x using instruments that were independently calibrated.

Atmospheric Reactivity Simulations

Atmospheric reactivity model simulations were carried out to derive MIR and other atmospheric reactivity values for MMB. The base mechanism, scenarios, and methods used were the same as those used when calculating the MIR and other atmospheric ozone reactivity scales for the SAPRC-07 mechanism by Carter (2009a), so the atmospheric reactivities calculated for MMB in this work are directly comparable with those given by Carter (2009a) for the ~1100 other types of VOCs represented using the SAPRC-07 mechanism. The mechanism used for MMB is the same as gave the best fits to the results of the chamber simulations, as discussed in the Results section below, and is given above. The inputs used in the reactivity scenarios are described by Carter (1994a,b).

RESULTS AND DISCUSSION

A chronological listing of the environmental chamber experiments carried out for this project is given in Table 7. These include experiments with MMB and appropriate characterization and control experiments needed for the data to be useful for mechanism evaluation. The results of the characterization experiments will be discussed first, followed by a discussion of the results of the mechanism evaluation experiments and of the model simulations of these experiments.

Characterization Results

The individual characterization experiments that are relevant to this project are summarized in Table 7. The characterization results are consistent with those discussed by Carter et al. (2005b), Carter and Malkina (2005, 2007), Carter (2007) and Carter (2009b,c), and the same characterization parameters were used for modeling. The only chamber effect parameter that is subject to change from time to time when modeling experiments in this chamber concerns the apparent HONO offgasing, which is believed to be responsible for both the chamber radical source and NO_x offgasing effects (Carter, 2004). This is represented in the chamber effects model by the parameter RN-I, which is the HONO offgasing rate used in the simulations divided by the light intensity as measured by the NO_2 photolysis rate. Figure 7 shows the HONO offgasing parameters that best fit the radical or NO_x - sensitive characterization experiments carried out in the UCR EPA during the period of the last several sets of reactors. Note that the best-fit parameters depend on the mechanism used (particularly the OH + NO_2 rate constant), and all these were calculated for SAPRC-07, the mechanism used in this work.

The experiments carried out for this project began shortly after the installation of a new set of reactors, and the applicable characterization data is for the last set of reactors shown on the figure. The two characterization experiments carried out with these reactors, shown on Table 7 and Figure 7, shows highly variable results for best fit RN-I parameter, but the results were within the range observed with the previous reactors. Because of the variability of the data with these new reactors, for modeling these runs we use the average RN-I parameter that fit the results of the experiments with the previous reactors, which was approximately 10 ppt. Although there is a large amount of scatter in the RN-I parameter that gave the best fit to the data in these characterization experiments, it should be noted that the simulation of the surrogate - NO_x incremental reactivity experiments, which are the experiments used for mechanism evaluation, are not very sensitive to this parameter. Test calculations showed that variation of this parameter within the range shown on Figure 7 has only a minor effect on the simulations of these experiments, and does not affect conclusions concerning the tetrahalopropene mechanism that gives the best fits to the data.

For modeling purposes, we use the same chamber effects parameters as used by Carter (2004), Carter and Malkina (2005), Carter et al. (2005b), and Carter (2007) for all the other chamber effect parameters. Simulations of the incremental reactivity experiments are also not very sensitive to these parameters.

Other control experiments carried out during this period included a side equivalency test (with the same reactive organic gas surrogate - NO_x mixture simultaneously irradiated in both reactors), and several pure air irradiations carried out when the reactors were new. The results of the side equivalency test carried out with this project, as with the recent projects previously (e.g., Carter, 2009b,c) indicated acceptable side equivalency. The results of the most recent side equivalency test are given in Table 8, in conjunction with the results of the reactivity experiments with MMB, discussed below.

Table 7. Summary of experiments carried out for this project.

Run [a]	Date	Type [b]	Purpose and Applicable Conditions	Results
	8/09	Reactors replaced after run EPA1031		
1032	8/30/09	Pure Air Irradiation	Experiment to clean and characterize new reactors.	Less than 1 ppb O_3 formed in both reactors. No PM data obtained.
1033	9/1/09	Pure Air Irradiation	Experiment to clean and characterize new reactors. Repeat EPA1032 but with PM data.	About 1 ppb O_3 formed in both reactors. No significant PM formed in either reactor, but some minor PM formation was beginning in Side A by the last hour of the experiment.
1034	9/2/09	CO - NO_x Irradiation	Characterization experiment to measure the chamber radical source. 35 ppm CO and 18 ppb NO_x injected into both reactors.	Results were consistent with chamber wall model assuming HONO input parameter RN-I = 5 ppt. This is somewhat lower than the default used for modeling runs in with the previous set of reactors but is in the range of results with those reactors.
1035	9/3/09	Side Equiv-alency Test	Control experiment to test for equivalent results in surrogate - NO_x irradiation in both reactors. Initial concentrations given on Table 8.	Results are summarized on Table 8. Good side equivalency obtained, except slightly more PM was formed in Side B, though PM levels were low in both reactors.
1045	9/25/09	MIR Incremental reactivity experiment	Incremental reactivity experiment to test mechanism for test compound at low ROG/NO_x ratios. Initial concentrations on Table 8.	Results are summarized on Table 8. Run had problems with GC data and other experimental problems, so the experiment was considered to be less reliable for model testing than subsequent runs. However, results were consistent with results of other MIR incremental reactivity experiments. No significant PM formation in either reactor.
1048	10/2/09	MIR Incremental reactivity experiment	Repeat of run EPA1045	Results are summarized on Table 8 and plots of selected data are given on Figure 8. See text. No significant PM formation in either reactor.
1052	10/7/09	MOIR/2 Incremental reactivity experiment	Incremental reactivity experiment to test mechanism for test compound at higher ROG/NO_x ratios. Initial concentrations on Table 8.	Results are summarized on Table 8 and plots of selected data are given on Figure 8. See text. No significant PM formation in either reactor.

Table 7 (continued)

Run [a]	Date	Type [b]	Purpose and Applicable Conditions	Results
1053	10/8/09	MIR Incremental reactivity experiment	Repeat of EPA1048 except with lower added MMB levels.	Results are summarized on Table 8 and plots of selected data are given on Figure 8. See text. More PM formation in both reactors than the other incremental reactivity experiments for this project, but lower PM levels formed in the added MMB reactor.
1056	10/13/09	MOIR/2 Incremental reactivity experiment	Repeat of EPA1052 except with higher added MMB levels.	Results are summarized on Table 8 and plots of selected data are given on Figure 8. See text. No significant PM formation in either reactor.
1075	12/1/09	CO - Air Irradiation	Characterization experiment to measure apparent NO_x offgasing . 55 ppm CO injected into both reactors.	Results were consistent with chamber wall model assuming HONO input parameter RN-I = 25 and 15 ppt on Sides A and B, respectively. These are higher than the default used for modeling runs in with the previous set of reactors but is in the range of results with the last two reactors.

[a] Gaps in run number indicate experiments carried out for other projects.

[b] All experiments are ~6-hour irradiations using blacklights. "Surrogate" indicates a ROG surrogate - NO_x mixture irradiated; "MIR" and "MOIR/2" mean the target initial NO_x and base ROG surrogate were 30 ppb and 0.55 ppmC and 25 ppb and 1.1 ppmC, respectively. "Incremental Reactivity" indicates that a reactant was added to one of the two reactors.

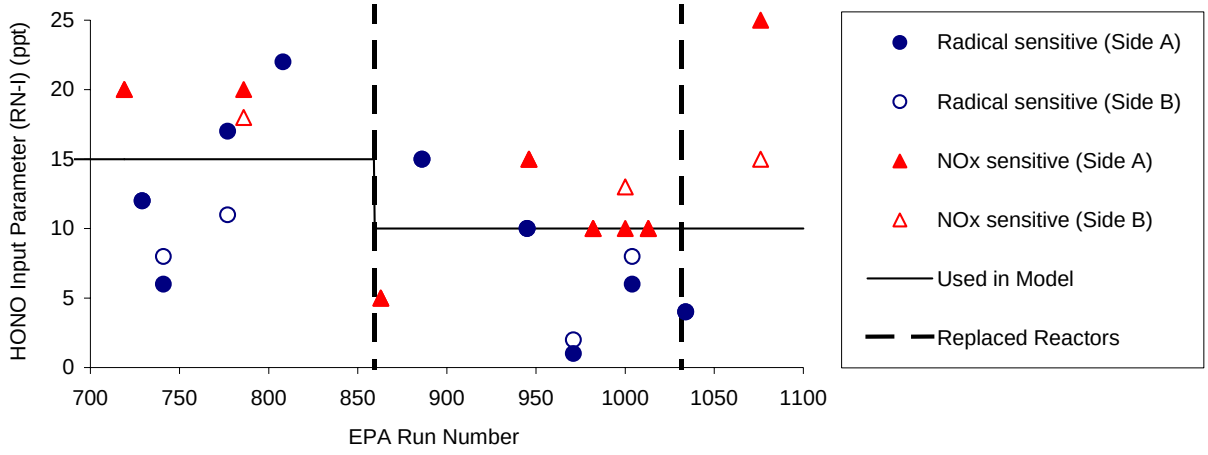

Figure 7. Plots of best fit HONO offgasing parameters against UCR EPA run number.

Incremental Reactivity and Mechanism Evaluation Results

The conditions and selected results of the incremental reactivity experiments used to evaluate the MMB mechanism are summarized on Table 8. These experiments consist of irradiations of a reactive organic gas (ROG) - NO_x mixture serving as a simplified model of the chemical system involved on O_3 formation in urban atmospheres, together in irradiations of the same mixture with MMB (the test compound) added. The experiment without the added test compound is referred to as the "base case" experiment, and the experiment where the test compound is added is the "test" experiment. The differences in O_3 formation and other measures of reactivity in these experiments provide a measure of the effects of the test compound in a system more closely representing atmospheric conditions than the simpler experiments discussed above, and provide a more realistic test of the mechanism's ability to predict its atmospheric reactivity.

As in previous incremental reactivity experiments carried out in this chamber (Carter and Malkina, 2005, 2007; Carter et al., 2005b), two types of base case experiments were employed. The first is a lower ROG/NO_x experiment designed to approximate conditions where O_3 formation is most sensitive to VOC emissions, which serve as the basis for the MIR reactivity scale, and are referred to as "MIR" experiments. The second is at higher ROG/NO_x ratios with NO_x levels at approximately half that yielding maximum ozone concentrations, and are referred to as "MOIR/2" experiments. For the MIR experiments the target initial NO_x was approximately 30 ppb and the target initial base case ROG was approximately 0.6 ppmC, while for the MOIR/2 experiments the target initial levels were approximately 25 ppb and 2.3 ppmC, respectively. In both cases, the base ROG surrogate mixture representing reactive organic gases from all sources consists of n-butane, n-octane, ethene, propene, trans-2-butene, toluene and m-xylene, and is based on a mixture derived previously (Carter et al., 1995c) as a simplification of ambient mixtures used in the atmospheric reactivity calculations. Earlier versions of this mixture also contained formaldehyde, but this was not included in the current experiments for experimental reasons. As

Table 8. Summary of initial concentrations and selected gas-phase results of the incremental reactivity experiments.

EPA Run No.	Test Side	Test Cmpd Added (ppm)	Base Run Initial Concentrations		6 Hr O_3 (ppb)		D([O_3]-[NO]) Change (ppb)		IntOH change (ppt-min)	5-6 Hr avg. PM ($\mu g/m^3$)	
			NO_x (ppb)	ROG (ppmC)	Base	Test	2 Hr	65 Hr		Base	Test
Side Equivalency Experiment											
1035	A		27	0.51	40	42	-1	1	[a]	0.00	0.11
Added MMB Experiments (MIR Conditions)											
1045	B	0.29	30	0.55	68	129	34	61	[a]	0.01	0.01
1048	B	0.28	29	0.45	46	110	23	64	-38	0.00	0.00
1053	B	0.19	26	0.51	51	101	19	49	-3	0.00	0.00
Added MMB Experiments (MOIR/2 Conditions)											
1052	A	0.23	23	0.99	88	123	32	36	-16	0.58	0.17
1056	B	0.34	24	0.87	83	124	32	41	[a]	0.06	0.00

[a] No useable data obtained for the time indicated.

discussed by Carter and Malkina (2005), this does not significantly affect the utility of the experiments for mechanism evaluation.

The measures of gas-phase reactivity used to evaluate the mechanisms in the incremental reactivity experiments are the effects of the test compound on $\Delta([O_3]\text{-}[NO])$, or $([O_3]_t\text{-}[NO]_t)\text{-}([O_3]_0\text{-}[NO]_0)$, and IntOH, the integrated OH radical levels. As discussed elsewhere (e.g., Johnson, 1983; Carter and Atkinson, 1987; Carter and Lurmann, 1991, Carter et al., 1993), $\Delta([O_3]\text{-}[NO])$ gives a direct measure of the amount of conversion of NO to NO_2 by peroxy radicals formed in the photooxidation reactions, which is the process that is directly responsible for ozone formation in the atmosphere. This gives a useful measure of factors affecting O_3 reactivity even early in the experiments where O_3 formation is suppressed by the unreacted NO. Although this is the primary measure of the effect of the VOC on O_3 formation, the effect on radical levels is also a useful measure for mechanism evaluation, because radical levels affect how rapidly all VOCs present, including the base ROG components, react to form ozone.

The integrated OH radical levels are not measured directly, but can be derived from the amounts of consumption of reactive VOCs that react only with OH radical levels. In particular,

$$\text{IntOH}_t = \frac{\ln([\text{tracer}]_0/[\text{tracer}]_t) - Dt}{k\text{OH}^{\text{tracer}}} \qquad \text{(I)}$$

where $[\text{tracer}]_0$ and $[\text{tracer}]_t$ are the initial and time t concentrations of the compound used as the OH tracer, $k\text{OH}^{\text{tracer}}$ its OH rate constant, and D is the dilution rate in the experiments. The latter is neglected in our IntOH analysis. The base ROG surrogate component m-xylene was used as the tracer to derive the IntOH levels in these experiments. The OH + m-xylene rate constant used was 2.36×10^{-11} cm^3 $molec^{-1}$ s^{-1} (Atkinson, 1989).

Plots of experimental $\Delta([O_3]\text{-}[NO])$ in the base case and test experiments, changes in $\Delta([O3]\text{-}[NO])$ and IntOH caused by adding the MMB, are shown on Figure 8 and changes in these quantities are also summarized on Table 8. It can be seen that the addition of the MMB caused a measurable increase in NO oxidation and O_3 formation in all the experiments, but also a decrease in the integrated OH radical in the experiments. This tendency to increase O_3 formation and NO oxidation is seen with many other VOCs with mechanisms similar to that for MMB, and is therefore expected.

Figure 8 also shows plots of model simulations of the incremental reactivity experiments, where they can be compared with the experimental data. The solid lines show the calculations using the estimated mechanism derived in this work, as shown in the previous section, and incorporate no adjustments to improve the fits of the model simulations to these data. Although the model gives good fits to the $\Delta([O_3]\text{-}[NO])$ data in the base case and added MMB MOIR/2 experiments and to the added MMB MIR experiments, the base mechanism tends to slightly underpredict the ozone in the base case MIR experiments, causing the model to slightly overpredict the effect of added MMB on $\Delta([O_3]\text{-}[NO])$ in the MIR runs. This overprediction is seen in the MIR experiments only and is fairly small and may be within the uncertainty of the data.

We were unable to find reasonable adjustments to the mechanism that improve the simulations of the results of the MIR experiments without significantly degrading the simulations of the other experiments or giving predictions that are inconsistent with our product data. Adjusting the branching ratios of the initial reaction either make this overprediction of incremental reactivity in the MIR experiments worse or give predicted product yields that are inconsistent with our experimental measurements discussed above. The only other mechanistic uncertainty that could be appropriately adjusted concerns the nitrate yields in the reactions of the C_6 peroxy radicals with NO, which are based on uncertain estimates and can significantly affect reactivity. However, increasing the yields to better

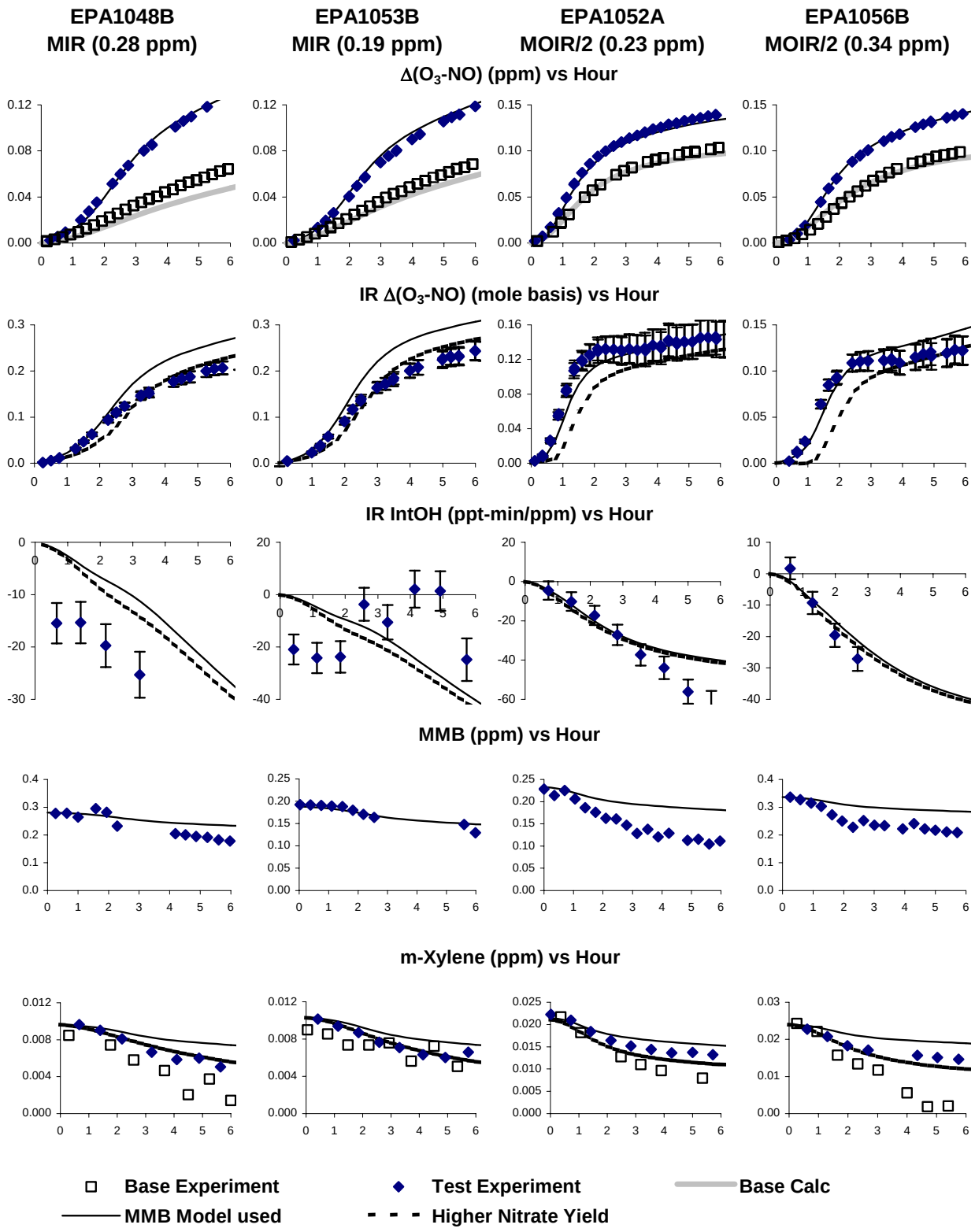

Figure 8. Experimental and calculated results of the incremental reactivity experiments with added MMB. (Results for run EPA1045 are similar to those for EPA1048 and are not shown.).

simulate final incremental reactivities in the MIR experiments result in significant underpredictions of reactivity in the MOIR/2 experiments and a tendency to underpredict NO oxidation rates in the early stages of the MIR experiments. This is shown by the calculations with the dotted lines on the incremental reactivity plots on Figure 8. Therefore, the originally estimated mechanism, used to derive the calculations shown by the solid lines on Figure 8 was used as the basis for the atmospheric reactivity calculations discussed in the following section.

Figure 8 also shows concentration-time plots measured for MMB in the added MMB experiments. It can be seen that the model underpredicted the consumption rate for MMB. However, the model also underpredicted the m-xylene consumption rate in both the base case and added MMB experiments, indicating that the base mechanism tends to underpredict overall radical levels. This tendency of the mechanism to underpredict overall radical levels is observed in most experiments where aromatics are present, and is attributed to uncertainties in the base aromatics mechanism (Carter, 2009a). The consumption rate of m-xylene relative to MMB is reasonably consistent with the ratio of rate constants used in the current mechanism for these compounds, to within the scatter of the data for these experiments. Therefore, this underprediction of the MMB consumption rate shown on Figure 8 does not necessarily indicate a problem with the mechanism used for MMB.

Atmospheric Reactivity Calculation

Conditions and maximum O_3 concentrations of the ambient scenarios used for reactivity assessment are summarized on Table 9. These are the same scenarios as used to calculate the atmospheric reactivities of the ~1100 types of VOCs using the SAPRC-07 mechanism by Carter (2009a), and are also the same as used in previous reactivity scales calculated using the SAPRC-99 (Carter, 2000a), and SAPRC-90 (Carter, 1994a) mechanisms. All of these are 1-day box model scenarios with varying inversion heights, initially present and emitted NO_x and reactive organics, and O_3 and background VOCs entrained from aloft as the inversion heights increase during the day (Carter, 1994a,b), with inputs designed to represent various urban areas around the United States (Baugues, 1990). As discussed previously, four types of scenarios are employed.

- Base. The base case scenarios have the NO_x and other inputs as originally specified by Baugues (1990) to represent the various urban areas around the United States. Note that these are not good representations of current conditions, since generally these scenarios predict much higher O_3 levels than currently occur, and these box model incorporate significant simplifications of transport, mixing, and emissions, and multi-day effects, which can be important. However, they do represent a variety of chemical conditions, which are the main factors reflecting *relative* atmospheric reactivities of VOCs. These scenarios represent a variety of relative NO_x levels, which is a major factor affecting absolute and relative reactivities of VOCs (Carter and Atkinson, 1989; Carter, 1994a). For this reason, other types of scenarios, discussed below, are derived to represent standard conditions of NO_x availability.
- MIR. The Maximum Incremental Reactivity (MIR) scenarios have the NO_x inputs adjusted so that the base ROG mixture used to represent all the anthropogenic VOC emissions has the maximum incremental reactivity relative to ozone formation. All the other inputs are the same as in the base case scenarios. Although the base ROG reactivity is used to define the MIR NO_x level, most other types of VOCs also have their maximum incremental reactivity at this same NO_x level. These scenarios represent the relatively high NO_x conditions where O_3 formation is the most sensitive to VOC emissions. The averages incremental reactivities in all these scenarios are used to derive the MIR scale that is used in regulatory applications in California (CARB 1993, 2000).
- MOIR. The Maximum Ozone Incremental Reactivity (MOIR) scenarios have the NO_x inputs adjusted to give the maximum daily maximum ozone concentration. All other inputs are the same

Table 9. Summary of conditions of scenarios used for reactivity assessment

Scenario	Max O_3 (ppb)				ROG / NOx				Max Height (kM)	ROG input (m.mol m^{-2})	O_3 aloft (ppb)	Final H (m)
	Base	MIR	MOIR	EBIR	Base	MIR	MOIR	EBIR				
Averaged Conditions		177	226	211		3.9	5.9	9.1	1.8	15	70	1823
Atlanta, GA	172	145	176	168	7.3	3.7	5.6	7.9	2.1	12	63	2146
Austin, TX	171	153	186	176	9.3	3.5	5.4	8.2	2.1	11	85	2108
Baltimore, MD	311	244	320	294	5.2	4.0	6.2	10.1	1.2	17	84	1169
Baton Rouge, LA	235	186	235	225	6.8	4.5	6.6	8.7	1.0	11	62	968
Birmingham, AL	239	204	258	243	6.9	2.8	4.3	6.4	1.8	13	81	1770
Boston, MA	192	165	200	190	6.5	2.9	4.4	6.8	2.6	14	105	2598
Charlotte, NC	139	138	162	158	7.8	1.9	3.0	4.1	3.0	7	92	3046
Chicago, IL	286	243	322	300	11.6	4.4	6.6	9.9	1.4	25	40	1392
Cincinnati, OH	195	158	198	182	6.4	3.5	5.3	9.1	2.8	17	70	2816
Cleveland, OH	242	195	242	228	6.6	4.4	6.9	10.3	1.7	16	89	1650
Dallas, TX	184	161	203	193	4.7	4.2	6.4	9.2	2.3	18	75	2250
Denver, CO	194	162	199	187	6.3	5.0	7.6	11.6	3.4	29	57	3358
Detroit, MI	237	183	239	219	6.8	3.8	5.8	10.0	1.8	17	68	1844
El Paso, TX	175	145	176	168	6.6	4.6	7.2	10.0	2.0	12	65	2000
Hartford, CT	168	148	185	173	8.4	2.9	4.5	7.3	2.3	11	78	2318
Houston, TX	300	227	300	278	6.1	4.1	6.2	9.5	1.7	25	65	1748
Indianapolis, IN	203	158	203	191	6.6	4.0	6.5	9.8	1.7	12	52	1675
Jacksonville, FL	150	126	157	150	7.6	3.7	5.5	7.6	1.5	8	40	1485
Kansas City, MO	152	127	158	146	7.1	3.1	4.9	8.5	2.2	9	65	2200
Lake Charles, LA	290	230	306	292	7.4	3.6	5.3	7.2	0.5	7	40	457
Los Angeles, CA	560	404	561	530	7.6	5.2	8.0	11.2	0.5	23	100	503
Louisville, KY	202	163	203	192	5.5	3.3	5.1	7.4	2.5	14	75	2518
Memphis, TN	224	180	232	216	6.8	3.4	5.1	7.8	1.8	15	58	1750
Miami, FL	129	122	149	143	9.6	2.9	4.5	6.4	2.7	9	57	2720
Nashville, TN	162	146	187	175	8.0	2.6	4.0	6.0	1.6	7	50	1608
New York, NY	373	303	380	358	8.1	4.8	6.7	9.8	1.5	39	103	1512
Philadelphia, PA	235	178	235	219	6.2	4.1	6.3	9.7	1.8	19	53	1800
Phoenix, AZ	268	209	269	245	7.6	5.0	7.8	13.0	3.3	40	60	3250
Portland, OR	159	130	163	157	6.5	3.1	4.9	7.0	1.6	6	66	1575
Richmond, VA	232	181	234	214	6.2	3.6	5.5	9.4	1.9	16	64	1932
Sacramento, CA	196	153	197	184	6.6	3.9	6.0	9.1	1.1	7	60	1103
St Louis, MO	305	239	312	289	6.1	4.7	7.2	11.6	1.6	26	82	1625
Salt Lake City, UT	180	158	190	177	8.5	3.5	5.5	9.1	2.2	11	85	2150
San Antonio, TX	120	102	122	118	3.9	3.0	4.7	6.5	2.3	6	60	2308
San Diego, CA	185	149	185	177	7.1	4.7	7.2	10.1	0.9	8	90	850
San Francisco, CA	225	347	458	436	4.8	6.1	9.0	12.0	0.7	25	70	650
Tampa, FL	212	173	219	210	4.4	3.5	5.2	7.0	1.0	8	68	991
Tulsa, OK	219	171	219	203	5.3	3.5	5.4	8.8	1.8	15	70	1830
Washington, DC	273	214	274	257	5.3	3.2	4.8	7.4	1.4	13	99	1421

as in the base and MIR scenarios. These scenarios represent NO_x conditions that are optimum for O_3 formation, which is always lower than those for MIR. The averages incremental reactivities in all these scenarios are used to derive the MOIR scale, which can be considered as an alternative to MIR (Carter, 1994a).

- EBIR. The Equal Benefit Incremental Reactivity (EBIR) scenarios have the NO_x inputs adjusted so that O_3 formation is equally sensitive to changes in total ROG or NO_x inputs. All the other inputs are the same as in the base, MIR, and MOIR scenarios. The NO_x inputs are always lower than those yielding maximum O_3 (MOIR), and represent the lowest NO_x levels where VOC control is at least as effective as NO_x control. The averages incremental reactivities in all these scenarios are used to derive the EBIR scale, which is a useful complement to the MIR scale in assessing how NO_x levels affect relative reactivities.
- Averaged Conditions. The averaged conditions scenarios have all inputs other than total NO_x derived to represent the average for the base case scenarios. The NO_x inputs are varied to assess how measures of reactivity depend on NO_x with other inputs held constant. Incremental reactivities in the MIR, MOIR, and EBIR averaged conditions scenarios (i.e., whose NO_x inputs are adjusted to represent those respective conditions) usually give good approximations to reactivities in those respective scales, though they are not used in deriving these scales.

Table 10 gives the calculated incremental ozone reactivities for MMB in these various scenarios, along with the incremental reactivities of the "base ROG" mixture used in the reactivity calculations to represent VOC emissions from all sources. Figure 9 gives a comparison of the MIR reactivity of MMB with those of selected isomers of MMB and with several other representative compounds and mixtures, including ethane, the standard used by the EPA as the dividing line between reactive and negligibly reactive for the purpose of determining VOC exemptions, ethanol, vehicle exhaust, toluene, and mixed xylene isomers. Table 10 shows that the reactivities of MMB vary from scenario to scenario to a similar extent as to those for the base ROG mixture, though its ozone impacts appear to be slightly less dependent on NO_x conditions than is the case for the base ROG mixture. MMB has the same average ozone impact as the base ROG in the relatively low NO_x EBIR scale, while it has ~15% lower reactivity than the base ROG in the relatively high NO_x MIR scale.

The ozone impact for MMB in the MIR scale is 2.71 grams O_3 per gram of VOC. Figure 9 shows that this is near the middle of the range of those for its isomers, is similar to but somewhat less than those the base ROG and the standard exhaust mixtures, is about twice that of ethanol, and is less than those of aromatics such as toluene and the xylenes. For comparison with MIR reactivities for other compounds calculated using the same mechanism and methodology, see the complete SAPRC-07 reactivity tabulations given by Carter (2009a).

The MMB MIR value derived in this work is about 3.5 times higher than the 0.78 grams O_3 per gram VOC value previously calculated for this compound, as given in the reactivity scales of Carter (2009a) dated September, 2009, and earlier. This is due in part to the factor of 2.3 increase in the OH radical rate constant relative to the estimated value used previously, in part to the increased relative importance of reaction routes that have more NO to NO_2 conversions and form more reactive products than initially estimated, and in part to the explicit representation of the $CH_3OC(CH_3)_2CH_2CHO$ product, which is calculated to be have a somewhat higher ozone impact than the generic RCHO species used to represent this aldehyde product previously.

Table 10. Calculated atmospheric incremental reactivities for 3-methoxy-3-methyl-1-butanol and the base ROG mixture

Scenario	3-Methoxy-3-Methyl-1-Butanol (MMB) (gm O_3 / gm VOC)				Base ROG Mixture (gm O_3 / gm VOC)			
	Base	MIR	MOIR	EBIR	Base	MIR	MOIR	EBIR
Averaged Conditions		2.71	1.28	0.79		3.62	1.47	0.79
Reactivity Scale Value (Scenario averages)	1.17±0.3	2.78±0.5	1.30±0.3	0.83±0.2	1.29±0.5	3.53±0.6	1.45±0.3	0.81±0.2
Atlanta, GA	0.95	2.63	1.32	0.85	0.78	3.29	1.48	0.86
Austin, TX	0.84	2.83	1.47	0.94	2.08	3.53	1.60	0.90
Baltimore, MD	1.79	2.88	1.31	0.81	1.08	3.66	1.39	0.71
Baton Rouge, LA	0.90	2.15	0.96	0.58	0.94	2.85	1.16	0.63
Birmingham, AL	1.04	3.51	1.64	1.10	0.90	4.35	1.76	1.02
Boston, MA	0.92	2.66	1.29	0.87	0.63	3.22	1.40	0.85
Charlotte, NC	0.77	2.85	1.57	1.21	0.47	3.35	1.64	1.17
Chicago, IL	0.52	2.61	1.07	0.62	1.34	3.44	1.23	0.61
Cincinnati, OH	1.36	3.10	1.59	1.03	1.48	3.83	1.66	0.91
Cleveland, OH	1.31	2.49	1.23	0.79	2.75	3.19	1.36	0.76
Dallas, TX	2.15	2.42	1.18	0.74	1.98	3.16	1.34	0.74
Denver, CO	1.57	2.29	1.07	0.62	1.21	3.07	1.26	0.64
Detroit, MI	1.20	2.97	1.39	0.87	1.68	3.73	1.47	0.78
El Paso, TX	1.38	2.34	1.18	0.73	0.92	3.17	1.40	0.75
Hartford, CT	1.01	3.36	1.68	1.12	1.41	4.08	1.79	1.05
Houston, TX	1.25	2.83	1.20	0.72	1.54	3.60	1.35	0.69
Indianapolis, IN	1.36	3.02	1.40	0.86	0.84	3.86	1.59	0.85
Jacksonville, FL	0.79	2.78	1.25	0.79	1.23	3.56	1.46	0.84
Kansas City, MO	1.28	3.41	1.72	1.12	0.62	4.12	1.80	1.02
Lake Charles, LA	0.56	2.88	1.01	0.58	0.94	3.76	1.24	0.66
Los Angeles, CA	0.78	1.73	0.70	0.44	1.55	2.40	0.82	0.41
Louisville, KY	1.38	3.22	1.54	0.98	1.01	4.00	1.76	1.01
Memphis, TN	0.98	3.34	1.36	0.84	0.60	4.18	1.52	0.83
Miami, FL	0.69	3.02	1.48	1.02	0.82	3.76	1.64	1.02
Nashville, TN	0.90	4.02	1.80	1.17	0.64	4.92	2.01	1.17
New York, NY	0.58	1.98	0.78	0.45	1.40	2.65	0.91	0.45
Philadelphia, PA	1.26	2.83	1.22	0.74	1.66	3.62	1.35	0.71
Phoenix, AZ	1.53	2.88	1.47	0.89	1.16	3.67	1.58	0.75
Portland, OR	1.11	3.07	1.51	1.02	1.33	3.80	1.68	1.03
Richmond, VA	1.31	3.07	1.46	0.93	1.42	3.90	1.54	0.83
Sacramento, CA	1.31	3.24	1.48	0.92	1.80	4.08	1.65	0.90
St Louis, MO	1.51	2.46	1.10	0.66	1.07	3.26	1.21	0.61
Salt Lake City, UT	1.14	3.02	1.65	1.07	2.11	3.72	1.75	0.97
San Antonio, TX	1.81	2.51	1.38	0.98	1.07	3.17	1.52	0.98
San Diego, CA	0.87	1.76	0.84	0.52	1.82	2.47	1.02	0.56
San Francisco, CA	1.32	1.55	0.68	0.40	2.18	2.16	0.81	0.40
Tampa, FL	1.73	2.63	1.13	0.70	1.54	3.46	1.35	0.77
Tulsa, OK	1.39	3.07	1.36	0.84	1.25	3.83	1.50	0.81
Washington, DC	1.18	2.90	1.32	0.87	1.23	3.69	1.43	0.82

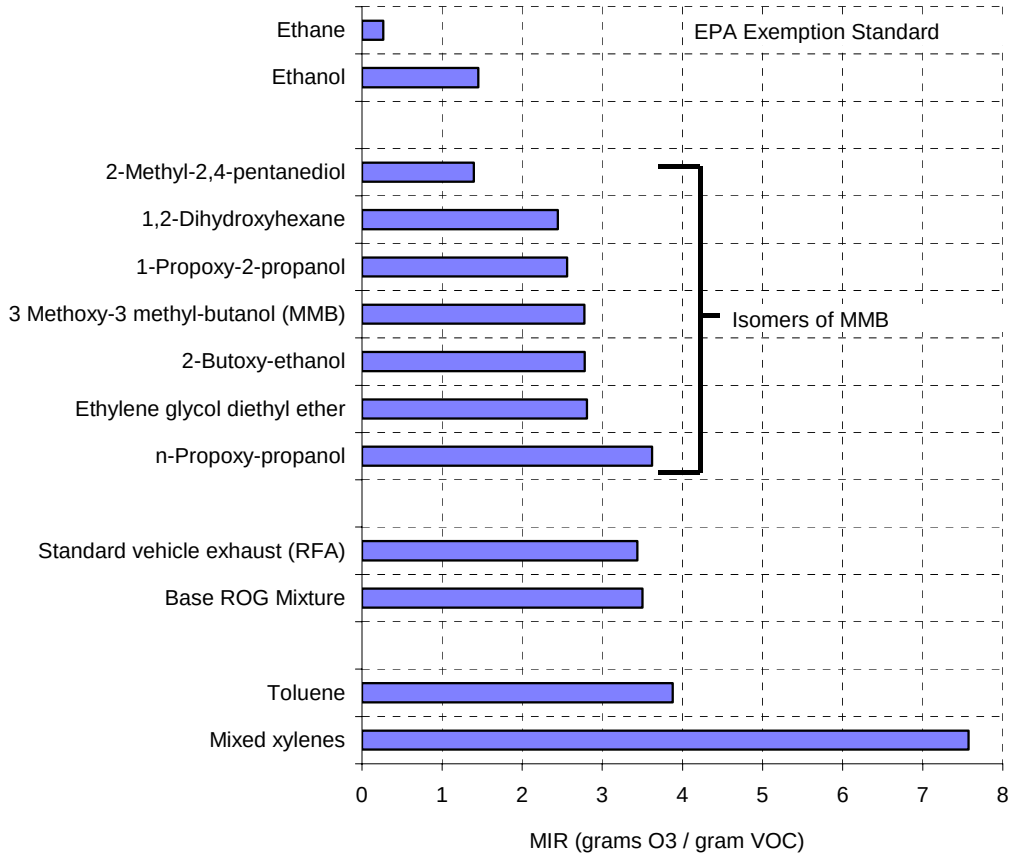

Figure 9. Comparisons of ozone reactivity of MMB in the MIR scale with those for isomeric compounds and other representative VOCs.

Effects of MMB on Secondary Aerosol Formation

Measurements of particle formation were also made during the course of the experiments, using the procedures discussed above and by Carter et al. (2005b), and representative results are summarized on Table 8. The addition of MMB was found not to significantly change the amounts of PM formed in the experiments, indicating that this compound is not a significant source of secondary organic aerosol (SOA). This is not unexpected, since the mechanism derived for this compound does not involve predicted formation of very low volatility products.

Figure 10 shows plots of average PM reactivities in incremental reactivity experiments for all VOCs for which PM data are available in UCR EPA chamber reactivity experiments. For this purpose, PM reactivities are defined as mass of additional PM formed after 5 hours of irradiation (uncorrected particle losses on the wall) when the test compounds was added to the surrogate - NO_x experiment, divided by mass of VOC added, assuming unit density of PM formed. It can be seen some VOCs form a significant amount of SOA under the conditions of these experiments, while others, such as MMB and ethylene and propylene glycols, do not. It is important to recognize that there are many factors that affect SOA formation in the environment, and PM reactivities in ambient airsheds may be different than measured in these chamber experiments. However, these results give at least a qualitative indication of relative SOA impacts of the various compounds studied, and indicate that the impacts of MMB in this regard are expected to be relatively low.

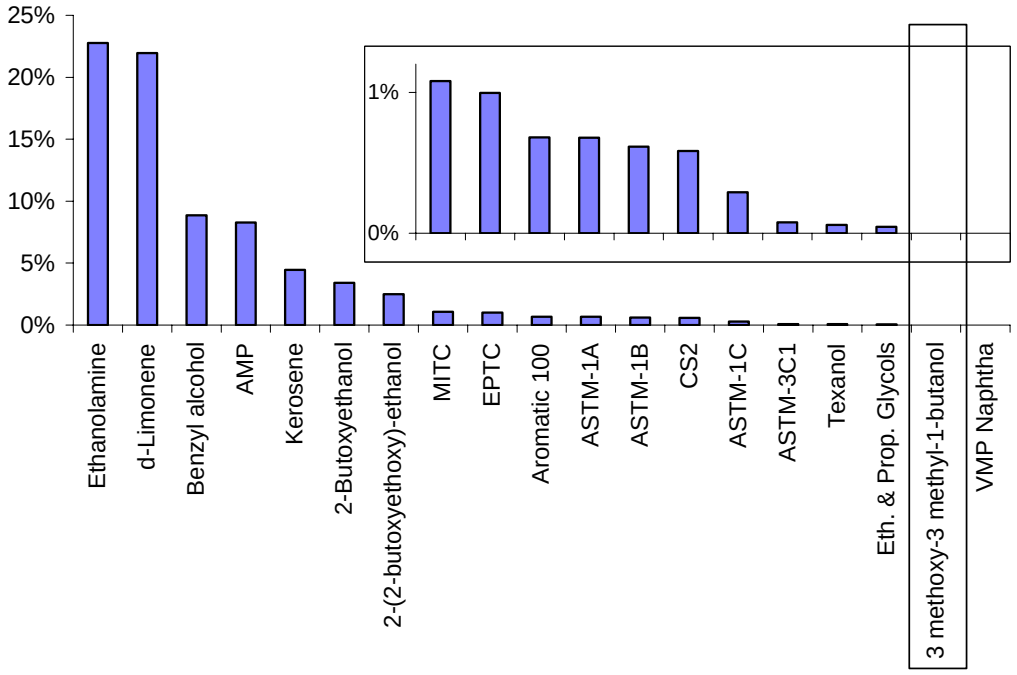

Figure 10. Plots of average PM reactivities in incremental reactivity experiments for all VOCs for which PM data are available in UCR EPA chamber reactivity experiments. Units are mass of PM formed after 5 hours of irradiation (uncorrected particle losses on the wall) divided by mass of VOC added, assuming unit density of PM formed.

CONCLUSIONS

This project was successful in obtaining information needed to reduce uncertainties in atmospheric ozone impact estimates for 3-methoxy-3-methyl-1-butanol (MMB). Until this study there were no data concerning the atmospheric reaction rate and mechanism for this compound, and all previous ozone impact quantifications for this compound were based entirely on estimates that were not experimentally evaluated. As part of this study, the rate constant for the reaction of MMB with OH radicals, its major atmospheric fate, was measured to be $(1.64 \pm 0.06) \times 10^{-11}$ cm^3 $molecule^{-1}$ s^{-1} at 296 ± 2 K. Acetone, methyl acetate, glycolaldehyde, and 3 methoxy-3-methyl-butanal were identified as products of this reaction. The yields of methyl acetate and acetone determined to be $3 \pm 1\%$ and $34 \pm 8\%$, respectively, and the yield of 3 methoxy-3-methyl-butanal was estimated to be approximately 33% based on estimated GC response factors, or to be 47% based on estimates of MMB reaction routes. These data, combined with estimates for reaction routes whose products were not quantified, were used derive a new atmospheric reaction mechanism that is consistent with the new kinetic and mechanistic data, and that gave ozone predictions that were consistent with the environmental chamber experiments carried out for this project.

The OH radical rate constant determined for MMB as part of this study was over a factor of two higher than that estimated using the structure-reactivity estimation methods of Kwok and Atkinson (1995), which was used to derive the previous estimated mechanism for MMB (Carter, 2009a). Generally, the estimation methods of Kwok and Atkinson (1995) perform much better for alcohols and ethers, so this level of discrepancy is unexpected. The product yield data determined in this work indicate that the major sources of the discrepancy are reactions at the $-CH_2-$ and $–CH_2OH-$ groups in MMB, which appear to be faster by approximately factors of ~5 and ~2, respectively, than estimated. The different branching ratios for the initial OH + MMB reaction also result in predictions of more reactive products in the reactions than were previously estimated to be the case.

The new MMB mechanism developed in this study resulted in the ozone impact for MMB being calculated to be 2.78 grams O_3 per gram VOC in the SAPRC-07 MIR scale. This is over a factor of three higher than the previous SAPRC-07 MIR value of 0.78 derived for this compound (Carter, 2009a), and reflects the effects of the increase in the OH reaction rate constant and the assumed formation of more reactive oxidation products. Although this increase is significant, the ozone impact of MMB is still somewhat less than the base ROG mixture used in the reactivity calculations to represent reactive VOC emissions from all anthropogenic sources, indicating that this compound can be considered to have approximately average or less than average ozone impact compared to other anthropogenic VOCs.

The ozone impact of MMB in the MIR scale is calculated to be about 10 times that of ethane, making this compound not appropriate for VOC exemption by the standards currently used by the EPA. This previously estimated reactivity of MMB was also higher than that of ethane, so this study does not change the status of MMB in this respect. The main effect of this study is that the ozone impact estimates for MMB are significantly less uncertain than was previously the case, and the chance of MMB having a significantly higher ozone impact than currently used as a result of this study is significantly reduced.

Data were also obtained concerning the effects of MMB on atmospheric particle formation. The addition of this compound to atmospheric reactive organic gas surrogate - NO_x irradiations either had no effect on the mass or particles formed, or slightly reduced it. This indicates that this compound does not form measurable amounts of secondary organic aerosol. This indicates an environmental advantage of using this compound compared to use of compounds that do form measurable secondary organic aerosol.

REFERENCES

Aschmann, S. M. and R. Atkinson (2008): Rate Constants for the Gas-Phase Reactions of OH Radicals with E-7-Tetradecene, 2-Methyl-1-tridecene and the C_7-C_{14} 1-Alkenes at 295 ± 1 K," Phys. Chem. Chem. Phys., 10, 4159-4164.

Atkinson, R. (1989): "Kinetics and Mechanisms of the Gas-Phase Reactions of the Hydroxyl Radical with Organic Compounds," J. Phys. Chem. Ref. Data, Monograph no 1.

Baugues, K. (1990): "Preliminary Planning Information for Updating the Ozone Regulatory Impact Analysis Version of EKMA," Draft Document, Source Receptor Analysis Branch, Technical Support Division, U. S. Environmental Protection Agency, Research Triangle Park, NC, January.

CARB (1993): "Proposed Regulations for Low-Emission Vehicles and Clean Fuels -- Staff Report and Technical Support Document," California Air Resources Board, Sacramento, CA, August 13, 1990. See also Appendix VIII of "California Exhaust Emission Standards and Test Procedures for 1988 and Subsequent Model Passenger Cars, Light Duty Trucks and Medium Duty Vehicles," as last amended September 22, 1993. Incorporated by reference in Section 1960.

CARB (2000): "Initial Statement of Reasons for the Proposed Amendments to the Regulation for Reducing Volatile Organic Compound Emissions from Aerosol Coating Products and Proposed Tables of Maximum Incremental Reactivity (MIR) Values, and Proposed Amendments to Method 310, 'Determination of Volatile Organic Compounds in Consumer Products'," California Air Resources Board, Sacramento, CA, May 5.

CARB (2008): "Air Resources Board Reactivity Programs." Web page at http://www.arb.ca.gov/ research/reactivity/reactivity.htm. Last updated June, 2008

Carter, W. P. L. (1994a): "Development of Ozone Reactivity Scales for Volatile Organic Compounds," J. Air & Waste Manage. Assoc., 44, 881-899.

Carter, W. P. L. (1994b): "Calculation of Reactivity Scales Using an Updated Carbon Bond IV Mechanism," Report Prepared for Systems Applications International Under Funding from the Auto/Oil Air Quality Improvement Research Program, April 12.

Carter, W. P. L. (2000a): "Documentation of the SAPRC-99 Chemical Mechanism for VOC Reactivity Assessment," Report to the California Air Resources Board, Contracts 92-329 and 95-308, May 8. Available at http://cert.ucr.edu/~carter/absts.htm#saprc99 and http://www.cert.ucr.edu/~carter /reactdat.htm.

Carter, W. P. L. (2000b): "Implementation of the SAPRC-99 Chemical Mechanism into the Models-3 Framework," Report to the United States Environmental Protection Agency, January 29. Available at http://www.cert.ucr.edu/~carter/absts.htm#s99mod3.

Carter, W. P. L. (2002): "Development of a Next Generation Environmental Chamber Facility for Chemical Mechanism and VOC Reactivity Research," Draft Research Plan and First Progress Report to the United States Environmental Protection Agency Cooperative Agreement CR 827331-01-0, January 3. Available at http://www.cert.ucr.edu/~carter/epacham.

Carter, W. P. L. (2004): “Evaluation of a Gas-Phase Atmospheric Reaction Mechanism for Low NO_x Conditions,” Final Report to California Air Resources Board Contract No. 01-305, May 5. Available at http://www.cert.ucr.edu/~carter/absts.htm#lnoxrpt.

Carter, W. P. L. (2007): "Investigation of the Atmospheric Ozone Impacts of Methyl Iodide," Final Report to Arysta LifeScience Corporation, Contract UCR-07041867, July 31. Available at http://www.cert.ucr.edu/~carter/absts.htm#ch3irep.

Carter, W. P. L. (2009a): "Development of the SAPRC-07 Chemical Mechanism and Updated Ozone Reactivity Scale," Revised final report to the California Air Resources Board Contract No. 03-318, June 22. Available at http://www.cert.ucr.edu/~carter/SAPRC.

Carter, W. P. L. (2009b). "Investigation of the Atmospheric Ozone Impacts of Trans 1,3,3,3-Tetra-fluoropropene," Final Report to Honeywell International Inc. Contract UCR-09010016, February 9. Available at http://www.cert.ucr.edu/~carter/absts.htm #ZEErept.

Carter, W. P. L. (2009c). "Investigation of the Atmospheric Ozone Impacts of 2,3,3,3-Tetra-fluoropropene," Final Report to Honeywell International Inc. Contract UCR-09010016, June 2. Available at http://www.cert.ucr.edu/~carter/absts.htm #YFrept.

Carter, W. P. L. and R. Atkinson (1987): “An Experimental Study of Incremental Hydrocarbon Reactivity,” Environ. Sci. Technol., 21, 670-679

Carter, W. P. L. and R. Atkinson (1989): “A Computer Modeling Study of Incremental Hydrocarbon Reactivity”, Environ. Sci. Technol., 23, 864.

Carter, W. P .L., and Lurmann, F. W. (1991) Evaluation of a detailed gas-phase atmospheric reaction mechanism using environmental chamber data. Atmos. Environ. 25A:2771-2806.

Carter, W. P. L., J. A. Pierce, I. L. Malkina, D. Luo and W. D. Long (1993): “Environmental Chamber Studies of Maximum Incremental Reactivities of Volatile Organic Compounds,” Report to Coordinating Research Council, Project No. ME-9, California Air Resources Board Contract No. A032-0692; South Coast Air Quality Management District Contract No. C91323, United States Environmental Protection Agency Cooperative Agreement No. CR-814396-01-0, University Corporation for Atmospheric Research Contract No. 59166, and Dow Corning Corporation. April 1. Available at http://www.cert.ucr.edu/~carter/absts.htm#rct1rept

Carter, W. P. L., D. Luo, I. L. Malkina, and J. A. Pierce (1995a): “Environmental Chamber Studies of Atmospheric Reactivities of Volatile Organic Compounds. Effects of Varying Chamber and Light Source,” Final report to National Renewable Energy Laboratory, Contract XZ-2-12075, Coordinating Research Council, Inc., Project M-9, California Air Resources Board, Contract A032-0692, and South Coast Air Quality Management District, Contract C91323, March 26.

Carter, W. P. L., D. Luo, I. L. Malkina, and D. Fitz (1995b): “The University of California, Riverside Environmental Chamber Data Base for Evaluating Oxidant Mechanism. Indoor Chamber Experiments through 1993,” Report submitted to the U. S. Environmental Protection Agency, EPA/AREAL, Research Triangle Park, NC., March 20..

Carter, W. P. L., D. Luo, I. L. Malkina, and J. A. Pierce (1995c): "Environmental Chamber Studies of Atmospheric Reactivities of Volatile Organic Compounds. Effects of Varying ROG Surrogate and NO_x," Final report to Coordinating Research Council, Inc., Project ME-9, California Air Resources Board, Contract A032-0692, and South Coast Air Quality Management District, Contract C91323. March 24. Available at http://www.cert.ucr.edu/~carter/absts.htm#rct2rept.

Carter, W. P. L. and I. L. Malkina (2005): "Evaluation of Atmospheric Impacts of Selected Coatings VOC Emissions," Final report to the California Air Resources Board Contract No. 00-333, March 15. Available at http://www.cert.ucr.edu/~carter/absts.htm#coatrpt.

Carter, W. P. L., D. R. Cocker III, D. R. Fitz, I. L. Malkina, K. Bumiller, C. G. Sauer, J. T. Pisano, C. Bufalino, and C. Song (2005a): "A New Environmental Chamber for Evaluation of Gas-Phase Chemical Mechanisms and Secondary Aerosol Formation", Atmos. Environ. 39 7768-7788.

Carter, W. P. L., I. L. Malkina, D. R. Cocker III, and C. Song (2005b): "Environmental Chamber Studies of VOC Species in Architectural Coatings and Mobile Source Emissions," Final Report to the South Coast Air Quality Management District Contract No. 03468, July 5. Available at http://www.cert.ucr.edu/~carter/absts.htm#scaqcham.

Carter, W. P. L. and I. L. Malkina (2007): "Investigation of the Atmospheric Impacts of Selected Pesticides," Final Report to the California Air Resources Board Contract 04-334, January 10. Available at http://www.cert.ucr.edu/~carter/absts.htm#pestrep.

Cocker, D. R., R. C. Flagan, and J. H. Seinfeld. (2001). "State-of-the-Art Chamber Facility for Studying Atmospheric Aerosol Chemistry," Environ. Sci. Technol. 35, 2594-2601.

Collins D. R., R. C. Flagan, and J. H. Seinfeld (2002). "Improved inversion of scanning DMA data," Aerosol Science Technology, 36, 2-9.

Dimitriades, B. (1999): "Scientific Basis of an Improved EPA Policy on Control of Organic Emissions for Ambient Ozone Reduction," J. Air & Waste Manage. Assoc. 49, 831-838

EPA (2005): "Interim Guidance on Control of Volatile Organic Compounds in Ozone State Implementation Plans," Federal Register, 70, 54046-54051, September 13.

Johnson, G. M. (1983): "Factors Affecting Oxidant Formation in Sydney Air," in "The Urban Atmosphere -- Sydney, a Case Study." Eds. J. N. Carras and G. M. Johnson (CSIRO, Melbourne), pp. 393-408.

Kwok, E. S. C., and R. Atkinson (1995): "Estimation of Hydroxyl Radical Reaction Rate Constants for Gas-Phase Organic Compounds Using a Structure-Reactivity Relationship: An Update," Atmos. Environ 29, 1685-1695.

Mellouki, A.; Teton, S.; Le Bras, G (1995): "Kinetics of OH reactions with a series of ethers," Int. J. Chem. Kinet. 27, 791-805.

RRWG (1999): "VOC Reactivity Policy White Paper," Prepared by the Reactivity Research Work Group Policy Team, October 1. Available at http://www.narsto.org/section.src?SID=10.

Tuazon, E. C., W. P. L. Carter, S. M. Aschmann, and R. Atkinson (1991): "Products of the Gas-Phase Reaction of Methyl tert-Butyl Ether with the OH Radical in the Presence of NO_x," Int. J. Chem. Kinet., 23, 1003-1015.

Tuazon, E. C., S. M. Aschmann, N. Nishino, J. Arey and R. Atkinson (2005): "Kinetics and Products of the OH Radical-Initiated Reaction of 3-Methyl-2-butenal," Phys. Chem. Chem. Phys., 7, 2298-2304.

Scanlon, J. T.; Willis, D. E (1985): "Calculation of flame ionization detector relative response factors using the effective carbon number concept," J. Chromat. Sci. 23, 333-340.

Smith, D. F, T. E. Kleindienst, E. E. Hudgens, C. D. McIver and J. J. Bufalini (1991): "The Photooxidation of Methyl Tertiary Butyl Ether," Int. J. Chem. Kinet. 23, 907-924.

Zafonte, L., P. L. Rieger, and J. R. Holmes (1977): "Nitrogen Dioxide Photolysis in the Los Angeles Atmosphere," Environ. Sci. Technol. 11, 483-487.

APPENDIX A. BASE MECHANISM LISTING

Table A-1. List of model species used in the base SAPRC-07 mechanism, including the VOC species used in the chamber and atmospheric reactivity simulations.

Name	Description
Constant Species.	
O2	Oxygen
M	Air
H2O	Water
H2	Hydrogen Molecules
HV	Light
Active Inorganic Species.	
O3	Ozone
NO	Nitric Oxide
NO2	Nitrogen Dioxide
NO3	Nitrate Radical
N2O5	Nitrogen Pentoxide
HONO	Nitrous Acid
HNO3	Nitric Acid
HNO4	Peroxynitric Acid
HO2H	Hydrogen Peroxide
CO	Carbon Monoxide
SO2	Sulfur Dioxide
H2	Hydrogen
Active Radical Species and Operators.	
OH	Hydroxyl Radicals
HO2	Hydroperoxide Radicals
MEO2	Methyl Peroxy Radicals
RO2C	Peroxy Radical Operator representing NO to NO_2 and NO_3 to NO_2 conversions, and the effects of peroxy radical reactions on acyl peroxy and other peroxy radicals.
RO2XC	Peroxy Radical Operator representing NO consumption (used in conjunction with organic nitrate formation), and the effects of peroxy radical reactions on NO_3, acyl peroxy radicals, and other peroxy radicals.
MECO3	Acetyl Peroxy Radicals
RCO3	Peroxy Propionyl and higher peroxy acyl Radicals
BZCO3	Peroxyacyl radical formed from Aromatic Aldehydes
MACO3	Peroxyacyl radicals formed from methacrolein and other acroleins.
Steady State Radical Species	
O3P	Ground State Oxygen Atoms
O1D	Excited Oxygen Atoms
TBUO	t-Butoxy Radicals
BZO	Phenoxy Radicals

Table A-1 (continued)

Name	Description
PAN and PAN Analogues	
PAN	Peroxy Acetyl Nitrate
PAN2	PPN and other higher alkyl PAN analogues
PBZN	PAN analogues formed from Aromatic Aldehydes
MAPAN	PAN analogue formed from Methacrolein
Explicit and Lumped Molecule Reactive Organic Product Species	
HCHO	Formaldehyde
CCHO	Acetaldehyde
RCHO	Lumped C3+ Aldehydes. Mechanism based on propionaldehyde
ACET	Acetone
MEK	Ketones and other non-aldehyde oxygenated products that react with OH radicals faster than 5×10^{-13} but slower than 5×10^{-12} cm^3 $molec^{-2}$ sec^{-1}. Mechanism based on methyl ethyl ketone.
MEOH	Methanol
HCOOH	Formic Acid
CCOOH	Acetic Acid. Also used for peroxyacetic acid.
RCOOH	Higher organic acids and peroxy acids. Mechanism based on propionic acid.
COOH	Methyl Hydroperoxide
ROOH	Lumped organic hydroperoxides with 2-4 carbons. Mechanism based n-propyl hydroperoxide.
R6OOH	Lumped organic hydroperoxides with 5 or more carbons (other than those formed following OH addition to aromatic rings, which are represented separately). Mechanism based on 3-hexyl hydroperoxide.
RAOOH	Organic hydroperoxides formed following OH addition to aromatic rings, which is represented separately because of their probable role in SOA formation. Mechanism based on two isomers expected to be formed in the m-xylene system.
GLY	Glyoxal
MGLY	Methyl Glyoxal
BACL	Biacetyl
CRES	Phenols and Cresols. Mechanism based on o-cresol.
NPHE	Nitrophenols
BALD	Aromatic aldehydes. Mechanism based on benzaldehyde
MACR	Methacrolein
MVK	Methyl Vinyl Ketone
IPRD	Lumped isoprene product species. Mechanism based on that of Carter and Atkinson (1996).
Aromatic unsaturated ring fragmentation products (see discussion of aromatic mechanisms)	
AFG1	Lumped photoreactive monounsaturated dicarbonyl aromatic fragmentation products that photolyze to form radicals.
AFG2	Lumped photoreactive monounsaturated dicarbonyl aromatic fragmentation products that photolyze to form non-radical products
AFG3	Lumped diunsaturatred dicarbonyl aromatic fragmentation product.

Table A-1 (continued)

Name	Description
Lumped Parameter Products	
PROD2	Ketones and other non-aldehyde oxygenated products that react with OH radicals faster than 5 x 10^{-12} cm^3 $molec^{-2}$ sec^{-1}. Mechanism based on $CH_3C(O)CH_2CH_2CH_2OH$, $CH_3C(O)$-$CH_2CH(CH_3)CH_2OH$, $CH_3CH_2C(O)CH_2CH_2CH(CH_3)OH$, $CH_3CH_2C(O)CH_2CH_2CH(OH)$-$CH_2CH_3$, and $CH_3CH_2CH_2CH(OH)CH_2$-$CH_2C(O)CH_2CH_3$ (PROD2-1 through 5), each weighed equally.
RNO3	Lumped Organic Nitrates. Mechanism based on $CH_3CH_2CH(CH_3)ONO_2$, $CH_3CH(OH)CH_2$-$CH_2CH_2ONO_2$, $CH_3CH_2CH(CH_3)CH(CH_3)ONO_2$, $CH_3CH_2CH_2CH_2CH_2CH(ONO_2)CH_2OH$, $CH_3CH_2C(CH_3)(ONO_2)CH_2CH(CH_3)CH_3$, and $CH_3CH_2CH_2CH_2CH_2CH_2CH_2CH(ONO_2)$-$CH_2CH_3$ (RNO3-1 through 6), each weighed equally.
Steady state operators used to represent radical or product formation in peroxy radical reactions.	
xHO2	Formation of HO_2 from alkoxy radicals formed in peroxy radical reactions with NO and NO_3 (100% yields) and RO_2 (50% yields)
xOH	As above, but for OH
xNO2	As above, but for NO_2
xMEO2	As above, but for MEO2
xMECO3	As above, but for MECO3
xRCO3	As above, but for RCO3
xMACO3	As above, but for MACO3
xTBUO	As above, but for TBUO
xCO	As above, but for CO
xHNO3	As above, but for HNO3
xHCHO	As above, but for HCHO
xCCHO	As above, but for CCHO
xRCHO	As above, but for RCHO
xACET	As above, but for ACET
xMEK	As above, but for MEK
xPROD2	As above, but for PROD2
xGLY	As above, but for GLY
xMGLY	As above, but for MGLY
xBACL	As above, but for BACL
xBALD	As above, but for BALD
xAFG1	As above, but for AFG1
xAFG2	As above, but for AFG2
xAFG3	As above, but for AFG3
xMACR	As above, but for MACR
xMVK	As above, but for MVK
xIPRD	As above, but for IPRD
xRNO3	As above, but for RNO3
xHCOOH	As above, but for HCOOH
xCCOOH	As above, but for CCOOH
xRCOOH	As above, but for RCOOH
zRNO3	Formation of RNO3 in the RO_2 + NO, reaction, or formation of corresponding non-nitrate products (represented by PROD2) formed from alkoxy radicals formed in RO_2 + NO_3 and (in 50% yields) RO_2 + RO_2 reactions.

Table A-1 (continued)

Name	Description
yROOH	Formation of ROOH following $RO_2 + HO_2$ reactions, or formation of H-shift disproportionation products (represented by MEK) in the $RO_2 + RCO_3$ and (in 50% yields) $RO_2 + RO_2$ reactions.
yR6OOH	As above, but with the $RO_2 + HO_2$ product represented by R6OOH and the H-shift products are represented by PROD2.
yRAOOH	As above, but with the $RO_2 + HO_2$ product represented by R6OOH
Non-Reacting Species	
CO2	Carbon Dioxide
SULF	Sulfates (SO_3 or H_2SO_4)
XC	Lost Carbon or carbon in unreactive products
XN	Lost Nitrogen or nitrogen in unreactive products
Primary Organics Represented explicitly	
CH4	Methane
ETHENE	Ethene
ISOPRENE	Isoprene
ACETYLEN	Acetylene
BENZENE	Benzene
ETHANE	Ethane (not part of the base mechanism, but used in atmospheric reactivity simulations)
Organics represented explicitly in the chamber simulations (not used in the atmospheric simulations)	
N-C4	n-Butane
N-C8	n-Octane
PROPENE	Propene
T-2-BUTE	trans-2-Butene
TOLUENE	Toluene
M-XYLENE	m-Xylene
Lumped model species used in the atmospheric reactivity simulations (not used in chamber simulations)	
ALK1	Alkanes and other non-aromatic compounds that react only with OH, and have kOH (OH radical rate constant) between 2 and 5×10^2 ppm^{-1} min^{-1}. (Primarily ethane)
ALK2	Alkanes and other non-aromatic compounds that react only with OH, and have kOH between 5×10^2 and 2.5×10^3 ppm^{-1} min^{-1}. (Primarily propane)
ALK3	Alkanes and other non-aromatic compounds that react only with OH, and have kOH between 2.5×10^3 and 5×10^3 ppm^{-1} min^{-1}.
ALK4	Alkanes and other non-aromatic compounds that react only with OH, and have kOH between 5×10^3 and 1×10^4 ppm^{-1} min^{-1}.
ALK5	Alkanes and other non-aromatic compounds that react only with OH, and have kOH greater than 1×10^4 ppm-1 min-1.
ARO1	Aromatics with kOH < 2×10^4 ppm^{-1} min^{-1}.
ARO2	Aromatics with kOH > 2×10^4 ppm^{-1} min^{-1}.
OLE1	Alkenes (other than ethene) with kOH < 7×10^4 ppm^{-1} min^{-1}.
OLE2	Alkenes with kOH > 7×10^4 ppm^{-1} min^{-1}.
TERP	Terpenes

Table A-2. Reactions and rate constants in the base SAPRC-07 mechanism used in this work. See Carter (2009a) for documentation.

Label	Reaction and Products [a]	Rate Parameters [b] k(300)	A	Ea	B
Inorganic Reactions					
1	NO2 + HV = NO + O3P	Phot Set= NO2-06			
2	O3P + O2 + M = O3 + M	5.68E-34	5.68E-34	0.00	-2.60
3	O3P + O3 = #2 O2	8.34E-15	8.00E-12	4.09	
4	O3P + NO = NO2	1.64E-12	Falloff, F=0.60, N=1.00		
		0:	9.00E-32	0.00	-1.50
		inf:	3.00E-11	0.00	0.00
5	O3P + NO2 = NO + O2	1.03E-11	5.50E-12	-0.37	
6	O3P + NO2 = NO3	3.24E-12	Falloff, F=0.60, N=1.00		
		0:	2.50E-31	0.00	-1.80
		inf:	2.20E-11	0.00	-0.70
7	O3 + NO = NO2 + O2	2.02E-14	3.00E-12	2.98	
8	O3 + NO2 = O2 + NO3	3.72E-17	1.40E-13	4.91	
9	NO + NO3 = #2 NO2	2.60E-11	1.80E-11	-0.22	
10	NO + NO + O2 = #2 NO2	1.93E-38	3.30E-39	-1.05	
11	NO2 + NO3 = N2O5	1.24E-12	Falloff, F=0.35, N=1.33		
		0:	3.60E-30	0.00	-4.10
		inf:	1.90E-12	0.00	0.20
12	N2O5 = NO2 + NO3	5.69E-02	Falloff, F=0.35, N=1.33		
		0:	1.30E-03	21.86	-3.50
		inf:	9.70E+14	22.02	0.10
13	N2O5 + H2O = #2 HNO3	2.50E-22			
14	N2O5 + H2O + H2O = #2 HNO3 + H2O	1.80E-39			
	N2O5 + HV = NO3 + NO + O3P	(Slow)			
	N2O5 + HV = NO3 + NO2	(Slow)			
15	NO2 + NO3 = NO + NO2 + O2	6.75E-16	4.50E-14	2.50	
16	NO3 + HV = NO + O2	Phot Set= NO3NO-06			
17	NO3 + HV = NO2 + O3P	Phot Set= NO3NO2-6			
18	O3 + HV = O1D + O2	Phot Set= O3O1D-06			
19	O3 + HV = O3P + O2	Phot Set= O3O3P-06			
20	O1D + H2O = #2 OH	1.99E-10			
21	O1D + M = O3P + M	3.28E-11	2.38E-11	-0.19	
22	OH + NO = HONO	7.31E-12	Falloff, F=0.60, N=1.00		
		0:	7.00E-31	0.00	-2.60
		inf:	3.60E-11	0.00	-0.10
23	HONO + HV = OH + NO	Phot Set= HONO-06			
24	OH + HONO = H2O + NO2	5.95E-12	2.50E-12	-0.52	
25	OH + NO2 = HNO3	1.05E-11	Falloff, F=0.60, N=1.00		
		0:	1.80E-30	0.00	-3.00
		inf:	2.80E-11	0.00	0.00
26	OH + NO3 = HO2 + NO2	2.00E-11			

Table A-2 (continued)

Label	Reaction and Products [a]	Rate Parameters [b] k(300)	A	Ea	B
27	OH + HNO3 = H2O + NO3	1.51E-13	k = k0+k3M/(1+k3M/k2)		
			k0: 2.40E-14	-0.91	0.00
			k2: 2.70E-17	-4.37	0.00
			k3: 6.50E-34	-2.65	0.00
28	HNO3 + HV = OH + NO2		Phot Set= HNO3		
29	OH + CO = HO2 + CO2	2.28E-13	k = k1 + k2 [M]		
			k1: 1.44E-13	0.00	0.00
			k2: 3.43E-33	0.00	0.00
30	OH + O3 = HO2 + O2	7.41E-14	1.70E-12	1.87	
31	HO2 + NO = OH + NO2	8.85E-12	3.60E-12	-0.54	
32	HO2 + NO2 = HNO4	1.12E-12	Falloff, F=0.60, N=1.00		
			0: 2.00E-31	0.00	-3.40
			inf: 2.90E-12	0.00	-1.10
33	HNO4 = HO2 + NO2	1.07E-01	Falloff, F=0.60, N=1.00		
			0: 3.72E-05	21.16	-2.40
			inf: 5.42E+15	22.20	-2.30
34	HNO4 + HV = #.61 {HO2 + NO2} + #.39 {OH + NO3}		Phot Set= HNO4-06		
35	HNO4 + OH = H2O + NO2 + O2	4.61E-12	1.30E-12	-0.76	
36	HO2 + O3 = OH + #2 O2	2.05E-15	2.03E-16	-1.38	4.57
37	HO2 + HO2 = HO2H + O2	2.84E-12	k = k1 + k2 [M]		
			k1: 2.20E-13	-1.19	0.00
			k2: 1.90E-33	-1.95	0.00
38	HO2 + HO2 + H2O = HO2H + O2 + H2O	6.09E-30	k = k1 + k2 [M]		
			k1: 3.08E-34	-5.56	0.00
			k2: 2.66E-54	-6.32	0.00
39	NO3 + HO2 = #.8 {OH + NO2 + O2} + #.2 {HNO3 + O2}	4.00E-12			
40	NO3 + NO3 = #2 NO2 + O2	2.41E-16	8.50E-13	4.87	
41	HO2H + HV = #2 OH		Phot Set= H2O2		
42	HO2H + OH = HO2 + H2O	1.80E-12	1.80E-12	0.00	
43	OH + HO2 = H2O + O2	1.10E-10	4.80E-11	-0.50	
44	OH + SO2 = HO2 + SULF	9.49E-13	Falloff, F=0.60, N=1.00		
			0: 3.30E-31	0.00	-4.30
			inf: 1.60E-12	0.00	0.00
45	OH + H2 = HO2 + H2O	7.02E-15	7.70E-12	4.17	
Methyl peroxy and methoxy reactions					
BR01	MEO2 + NO = NO2 + HCHO + HO2	7.64E-12	2.30E-12	-0.72	
BR02	MEO2 + HO2 = COOH + O2	4.65E-12	3.46E-13	-1.55	0.36
BR03	MEO2 + HO2 = HCHO + O2 + H2O	4.50E-13	3.34E-14	-1.55	-3.53
BR04	MEO2 + NO3 = HCHO + HO2 + NO2	1.30E-12			
BR05	MEO2 + MEO2 = MEOH + HCHO + O2	2.16E-13	6.39E-14	-0.73	-1.80
BR06	MEO2 + MEO2 = #2 {HCHO + HO2}	1.31E-13	7.40E-13	1.03	
Active Peroxy Racical Operators					
BR07	RO2C + NO = NO2	9.23E-12	2.60E-12	-0.76	

Table A-2 (continued)

Label	Reaction and Products [a]	Rate Parameters [b] k(300)	A	Ea	B
BR08	RO2C + HO2 =	7.63E-12	3.80E-13	-1.79	
BR09	RO2C + NO3 = NO2	2.30E-12			
BR10	RO2C + MEO2 = #.5 {RO2C + xHO2 + xHCHO + O2} + #.25 {HCHO + MEOH}	2.00E-13			
BR11	RO2C + RO2C =	3.50E-14			
BR12	RO2XC + NO = XN	Same k as rxn BR07			
BR13	RO2XC + HO2 =	Same k as rxn BR08			
BR14	RO2XC + NO3 = NO2	Same k as rxn BR09			
BR15	RO2XC + MEO2 = #.5 {RO2C + xHO2 + xHCHO + O2} + #.25 {HCHO + MEOH}	Same k as rxn BR10			
BR16	RO2XC + RO2C =	Same k as rxn BR11			
BR17	RO2XC + RO2XC =	Same k as rxn BR11			
Reactions of Acyl Peroxy Radicals, PAN, and PAN analogues					
BR18	MECO3 + NO2 = PAN	9.37E-12	Falloff, F=0.30, N=1.41		
		0:	2.70E-28	0.00	-7.10
		inf:	1.21E-11	0.00	-0.90
BR19	PAN = MECO3 + NO2	6.27E-04	Falloff, F=0.30, N=1.41		
		0:	4.90E-03	24.05	0.00
		inf:	4.00E+16	27.03	0.00
BR20	PAN + HV = #.6 {MECO3 + NO2} + #.4 {MEO2 + CO2 + NO3}	Phot Set= PAN			
BR21	MECO3 + NO = MEO2 + CO2 + NO2	1.97E-11	7.50E-12	-0.58	
BR22	MECO3 + HO2 = CCOOH + #.7 O2 + #.3 O3	1.36E-11	5.20E-13	-1.95	
BR23	MECO3 + NO3 = MEO2 + CO2 + NO2 + O2	Same k as rxn BR09			
BR24	MECO3 + MEO2 = #.1 {CCOOH + HCHO + O2} + #.9 {HCHO + HO2 + MEO2 + CO2}	1.06E-11	2.00E-12	-0.99	
BR25	MECO3 + RO2C = MEO2 + CO2	1.56E-11	4.40E-13	-2.13	
BR26	MECO3 + RO2XC = MEO2 + CO2	Same k as rxn BR25			
BR27	MECO3 + MECO3 = #2 {MEO2 + CO2} + O2	1.54E-11	2.90E-12	-0.99	
BR28	RCO3 + NO2 = PAN2	1.21E-11	1.21E-11	0.00	-1.07
BR29	PAN2 = RCO3 + NO2	5.48E-04	8.30E+16	27.70	
BR30	PAN2 + HV = #.6 {RCO3 + NO2} + #.4 {RO2C + xHO2 + yROOH + xCCHO + CO2 + NO3}	Phot Set= PAN			
BR31	RCO3 + NO = NO2 + RO2C + xHO2 + yROOH + xCCHO + CO2	2.08E-11	6.70E-12	-0.68	
BR32	RCO3 + HO2 = RCOOH + #.75 O2 + #.25 O3	Same k as rxn BR22			
BR33	RCO3 + NO3 = NO2 + RO2C + xHO2 + yROOH + xCCHO + CO2 + O2	Same k as rxn BR09			
BR34	RCO3 + MEO2 = HCHO + HO2 + RO2C + xHO2 + xCCHO + yROOH + CO2	Same k as rxn BR24			
BR35	RCO3 + RO2C = xHO2 + xCCHO + yROOH + CO2	Same k as rxn BR25			
BR36	RCO3 + RO2XC = xHO2 + xCCHO + yROOH + CO2	Same k as rxn BR25			
BR37	RCO3 + MECO3 = #2 CO2 + MEO2 + RO2C + xHO2 + yROOH + xCCHO + O2	Same k as rxn BR27			

Table A-2 (continued)

Label	Reaction and Products [a]	Rate Parameters [b] k(300)	A	Ea	B
BR38	RCO3 + RCO3 = #2 {RO2C + xHO2 + xCCHO + yROOH + CO2}	Same k as rxn BR27			
BR39	BZCO3 + NO2 = PBZN	1.37E-11			
BR40	PBZN = BZCO3 + NO2	4.27E-04	7.90E+16	27.82	
BR41	PBZN + HV = #.6 {BZCO3 + NO2} + #.4 {CO2 + BZO + RO2C + NO3}	Phot Set= PAN			
BR42	BZCO3 + NO = NO2 + CO2 + BZO + RO2C	Same k as rxn BR31			
BR43	BZCO3 + HO2 = RCOOH + #.75 O2 + #.25 O3 + #4 XC	Same k as rxn BR22			
BR44	BZCO3 + NO3 = NO2 + CO2 + BZO + RO2C + O2	Same k as rxn BR09			
BR45	BZCO3 + MEO2 = HCHO + HO2 + RO2C + BZO + CO2	Same k as rxn BR24			
BR46	BZCO3 + RO2C = RO2C + BZO + CO2	Same k as rxn BR25			
BR47	BZCO3 + RO2XC = RO2C + BZO + CO2	Same k as rxn BR25			
BR48	BZCO3 + MECO3 = #2 CO2 + MEO2 + BZO + RO2C	Same k as rxn BR27			
BR49	BZCO3 + RCO3 = #2 CO2 + RO2C + xHO2 + yROOH + xCCHO + BZO + RO2C	Same k as rxn BR27			
BR50	BZCO3 + BZCO3 = #2 {BZO + RO2C + CO2}	Same k as rxn BR27			
BR51	MACO3 + NO2 = MAPAN	Same k as rxn BR28			
BR52	MAPAN = MACO3 + NO2	4.79E-04	1.60E+16	26.80	
BR53	MAPAN + HV = #.6 {MACO3 + NO2} + #.4 {CO2 + HCHO + MECO3 + NO3}	Phot Set= PAN			
BR54	MACO3 + NO = NO2 + CO2 + HCHO + MECO3	Same k as rxn BR31			
BR55	MACO3 + HO2 = RCOOH + #.75 O2 + #.25 O3 + XC	Same k as rxn BR22			
BR56	MACO3 + NO3 = NO2 + CO2 + HCHO + MECO3 + O2	Same k as rxn BR09			
BR57	MACO3 + MEO2 = #2 HCHO + HO2 + CO2 + MECO3	Same k as rxn BR24			
BR58	MACO3 + RO2C = CO2 + HCHO + MECO3	Same k as rxn BR25			
BR59	MACO3 + RO2XC = CO2 + HCHO + MECO3	Same k as rxn BR25			
BR60	MACO3 + MECO3 = #2 CO2 + MEO2 + HCHO + MECO3 + O2	Same k as rxn BR27			
BR61	MACO3 + RCO3 = HCHO + MECO3 + RO2C + xHO2 + yROOH + xCCHO + #2 CO2	Same k as rxn BR27			
BR62	MACO3 + BZCO3 = HCHO + MECO3 + BZO + RO2C + #2 CO2	Same k as rxn BR27			
BR63	MACO3 + MACO3 = #2 {HCHO + MECO3 + CO2}	Same k as rxn BR27			
Other Organic Radical Species					
BR64	TBUO + NO2 = RNO3 + #-2 XC	2.40E-11			
BR65	TBUO = ACET + MEO2	1.18E+03	7.50E+14	16.20	
BR66	BZO + NO2 = NPHE	3.79E-11	2.30E-11	-0.30	
BR67	BZO + HO2 = CRES + #-1 XC	Same k as rxn BR08			
BR68	BZO = CRES + RO2C + xHO2 + #-1 XC	1.00E-03			

Table A-2 (continued)

Label	Reaction and Products [a]	Rate Parameters [b] k(300)	A	Ea	B
Steady-State Peroxy Radical operators (for formation of inorganic and radical products) [c]					
RO01	xHO2 = HO2	k is variable parameter: RO2RO			
RO02	xHO2 =	k is variable parameter: RO2XRO			
RO03	xOH = OH	k is variable parameter: RO2RO			
RO04	xOH =	k is variable parameter: RO2XRO			
RO05	xNO2 = NO2	k is variable parameter: RO2RO			
RO06	xNO2 = XN	k is variable parameter: RO2XRO			
RO07	xMEO2 = MEO2	k is variable parameter: RO2RO			
RO08	xMEO2 = XC	k is variable parameter: RO2XRO			
RO09	xMECO3 = MECO3	k is variable parameter: RO2RO			
RO10	xMECO3 = #2 XC	k is variable parameter: RO2XRO			
RO11	xRCO3 = RCO3	k is variable parameter: RO2RO			
RO12	xRCO3 = #3 XC	k is variable parameter: RO2XRO			
RO13	xMACO3 = MACO3	k is variable parameter: RO2RO			
RO14	xMACO3 = #4 XC	k is variable parameter: RO2XRO			
RO15	xTBUO = TBUO	k is variable parameter: RO2RO			
RO16	xTBUO = #4 XC	k is variable parameter: RO2XRO			
RO17	xCO = CO	k is variable parameter: RO2RO			
RO18	xCO = XC	k is variable parameter: RO2XRO			
Explicit and Lumped Molecule Organic Products					
BP01	HCHO + HV = #2 HO2 + CO	Phot Set= HCHOR-06			
BP02	HCHO + HV = H2 + CO	Phot Set= HCHOM-06			
BP03	HCHO + OH = HO2 + CO + H2O	8.47E-12	5.40E-12	-0.27	
BP04	HCHO + HO2 = HOCOO	Assumed to be negligible			
BP07	HCHO + NO3 = HNO3 + HO2 + CO	6.06E-16	2.00E-12	4.83	
BP08	CCHO + OH = MECO3 + H2O	1.49E-11	4.40E-12	-0.73	
BP09	CCHO + HV = CO + HO2 + MEO2	Phot Set= CCHO_R			
BP10	CCHO + NO3 = HNO3 + MECO3	2.84E-15	1.40E-12	3.70	
BP11	RCHO + OH = #.965 RCO3 + #.035 {RO2C + xHO2 + xCO + xCCHO + yROOH}	1.97E-11	5.10E-12	-0.80	
BP12	RCHO + HV = RO2C + xHO2 + yROOH + xCCHO + CO + HO2	Phot Set= C2CHO			
BP13	RCHO + NO3 = HNO3 + RCO3	6.74E-15	1.40E-12	3.18	
BP14	ACET + OH = RO2C + xMECO3 + xHCHO + yROOH	1.91E-13	4.56E-14	-0.85	3.65
BP15	ACET + HV = #.62 MECO3 + #1.38 MEO2 + #.38 CO	Phot Set= ACET-06, qy= 0.5			
BP16	MEK + OH = #.967 RO2C + #.039 {RO2XC + zRNO3} + #.376 xHO2 + #.51 xMECO3 + #.074 xRCO3 + #.088 xHCHO + #.504 xCCHO + #.376 xRCHO + yROOH + #.3 XC	1.20E-12	1.30E-12	0.05	2.00
BP17	MEK + HV = MECO3 + RO2C + xHO2 + xCCHO + yROOH	Phot Set= MEK-06, qy= 0.175			
BP18	MEOH + OH = HCHO + HO2	9.02E-13	2.85E-12	0.69	
BP19	HCOOH + OH = HO2 + CO2	4.50E-13			

Table A-2 (continued)

Label	Reaction and Products [a]	Rate Parameters [b] k(300)	A	Ea	B
BP20	CCOOH + OH = #.509 MEO2 + #.491 RO2C + #.509 CO2 + #.491 xHO2 + #.491 xMGLY + #.491 yROOH + #-0.491 XC	7.26E-13	4.20E-14	-1.70	
BP21	RCOOH + OH = RO2C + xHO2 + #.143 CO2 + #.142 xCCHO + #.4 xRCHO + #.457 xBACL + yROOH + #-0.455 XC	1.20E-12			
BP22	COOH + OH = H2O + #.3 {HCHO + OH} + #.7 MEO2	7.40E-12	3.80E-12	-0.40	
BP23	COOH + HV = HCHO + HO2 + OH	Phot Set= COOH			
BP24	ROOH + OH = #.744 OH + #.251 RO2C + #.004 RO2XC + #.004 zRNO3 + #.744 RCHO + #.239 xHO2 + #.012 xOH + #.012 xHCHO + #.012 xCCHO + #.205 xRCHO + #.034 xPROD2 + #.256 yROOH + #-0.115 XC	2.50E-11			
BP25	ROOH + HV = RCHO + HO2 + OH	Phot Set= COOH			
BP26	R6OOH + OH = #.84 OH + #.222 RO2C + #.029 RO2XC + #.029 zRNO3 + #.84 PROD2 + #.09 xHO2 + #.041 xOH + #.02 xCCHO + #.075 xRCHO + #.084 xPROD2 + #.16 yROOH + #.02 XC	5.60E-11			
BP27	R6OOH + HV = OH + #.142 HO2 + #.782 RO2C + #.077 RO2XC + #.077 zRNO3 + #.085 RCHO + #.142 PROD2 + #.782 xHO2 + #.026 xCCHO + #.058 xRCHO + #.698 xPROD2 + #.858 yR6OOH + #.017 XC	Phot Set= COOH			
BP28	RAOOH + OH = #.139 OH + #.148 HO2 + #.589 RO2C + #.124 RO2XC + #.124 zRNO3 + #.074 PROD2 + #.147 MGLY + #.139 IPRD + #.565 xHO2 + #.024 xOH + #.448 xRCHO + #.026 xGLY + #.030 xMEK + #.252 xMGLY + #.073 xAFG1 + #.073 xAFG2 + #.713 yR6OOH + #2.674 XC	1.41E-10			
BP29	RAOOH + HV = OH + HO2 + #.5 {GLY + MGLY + AFG1 + AFG2} + #.5 XC	Phot Set= COOH			
BP30	GLY + HV = #2 {CO + HO2}	Phot Set= GLY-07R			
BP31	GLY + HV = HCHO + CO	Phot Set= GLY-07M			
BP32	GLY + OH = #.63 HO2 + #1.26 CO + #.37 RCO3 + #-.37 XC	1.10E-11			
BP33	GLY + NO3 = HNO3 + #.63 HO2 + #1.26 CO + #.37 RCO3 + #-.37 XC	1.02E-15	2.80E-12	4.72	
BP34	MGLY + HV = HO2 + CO + MECO3	Phot Set= MGLY-06			
BP35	MGLY + OH = CO + MECO3	1.50E-11			
BP36	MGLY + NO3 = HNO3 + CO + MECO3	2.53E-15	1.40E-12	3.77	
BP37	BACL + HV = #2 MECO3	Phot Set= BACL-07			
BP38	CRES + OH = #.2 BZO + #.8 {RO2C + xHO2 + yR6OOH} + #.25 xMGLY + #5.05 XC	4.03E-11	1.70E-12	-1.89	

Table A-2 (continued)

Label	Reaction and Products [a]	Rate Parameters [b] k(300)	A	Ea	B
BP39	CRES + NO3 = HNO3 + BZO + XC	1.40E-11			
BP40	NPHE + OH = BZO + XN	3.50E-12			
BP41	NPHE + HV = HONO + #6 XC	Phot Set= NO2-06, qy= 1.5e-3			
BP42	NPHE + HV = #6 XC + XN	Phot Set= NO2-06, qy= 1.5e-2			
BP43	BALD + OH = BZCO3	1.20E-11			
BP44	BALD + HV = #7 XC	Phot Set= BALD-06, qy= 0.06			
BP45	BALD + NO3 = HNO3 + BZCO3	2.73E-15	1.34E-12	3.70	
Lumped Unsaturated Aromatic Ring-Opening Products					
BP46	AFG1 + OH = #.217 MACO3 + #.723 RO2C + #.060 {RO2XC + zRNO3} + #.521 xHO2 + #.201 xMECO3 + #.334 xCO + #.407 xRCHO + #.129 xMEK + #.107 xGLY + #.267 xMGLY + #.783 yR6OOH + #.284 XC	7.40E-11			
BP47	AFG1 + O3 = #.826 OH + #.522 HO2 + #.652 RO2C + #.522 CO + #.174 CO2 + #.432 GLY + #.568 MGLY + #.652 xRCO3 + #.652 xHCHO + #.652 yR6OOH + #-.872 XC	9.66E-18			
BP48	AFG1 + HV = #1.023 HO2 + #.173 MEO2 + #.305 MECO3 + #.500 MACO3 + #.695 CO + #.195 GLY + #.305 MGLY + #.217 XC	Phot Set= AFG1			
BP49	AFG2 + OH = #.217 MACO3 + #.723 RO2C + #.060 {RO2XC + zRNO3} + #.521 xHO2 + #.201 xMECO3 + #.334 xCO + #.407 xRCHO + #.129 xMEK + #.107 xGLY + #.267 xMGLY + #.783 yR6OOH + #.284 XC	7.40E-11			
BP50	AFG2 + O3 = #.826 OH + #.522 HO2 + #.652 RO2C + #.522 CO + #.174 CO2 + #.432 GLY + #.568 MGLY + #.652 xRCO3 + #.652 xHCHO + #.652 yR6OOH + #-.872 XC	9.66E-18			
BP51	AFG2 + HV = PROD2 + #-1 XC	Phot Set= AFG1			
BP52	AFG3 + OH = #.206 MACO3 + #.733 RO2C + #.117 {RO2XC + zRNO3} + #.561 xHO2 + #.117 xMECO3 + #.114 xCO + #.274 xGLY + #.153 xMGLY + #.019 xBACL + #.195 xAFG1 + #.195 xAFG2 + #.231 xIPRD + #.794 yR6OOH + #.938 XC	9.35E-11			
BP53	AFG3 + O3 = #.471 OH + #.554 HO2 + #.013 MECO3 + #.258 RO2C + #.007 {RO2XC + zRNO3} + #.580 CO + #.190 CO2 + #.366 GLY + #.184 MGLY + #.350 AFG1 + #.350 AFG2 + #.139 AFG3 + #.003 MACR + #.004 MVK + #.003 IPRD + #.095 xHO2 + #.163 xRCO3 + #.163 xHCHO + #.095 xMGLY + #.264 yR6OOH + #-.575 XC	1.43E-17			
Isoprene Products					
BP54	MACR + OH = #.5 MACO3 + #.5 {RO2C + xHO2} + #.416 xCO + #.084 xHCHO + #.416 xMEK + #.084 xMGLY + #.5 yROOH + #-0.416 XC	2.84E-11	8.00E-12	-0.76	

Table A-2 (continued)

Label	Reaction and Products [a]	Rate Parameters [b] k(300)	A	Ea	B
BP55	MACR + O3 = #.208 OH + #.108 HO2 + #.1 RO2C + #.45 CO + #.117 CO2 + #.1 HCHO + #.9 MGLY + #.333 HCOOH + #.1 xRCO3 + #.1 xHCHO + #.1 yROOH + #-0.1 XC	1.28E-18	1.40E-15	4.17	
BP56	MACR + NO3 = #.5 {MACO3 + RO2C + HNO3 + xHO2 + xCO} + #.5 yROOH + #1.5 XC + #.5 XN	3.54E-15	1.50E-12	3.61	
BP57	MACR + O3P = RCHO + XC	6.34E-12			
BP58	MACR + HV = #.33 OH + #.67 HO2 + #.34 MECO3 + #.33 MACO3 + #.33 RO2C + #.67 CO + #.34 HCHO + #.33 xMECO3 + #.33 xHCHO + #.33 yROOH	Phot Set= MACR-06			
BP59	MVK + OH = #.975 RO2C + #.025 {RO2XC + zRNO3} + #.3 xHO2 + #.675 xMECO3 + #.3 xHCHO + #.675 xRCHO + #.3 xMGLY + yROOH + #-0.725 XC	1.99E-11	2.60E-12	-1.21	
BP60	MVK + O3 = #.164 OH + #.064 HO2 + #.05 {RO2C + xHO2} + #.475 CO + #.124 CO2 + #.05 HCHO + #.95 MGLY + #.351 HCOOH + #.05 xRCO3 + #.05 xHCHO + #.05 yROOH + #-0.05 XC	5.36E-18	8.50E-16	3.02	
BP61	MVK + NO3 = #4 XC + XN	(Slow)			
BP62	MVK + O3P = #.45 RCHO + #.55 MEK + #.45 XC	4.32E-12			
BP63	MVK + HV = #.4 MEO2 + #.6 CO + #.6 PROD2 + #.4 MACO3 + #-2.2 XC	Phot Set= MVK-06			
BP64	IPRD + OH = #.289 MACO3 + #.67 {RO2C + xHO2} + #.041 {RO2XC + zRNO3} + #.336 xCO + #.055 xHCHO + #.129 xCCHO + #.013 xRCHO + #.15 xMEK + #.332 xPROD2 + #.15 xGLY + #.174 xMGLY + #-0.504 XC + #.711 yR6OOH	6.19E-11			
BP65	IPRD + O3 = #.285 OH + #.4 HO2 + #.048 {RO2C + xRCO3} + #.498 CO + #.14 CO2 + #.124 HCHO + #.21 MEK + #.023 GLY + #.742 MGLY + #.1 HCOOH + #.372 RCOOH + #.047 xCCHO + #.001 xHCHO + #.048 yR6OOH + #-.329 XC	4.18E-18			
BP66	IPRD + NO3 = #.15 {MACO3 + HNO3} + #.799 {RO2C + xHO2} + #.051 {RO2XC + zRNO3} + #.572 xCO + #.227 xHCHO + #.218 xRCHO + #.008 xMGLY + #.572 xRNO3 + #.85 yR6OOH + #.278 XN + #-.815 XC	1.00E-13			
BP67	IPRD + HV = #1.233 HO2 + #.467 MECO3 + #.3 RCO3 + #1.233 CO + #.3 HCHO + #.467 CCHO + #.233 MEK + #-.233 XC	Phot Set= MACR-06			

Table A-2 (continued)

Label	Reaction and Products [a]	Rate Parameters [b] k(300)	A	Ea	B
Lumped Parameter Organic Products					
BP68	PROD2 + OH = #.472 HO2 + #.379 xHO2 + #.029 xMECO3 + #.049 xRCO3 + #.473 RO2C + #.071 RO2XC + #.071 zRNO3 + #.002 HCHO + #.211 xHCHO + #.001 CCHO + #.083 xCCHO + #.143 RCHO + #.402 xRCHO + #.115 xMEK + #.329 PROD2 + #.007 xPROD2 + #.528 yR6OOH + #.877 XC	1.55E-11			
BP69	PROD2 + HV = #.913 xHO2 + #.4 MECO3 + #.6 RCO3 + #1.59 RO2C + #.087 RO2XC + #.087 zRNO3 + #.303 xHCHO + #.163 xCCHO + #.78 xRCHO + yR6OOH + #-.091 XC	Phot Set= MEK-06, qy= 4.86e-3			
BP70	RNO3 + OH = #.189 HO2 + #.305 xHO2 + #.019 NO2 + #.313 xNO2 + #.976 RO2C + #.175 RO2XC + #.175 zRNO3 + #.011 xHCHO + #.429 xCCHO + #.001 RCHO + #.036 xRCHO + #.004 xACET + #.01 MEK + #.17 xMEK + #.008 PROD2 + #.031 xPROD2 + #.189 RNO3 + #.305 xRNO3 + #.157 yROOH + #.636 yR6OOH + #.174 XN + #.04 XC	7.20E-12			
BP71	RNO3 + HV = #.344 HO2 + #.554 xHO2 + NO2 + #.721 RO2C + #.102 RO2XC + #.102 zRNO3 + #.074 HCHO + #.061 xHCHO + #.214 CCHO + #.23 xCCHO + #.074 RCHO + #.063 xRCHO + #.008 xACET + #.124 MEK + #.083 xMEK + #.19 PROD2 + #.261 xPROD2 + #.066 yROOH + #.591 yR6OOH + #.396 XC	Phot Set= IC3ONO2			
Steady-State Peroxy Radical operators (for formation of organic product species) [c]					
PO01	xHCHO = HCHO	k is variable parameter: RO2RO			
PO02	xHCHO = XC	k is variable parameter: RO2XRO			
PO03	xCCHO = CCHO	k is variable parameter: RO2RO			
PO04	xCCHO = #2 XC	k is variable parameter: RO2XRO			
PO05	xRCHO = RCHO	k is variable parameter: RO2RO			
PO06	xRCHO = #3 XC	k is variable parameter: RO2XRO			
PO07	xACET = ACET	k is variable parameter: RO2RO			
PO08	xACET = #3 XC	k is variable parameter: RO2XRO			
PO09	xMEK = MEK	k is variable parameter: RO2RO			
PO10	xMEK = #4 XC	k is variable parameter: RO2XRO			
PO11	xPROD2 = PROD2	k is variable parameter: RO2RO			
PO12	xPROD2 = #6 XC	k is variable parameter: RO2XRO			
PO13	xGLY = GLY	k is variable parameter: RO2RO			
PO14	xGLY = #2 XC	k is variable parameter: RO2XRO			
PO15	xMGLY = MGLY	k is variable parameter: RO2RO			
PO16	xMGLY = #3 XC	k is variable parameter: RO2XRO			
PO17	xBACL = BACL	k is variable parameter: RO2RO			
PO18	xBACL = #4 XC	k is variable parameter: RO2XRO			
PO19	xBALD = BALD	k is variable parameter: RO2RO			

Table A-2 (continued)

Label	Reaction and Products [a]	Rate Parameters [b] k(300)	A	Ea	B
PO20	xBALD = #7 XC	k is variable parameter: RO2XRO			
PO21	xAFG1 = AFG1	k is variable parameter: RO2RO			
PO22	xAFG1 = #5 XC	k is variable parameter: RO2XRO			
PO23	xAFG2 = AFG2	k is variable parameter: RO2RO			
PO24	xAFG2 = #5 XC	k is variable parameter: RO2XRO			
PO25	xAFG3 = AFG3	k is variable parameter: RO2RO			
PO26	xAFG3 = #7 XC	k is variable parameter: RO2XRO			
PO27	xMACR = MACR	k is variable parameter: RO2RO			
PO28	xMACR = #4 XC	k is variable parameter: RO2XRO			
PO29	xMVK = MVK	k is variable parameter: RO2RO			
PO30	xMVK = #4 XC	k is variable parameter: RO2XRO			
PO31	xIPRD = IPRD	k is variable parameter: RO2RO			
PO32	xIPRD = #5 XC	k is variable parameter: RO2XRO			
PO33	xRNO3 = RNO3	k is variable parameter: RO2RO			
Steady-State Peroxy Radical Operator (for formation of organic nitrates in peroxy + NO reactions) [d]					
PO34	xRNO3 = #6 XC + XN	k is variable parameter: RO2XRO			
PO35	zRNO3 = RNO3 + #-1 XN	k is variable parameter: RO2NO			
PO36	zRNO3 = PROD2 + HO2	k is variable parameter: RO22NN			
PO37	zRNO3 = #6 XC	k is variable parameter: RO2XRO			
Steady-State Peroxy Radical Operators (for formation of hydroperoxides in peroxy + HO_2 reactions) [e]					
PO38	yROOH = ROOH + #-3 XC	k is variable parameter: RO2HO2			
PO39	yROOH = MEK + #-4 XC	k is variable parameter: RO2RO2M			
PO40	yROOH =	k is variable parameter: RO2RO			
PO41	yR6OOH = R6OOH + #-6 XC	k is variable parameter: RO2HO2			
PO42	yR6OOH = PROD2 + #-6 XC	k is variable parameter: RO2RO2M			
PO43	yR6OOH =	k is variable parameter: RO2RO			
PO44	yRAOOH = RAOOH + #-8 XC	k is variable parameter: RO2HO2			
PO45	yRAOOH = PROD2 + #-6 XC	k is variable parameter: RO2RO2M			
PO46	yRAOOH =	k is variable parameter: RO2RO			
Explicitly Represented Primary Organics					
BE01	CH4 + OH = H2O + MEO2	6.62E-15	1.85E-12	3.36	
BE02	ETHENE + OH = RO2C + xHO2 + #1.61 xHCHO + #.195 xCCHO + yROOH	8.15E-12	Falloff, F=0.60, N=1.00		
		0:	1.00E-28	0.00	-4.50
		inf:	8.80E-12	0.00	-0.85
BE03	ETHENE + O3 = #.16 OH + #.16 HO2 + #.51 CO + #.12 CO2 + HCHO + #.37 HCOOH	1.68E-18	9.14E-15	5.13	
BE04	ETHENE + NO3 = RO2C + xHO2 + xRCHO + yROOH + #-1 XC + XN	2.24E-16	3.30E-12	5.72	2.00
BE05	ETHENE + O3P = #.8 HO2 + #.51 MEO2 + #.29 RO2C + #.51 CO + #.1 CCHO + #.29 xHO2 + #.278 xCO + #.278 xHCHO + #.012 xGLY + #.29 yROOH + #.2 XC	7.43E-13	1.07E-11	1.59	

Table A-2 (continued)

Label	Reaction and Products [a]	Rate Parameters [b] k(300)	A	Ea	B
BE06	ISOPRENE + OH = #.986 RO2C + #.093 {RO2XC + zRNO3} + #.907 xHO2 + #.624 xHCHO + #.23 xMACR + #.32 xMVK + #.357 xIPRD + yR6OOH + #-0.167 XC	9.96E-11	2.54E-11	-0.81	
BE07	ISOPRENE + O3 = #.266 OH + #.066 HO2 + #.192 RO2C + #.008 {RO2XC + zRNO3} + #.275 CO + #.122 CO2 + #.4 HCHO + #.1 PROD2 + #.39 MACR + #.16 MVK + #.15 IPRD + #.204 HCOOH + #.192 {xMACO3 + xHCHO} + #.2 yR6OOH + #-0.559 XC	1.34E-17	7.86E-15	3.80	
BE08	ISOPRENE + NO3 = #.936 RO2C + #.064 {RO2XC + zRNO3} + #.749 xHO2 + #.187 xNO2 + #.936 xIPRD + yR6OOH + #-0.064 XC + #.813 XN	6.81E-13	3.03E-12	0.89	
BE09	ISOPRENE + O3P = #.25 MEO2 + #.24 RO2C + #.01 {RO2XC + zRNO3} + #.75 PROD2 + #.24 xMACO3 + #.24 xHCHO + #.25 yR6OOH + #-1.01 XC	3.50E-11			
BE10	ACETYLEN + OH = #.7 OH + #.3 HO2 + #.3 CO + #.7 GLY + #.3 HCOOH	7.56E-13	Falloff, F=0.60, N=1.00		
BE11	ACETYLEN + O3 = #.5 OH + #1.5 HO2 + #1.5 CO + #.5 CO2	1.16E-20	1.00E-14	8.15	
BE12	BENZENE + OH = #.116 OH + #.29 {RO2C + xHO2} + #.024 {RO2XC + zRNO3} + #.57 {HO2 + CRES} + #.116 AFG3 + #.290 xGLY + #.029 xAFG1 + #.261 xAFG2 + #.314 yRAOOH + #-.976 XC	1.22E-12	2.33E-12	0.38	
<u>Reactions of Compounds represented explicitly in the chamber simulations</u>					
CH05	N-C4 + OH = #1.334 RO2C + #.079 RO2XC + #.079 zRNO3 + #.921 xHO2 + #.632 xCCHO + #.120 xRCHO + #.485 xMEK + yROOH + #-.038 XC	2.38e-12	1.63e-12	-0.23	
CH09	N-C8 + OH = #1.432 RO2C + #.354 RO2XC + #.354 zRNO3 + #.646 xHO2 + #.024 xRCHO + #.622 xPROD2 + yR6OOH + #2.072 XC	8.16e-12	2.45e-12	-0.72	
CH11	PROPENE + OH = #.984 RO2C + #.016 RO2XC + #.016 zRNO3 + #.984 xHO2 + #.984 xHCHO + #.984 xCCHO + yROOH + #-.048 XC	2.60e-11	4.85e-12	-1.00	
CH12	PROPENE + O3 = #.350 OH + #.165 HO2 + #.355 MEO2 + #.525 CO + #.215 CO2 + #.500 HCHO + #.500 CCHO + #.185 HCOOH + #.075 CCOOH + #.070 XC	1.05e-17	5.51e-15	3.73	
CH13	PROPENE + NO3 = #.949 RO2C + #.051 RO2XC + #.051 zRNO3 + #.949 xHO2 + yROOH + #2.694 XC + XN	9.73e-15	4.59e-13	2.30	
CH14	PROPENE + O3P = #.450 RCHO + #.550 MEK + #-.550 XC	4.01e-12	1.02e-11	0.56	
CH16	T-2-BUTE + OH = #.965 RO2C + #.035 RO2XC + #.035 zRNO3 + #.965 xHO2 + #1.930 xCCHO + yROOH + #-.070 XC	6.32e-11	1.01e-11	-1.09	

Table A-2 (continued)

Label	Reaction and Products [a]	Rate Parameters [b] k(300)	A	Ea	B
CH17	T-2-BUTE + O3 = #.540 OH + #.170 HO2 + #.710 MEO2 + #.540 CO + #.310 CO2 + CCHO + #.150 CCOOH + #.140 XC	1.95e-16	6.64e-15	2.10	
CH18	T-2-BUTE + NO3 = #.920 RO2C + #.080 RO2XC + #.080 zRNO3 + #.705 xNO2 + #.215 xHO2 + #1.410 xCCHO + #.215 xRNO3 + yROOH + #-.590 XC + #.080 XN	3.93e-13	1.10e-13	-0.76	
CH19	T-2-BUTE + O3P = MEK	1.99e-11	1.09e-11	-0.36	
CH21	TOLUENE + OH = #.312 {OH + AFG3} + #.181 {HO2 + CRES} + #.454 {RO2C + xHO2} + #.054 {RO2XC +zRNO3} + #.238 xGLY + #.151 xMGLY + #.065 xBALD + #.195 xAFG1 + #.195 xAFG2 + #.073 yR6OOH + #.435 yRAOOH + #-.109 XC	5.58e-12	1.81e-12	-0.67	
CH23	M-XYLENE + OH = #.239 {OH + AFG3} + #.159 {HO2 + CRES} + #.52 {RO2C +xHO2} + #.082 {RO2XC + zRNO3} + #.100 xGLY + #.380 xMGLY + #.041 xBALD + #.336 xAFG1 + #.144 xAFG2 + #.047 yR6OOH + #.555 yRAOOH+ #.695 XC	2.31e-11			
Reactions of Ethane used in its Atmospheric Reactivity Simulations					
C201	ETHANE + OH = RO2C + xHO2 + xCCHO + yROOH	2.54E-13	1.34E-12	0.992	2.0
Reactions of Lumped Species used in Atmospheric Reactivity Simulations					
BL01	ALK1 + OH = RO2C + xHO2 + xCCHO + yROOH	2.54e-13	1.34e-12	0.99	
BL02	ALK2 + OH = #.965 RO2C + #.035 {RO2XC + zRNO3} + #.965 xHO2 + #.261 xRCHO + #.704 xACET + yROOH + #-.105 XC	1.11e-12	1.49e-12	0.17	
BL03	ALK3 + OH = #1.253 RO2C + #.07 {RO2XC + zRNO3} + #.694 xHO2 + #.236 xTBUO + #.026 xHCHO + #.445 xCCHO + #.122 xRCHO + #.024 xACET + #.332 xMEK + yROOH + #-.046 XC	2.31e-12	1.51e-12	-0.25	
BL04	ALK4 + OH = #1.773 RO2C + #.144 {RO2XC + zRNO3} + #.834 xHO2 + #.011 xMEO2 + #.011 xMECO3 + #.002 xCO + #.030 xHCHO + #.454 xCCHO + #.242 xRCHO + #.442 xACET + #.110 xMEK + #.128 xPROD2 + yR6OOH + #-.097 XC	4.26e-12	3.67e-12	-0.09	
BL05	ALK5 + OH = #1.597 RO2C + #.348 {RO2XC + zRNO3} + #.652 xHO2 + #.037 xHCHO + #.099 xCCHO + #.199 xRCHO + #.066 xACET + #.080 xMEK + #.425 xPROD2 + yR6OOH + #2.012 XC	9.22e-12	2.65e-12	-0.74	
BL06	OLE1 + OH = #1.138 RO2C + #.095 {RO2XC + zRNO3} + #.904 xHO2 + #.001 xMEO2 + #.700 xHCHO + #.301 xCCHO + #.470 xRCHO + #.005 xACET + #.119 xPROD2 + #.026 xMACR + #.008 xMVK + #.006 xIPRD + yROOH + #.822 XC	3.29e-11	6.18e-12	-1.00	

Table A-2 (continued)

Label	Reaction and Products [a]	Rate Parameters [b] k(300)	A	Ea	B
BL07	OLE1 + O3 = #.193 OH + #.116 HO2 + #.104 MEO2 + #.063 RO2C + #.004 {RO2XC + zRNO3} + #.368 CO + #.125 CO2 + #.500 HCHO + #.147 CCHO + #.353 RCHO + #.006 MEK + #.189 PROD2 + #.185 HCOOH + #.022 CCOOH + #.112 RCOOH + #.040 xHO2 + #.007 xCCHO + #.031 xRCHO + #.002 xACET + #.044 yR6OOH + #.69 XC	1.09e-17	3.15e-15	3.38	
BL08	OLE1 + NO3 = #1.312 RO2C + #.176 {RO2XC + zRNO3} + #.824 xHO2 + #.009 xCCHO + #.002 xRCHO + #.024 xACET + #.546 xRNO3 + yR6OOH + #.454 XN + #.572 XC	1.44e-14	4.73e-13	2.08	
BL09	OLE1 + O3P = #.450 RCHO + #.437 MEK + #.113 PROD2 + #1.224 XC	5.02e-12	1.49e-11	0.65	
BL10	OLE2 + OH = #.966 RO2C + #.086 {RO2XC + zRNO3} + #.914 xHO2 + #.209 xHCHO + #.787 xCCHO + #.483 xRCHO + #.136 xACET + #.076 xMEK + #.021 xPROD2 + #.027 xMACR + #.002 xMVK + #.037 xIPRD + yR6OOH + #.113 XC	6.41e-11	1.26e-11	-0.97	
BL11	OLE2 + O3 = #.421 OH + #.093 HO2 + #.290 MEO2 + #.199 RO2C + #.003 {RO2XC + zRNO3} + #.296 CO + #.162 CO2 + #.152 HCHO + #.426 CCHO + #.316 RCHO + #.048 ACET + #.031 MEK + #.042 PROD2 + #.028 MACR + #.021 MVK + #.033 HCOOH + #.061 CCOOH + #.222 RCOOH + #.039 xHO2 + #.147 xMECO3 + #.007 xRCO3 + #.108 xHCHO + #.066 xCCHO + #.019 xRCHO + #.196 yR6OOH + #.133 XC	1.24e-16	8.15e-15	2.49	
BL12	OLE2 + NO3 = #1.185 RO2C + #.136 {RO2XC + zRNO3} + #.409 xNO2 + #.423 xHO2 + #.033 xMEO2 + #.074 xHCHO + #.546 xCCHO + #.153 xRCHO + #.110 xACET + #.002 xMEK + #.026 xMVK + #.007 xIPRD + #.322 xRNO3 + yR6OOH + #.270 XN + #.117 XC	7.70e-13	2.15e-13	-0.76	
BL13	OLE2 + O3P = #.014 HO2 + #.013 RO2C + #.074 RCHO + #.709 MEK + #.203 PROD2 + #.007 xHO2 + #.007 xMACO3 + #.006 xCO + #.006 xMACR + #.014 yR6OOH + #.666 XC	2.06e-11	1.43e-11	-0.22	
BL14	ARO1 + OH = #.283 OH + #.166 HO2 + #.483 RO2C + #.068 {RO2XC + zRNO3} + #.166 CRES + #.283 AFG3 + #.483 xHO2 + #.217 xGLY + #.138 xMGLY + #.049 xBALD + #.079 xPROD2 + #.164 xAFG1 + #.192 xAFG2 + #.150 yR6OOH + #.402 yRAOOH+ #.004 XC	6.18e-12			
BL15	ARO2 + OH = #.199 OH + #.108 HO2 + #.582 RO2C + #.111 RO2XC + #.111 zRNO3 + #.108 CRES + #.199 AFG3 + #.582 xHO2 + #.111 xGLY + #.291 xMGLY + #.104 xBACL + #.033 xBALD + #.042 xPROD2 + #.223 xAFG1 + #.211 xAFG2 + #.074 xAFG3 + #.090 yR6OOH + #.603 yRAOOH+ #1.503 XC	2.20e-11			

Table A-2 (continued)

Label	Reaction and Products [a]	Rate Parameters [b] k(300)	A	Ea	B
BL16	TERP + OH = #1.147 RO2C + #.2 {RO2XC + zRNO3} + #.759 xHO2 + #.042 xRCO3 + #.002 xCO + #.264 xHCHO + #.533 xRCHO + #.036 xACET + #.005 xMEK + #.255 xPROD2 + #.009 xMGLY + #.014 xBACL + #.002 xMVK + #.001 xIPRD + yR6OOH + #5.055 XC	7.98e-11	1.87e-11	-0.86	
BL17	TERP + O3 = #.585 OH + #.052 HO2 + #.875 RO2C + #.203 RO2XC + #.203 zRNO3 + #.166 CO + #.045 CO2 + #.079 HCHO + #.004 MEK + #.409 PROD2 + #.107 HCOOH + #.043 RCOOH + #.067 xHO2 + #.126 xMECO3 + #.149 xRCO3 + #.019 xCO + #.150 xHCHO + #.220 xRCHO + #.165 xACET + #.001 xGLY + #.002 xMGLY + #.055 xBACL + #.001 xMACR + #.001 xIPRD + #.545 yR6OOH + #3.526 XC	6.99e-17	1.02e-15	1.60	
BL18	TERP + NO3 = #1.508 RO2C + #.397 RO2XC + #.397 zRNO3 + #.422 xNO2 + #.162 xHO2 + #.019 xRCO3 + #.010 xCO + #.017 xHCHO + #.001 xCCHO + #.509 xRCHO + #.174 xACET + #.001 xMGLY + #.003 xMACR + #.001 xMVK + #.002 xIPRD + #.163 xRNO3 + yR6OOH + #4.476 XC + #.415 XN	6.53e-12	1.28e-12	-0.97	
BL19	TERP + O3P = #.147 RCHO + #.853 PROD2 + #4.441 XC	3.71e-11			

[a] Format of reaction listing: "=" separates reactants from products; "*#number*" indicates stoichiometric coefficient, "*#coefficient* {*product list*}" means that the stoichiometric coefficient is applied to all the products listed.

[b] Except as indicated, the rate constants are given by $k(T) = A \cdot (T/300)^B \cdot e^{-Ea/RT}$, where the units of k and A are cm^3 $molec^{-1}$ s^{-1}, Ea are kcal mol^{-1}, T is ^oK, and R=0.0019872 kcal mol^{-1} deg^{-1}. If A, Ea, and B are not given the rate constants are assumed to be temperature independent. The following special rate constant expressions are used:

Phot Set = *name*: The absorption cross sections and (if applicable) quantum yields for the photolysis reaction are given by Carter (2009). Here, "*name*" indicates the photolysis set used. If a "qy=*number*" notation is given, the number given is the overall quantum yield, which is assumed to be wavelength independent. Photolysis rates used in chamber and ambient simulations are given in Table A-3.

Falloff: The rate constant as a function of temperature and pressure is calculated using $k(T,M) = \{k0(T)\cdot[M]/[1 + k0(T)\cdot[M]/kinf(T)]\}\cdot F^Z$, where $Z = \{1 + [\log10\{k0(T)\cdot[M])/kinf(T)\}/N]^2\}^{-1}$, [M] is the total pressure in molecules cm^{-3}, F and N are as indicated on the table, and the temperature dependences of k0 and kinf are as indicated on the table.

k = k0+k3M(1+k3M/k2): The rate constant as a function of temperature and pressure is calculated using $k(T,M) = k0(T) + k3(T)\cdot[M] \cdot(1 + k3(T)\cdot[M]/k2(T))$, where [M] is the total bath gas (air) concentration in molecules cm-3, and the temperature dependences for k0, k2 and k3 are as indicated on the table.

k = k1 + k2 [M]: The rate constant as a function of temperature and pressure is calculated using $k(T,M) = k1(T) + k2(T)\cdot[M]$, where [M] is the total bath gas (air) concentration in molecules cm-3, and the temperature dependences for k1, and k2 are as indicated on the table.

Table A-2 (continued)

Same K as Rxn xx: Uses the same rate constant as the reaction with the same label.

k is variable parameter *name*: The rate constant is calculated using variable parameters that are calculated using concentrations of various species. See Footnotes [c], [d], and [e], below.

[c] The xPROD chemical operator species are used to represent the formation of radicals and products from alkoxy radicals formed in the reactions of peroxy radicals with NO, NO_3, acyl peroxy radicals, and, in ~50% yields, with other peroxy radicals. These products are not formed when peroxy radicals react with HO_2, and, in ~50% yields, with other peroxy radicals, since those reactions are assumed not form alkoxy radicals, but instead form hydroperoxides or H-shift disproportion products that are represented by separate yROOH chemical operator species, discussed in a separate footnote. The reactions of peroxy radicals with other peroxy radicals are assumed to form alkoxy radicals 50% of the time, so the products from alkoxy radical reactions are represented as being formed in 50% yields in these reactions. The consumption and products formed from these species can be represented in several ways. The most straightforward method is to include a reaction for each of the types of peroxy radical reactions, as follows:

xPROD + NO → NO + PROD
xPROD + HO2 → HO2
xPROD + NO3 → NO3 + PROD
xPROD + MECO3 → MECO3 + PROD (& similar reactions for RCO3, BZCO3, and MACO3)
xPROD + MEO2 → MEO2 + 1/2 PROD
xPROD + RO2C → RO2C + 1/2 PROD (& a similar reaction for RO2XC)

where "PROD" represents the product species for the operator (e.g, HO2 for xHO2). The rate constants for these reactions should be the same as the rate constant for the corresponding reactions of RO2C or RO2XC. This is a somewhat cumbersome method because it requires 9 reactions for each of the many xPROD species. An alternative method, implemented in this table, uses the coefficient "RO2RO" to determine the rate of formation of the product species and "RO2XRO" to represent processes where the product is not formed. These are calculated as follows, where the k(RO2+..)'s refer to the rate constants for the reactions of RO2C or RO2XC with the indicated reactant.

RO2RO = k(RO2+NO)[NO] + k(RO2+NO3)[NO3] + k(RO2+MECO3){[MECO3]+[RCO3]+ [BZCO3]+[MACO3]) + 0.5 k(RO2+MEO2)[MEO2] + 0.5 k(RO2+RO2) {[RO2C]+[RO2XC])
RO2XRO = k(RO2+HO2)[HO2] + 0.5 k(RO2+MEO2)[MEO2] + 0.5 k(RO2+RO2){[RO2C]+ [RO2XC])

The steady state approximation must be used for these operators when this representation is used, and the operators must not be allowed to be diluted or transported.

[d] The zRNO3 chemical operator species is used to represent the formation organic nitrates formed when peroxy radicals react with NO, or formation of of radicals and products from alkoxy radicals formed in the reactions of peroxy radicals with NO_3, acyl peroxy radicals, and (in ~50% yields) with other peroxy radicals. These products are not formed when peroxy radicals react with HO_2 and (in the other ~50% of the time) with other peroxy radicals, since those reactions are assumed not form organic nitrates or alkoxy radicals, but instead form hydroperoxides or H-shift disproportion products that are represented by separate yROOH chemical operator species, discussed in a separate footnote. At present the mechanism has only one zRNO3 operator to correspond to the single lumped organic nitrate model species, but other such operators can be added if it is desired to have separate organic nitrate model species, such as, for example, those to represent semi-volatile organic nitrates that may contribute to SOA. In the case of zRNO3, the products resulting if alkoxy radicals are formed in the RCO3 or RO2 reactions would depend on reactant and individual radicals, and are approximated by PROD2 and HO2 (as might occur following the reaction of a peroxy radical with O_2 to form HO_2 and a ketone species). As with the xPROD species, the consumption and products

Table A-2 (continued)

formed from these species can be represented in several ways, with the most straightforward method being to include a reaction for each of the types of peroxy radical reactions, as follows:

zRNO3 + NO → NO + RNO3
zRNO3 + HO2 → HO2
zRNO3 + NO3 → NO3 + PROD2 + HO2
zRNO3 + MECO3 → MECO3 + PROD2 + HO2 (& similar reactions for RCO3, BZCO3, and MACO3)
zRNO3 + MEO2 → MEO2 + 1/2 {PROD2 + HO2}
zRNO3 + RO2C → RO2C + 1/2 {PROD2 + HO2} (& a similar reaction for RO2XC)

The rate constants for these reactions should be the same as the rate constant for the corresponding reactions of RO2C or RO2XC. As with xPROD, an alternative method, requiring fewer reactions, is implemented in this table. In this case, the coefficient "RO2NO" is used to determine the rate of formation of organic nitrates, "RO22NN" is used to determine the rate of formation of the alkoxy radical products, and "RO2XRO" is used to represent processes where these products are is not formed, and is the same as used for xPROD. These are calculated as follows, where the k(RO2+..)'s refer to the rate constants for the reactions of RO2C or RO2XC with the indicated reactant.

RO2NO = k(RO2+NO)[NO]
RO22NN = k(RO2+NO3)[NO3] + k(RO2+MECO3){[MECO3]+[RCO3]+[BZCO3]+ [MACO3]) + 0.5 k(RO2+MEO2)[MEO2] + 0.5 k(RO2+RO2){[RO2C]+ [RO2XC])
RO2XRO = k(RO2+HO2)[HO2] + 0.5 k(RO2+MEO2)[MEO2] + 0.5 k(RO2+RO2){[RO2C]+ [RO2XC]) (same as used for xPROD)

The steady state approximation must be used for these operators when this representation is used, and the operators must not be allowed to be diluted or transported.

[e] The yROOH chemical operator species is used to represent the formation of organic hydroperoxides formed with peroxy radicals react with HO_2, or of H-shift disproportionation products formed when peroxy radicals react (in 50% yields) with other peroxy radicals. Note that the products formed when peroxy radicals react to form alkoxy radicals or organic nitrates (in the NO reaction) are represented using separate xPROD or zRNO3 species, and together these three types of operators represent all the products and radicals formed. Separate such yROOH species are used to represent formation of hydroperoxides or H-shift disproportion products in different molecular weight ranges or volatilities, and more can be added as needed for appropriate predictions of SOA formation. The hydroperoxide formed in the HO2 reaction is represented by either ROOH, R6OOH, or RAOOH, and the H-shift disproportion products are represented by either MEK (for yROOH) or PROD2 (for the others). As with the xPROD and zRNO3 species, the consumption and products formed from these species can be represented in several ways, with the most straightforward method being to include a reaction for each of the types of peroxy radical reactions, as follows for yROOH (the reactions for the other two are analogous).

yROOH + NO → NO
yROOH + HO2 → HO2 + ROOH
yROOH + NO3 → NO3
yROOH + MECO3 → MECO3 (& similar reactions for RCO3, BZCO3, and MACO3)
yROOH + MEO2 → MEO2 + 1/2 MEK
yROOH + RO2C → RO2C + 1/2 MEK (& a similar reaction for RO2XC)

The rate constants for these reactions should be the same as the rate constant for the corresponding reactions of RO2C or RO2XC. As with the other operators, an alternative method, requiring fewer reactions, is implemented in this table. In this case, the coefficient "RO2HO2" is used to determine the rate of formation of organic hydroperoxides, "RO2RO2M" to determine the rate of formation of H-shift disproportion products, and "RO2RO" is used to represent processes where these products

Table A-2 (continued)

are is not formed. Note that the latter is the same as the coefficient that is used to represent the formation products from the xPROD species. These are calculated as follows, where the k(RO2+..)'s refer to the rate constants for the reactions of RO2C or RO2XC with the indicated reactant.

RO2HO2 = k(RO2+HO2)[HO2]
RO2RO2M = 0.5 k(RO2+RO2){[RO2C]+ [RO2XC])
RO2RO = k(RO2+NO)[NO] + k(RO2+NO3)[NO3] + k(RO2+MECO3){[MECO3]+[RCO3]+ [BZCO3]+[MACO3]) + 0.5 k(RO2+MEO2) [MEO2] + 0.5 k(RO2+RO2) {[RO2C]+[RO2XC])

The steady state approximation must be used for these operators when this representation is used, and the operators must not be allowed to be diluted or transported.

Table A-3. Summary of photolysis rates used in chamber and ambient simulations.

Phot File	Chamber [a]	Photolysis rates (min-1) Ambient simulations (as function of solar zenith angle) [b] Z=0	Z=10	Z=20	Z=30	Z=40	Z=50	Z=60	Z=70	Z=78	Z=86
Base Mechanism [c]											
NO2-06	0.115	0.723	0.718	0.702	0.676	0.631	0.560	0.430	0.253	0.093	0.005
NO3NO-06	2.44e-4	1.91e+0	1.91e+0	1.90e+0	1.89e+0	1.87e+0	1.82e+0	1.65e+0	1.37e+0	9.15e-1	4.85e-1
NO3NO2-6	4.83e-2	1.54e+1	1.54e+1	1.53e+1	1.52e+1	1.49e+1	1.44e+1	1.29e+1	1.03e+1	6.50e+0	2.80e+0
O3O1D-06	1.83e-4	3.06e-3	2.96e-3	2.68e-3	2.24e-3	1.67e-3	1.06e-3	4.91e-4	1.33e-4	2.01e-5	3.66e-7
O3O3P-06	4.84e-4	3.66e-2	3.66e-2	3.62e-2	3.57e-2	3.48e-2	3.32e-2	2.95e-2	2.37e-2	1.57e-2	8.36e-3
HONO-06	2.81e-2	1.14e-1	1.13e-1	1.10e-1	1.06e-1	9.78e-2	8.54e-2	6.38e-2	3.55e-2	1.18e-2	4.32e-4
HNO3	4.42e-6	5.40e-5	5.28e-5	4.91e-5	4.31e-5	3.49e-5	2.50e-5	1.40e-5	4.99e-6	9.91e-7	2.29e-8
HNO4-06	6.66e-5	5.42e-4	5.32e-4	5.01e-4	4.52e-4	3.81e-4	2.90e-4	1.77e-4	7.28e-5	1.70e-5	4.56e-7
H2O2	9.00e-5	5.64e-4	5.56e-4	5.29e-4	4.86e-4	4.21e-4	3.33e-4	2.14e-4	9.43e-5	2.35e-5	6.64e-7
PAN	7.17e-6	6.12e-5	6.00e-5	5.65e-5	5.08e-5	4.26e-5	3.22e-5	1.95e-5	7.90e-6	1.81e-6	4.80e-8
HCHOR-06	2.53e-4	2.76e-3	2.72e-3	2.59e-3	2.36e-3	2.03e-3	1.58e-3	9.85e-4	4.05e-4	9.08e-5	2.35e-6
HCHOM-06	6.12e-4	3.12e-3	3.08e-3	2.97e-3	2.77e-3	2.47e-3	2.02e-3	1.37e-3	6.41e-4	1.69e-4	5.00e-6
CCHO_R	2.53e-5	4.16e-4	4.06e-4	3.75e-4	3.27e-4	2.60e-4	1.81e-4	9.50e-5	2.99e-5	4.86e-6	8.30e-8
C2CHO	1.05e-4	1.40e-3	1.37e-3	1.28e-3	1.14e-3	9.29e-4	6.74e-4	3.80e-4	1.36e-4	2.62e-5	5.79e-7
ACET-06	3.85e-6	6.47e-5	6.28e-5	5.69e-5	4.78e-5	3.60e-5	2.32e-5	1.10e-5	3.05e-6	4.50e-7	7.35e-9
MEK-06	6.96e-5	9.66e-4	9.45e-4	8.80e-4	7.78e-4	6.33e-4	4.56e-4	2.54e-4	8.86e-5	1.66e-5	3.53e-7
COOH	7.11e-5	3.94e-4	3.89e-4	3.71e-4	3.42e-4	2.99e-4	2.40e-4	1.58e-4	7.21e-5	1.89e-5	5.51e-7
GLY-07R	9.60e-4	9.06e-3	9.00e-3	8.78e-3	8.44e-3	7.86e-3	6.97e-3	5.39e-3	3.29e-3	1.35e-3	1.31e-4
GLY-07M	4.40e-4	3.18e-3	3.14e-3	3.00e-3	2.78e-3	2.44e-3	1.98e-3	1.33e-3	6.41e-4	1.91e-4	8.80e-6
MGLY-06	1.02e-3	1.56e-2	1.56e-2	1.52e-2	1.47e-2	1.38e-2	1.24e-2	9.83e-3	6.27e-3	2.72e-3	2.87e-4
BACL-07	2.06e-3	2.67e-2	2.66e-2	2.61e-2	2.54e-2	2.40e-2	2.18e-2	1.75e-2	1.12e-2	4.81e-3	4.67e-4
BALD-06	1.32e-2	5.10e-2	5.05e-2	4.88e-2	4.61e-2	4.17e-2	3.52e-2	2.49e-2	1.26e-2	3.71e-3	1.17e-4
AFG1	6.82e-2	3.87e-1	3.83e-1	3.70e-1	3.50e-1	3.17e-1	2.69e-1	1.94e-1	1.04e-1	3.51e-2	1.99e-3
MACR-06	3.43e-5	1.97e-4	1.94e-4	1.86e-4	1.72e-4	1.51e-4	1.21e-4	7.98e-5	3.64e-5	9.42e-6	2.74e-7
MVK-06	1.32e-5	7.50e-5	7.40e-5	7.07e-5	6.54e-5	5.73e-5	4.60e-5	3.02e-5	1.37e-5	3.51e-6	1.01e-7
IC3ONO2	1.82e-5	2.35e-4	2.30e-4	2.15e-4	1.91e-4	1.57e-4	1.15e-4	6.57e-5	2.41e-5	4.80e-6	1.11e-7

[a] Photolysis rates for a chamber experiment with blacklight light source. The chamber photolysis rates are for the experiments carried out for this project.

[b] See Carter (1994) for documentation of solar actinic fluxes used in the atmospheric reactivity calculations.

[c] Calculated using absorption coefficients and cross sections given by Carter (2009)